AD 702727

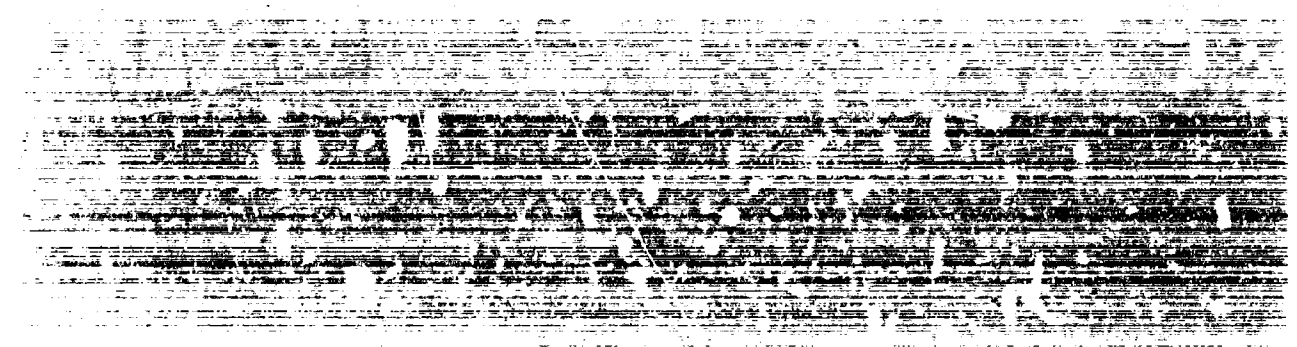

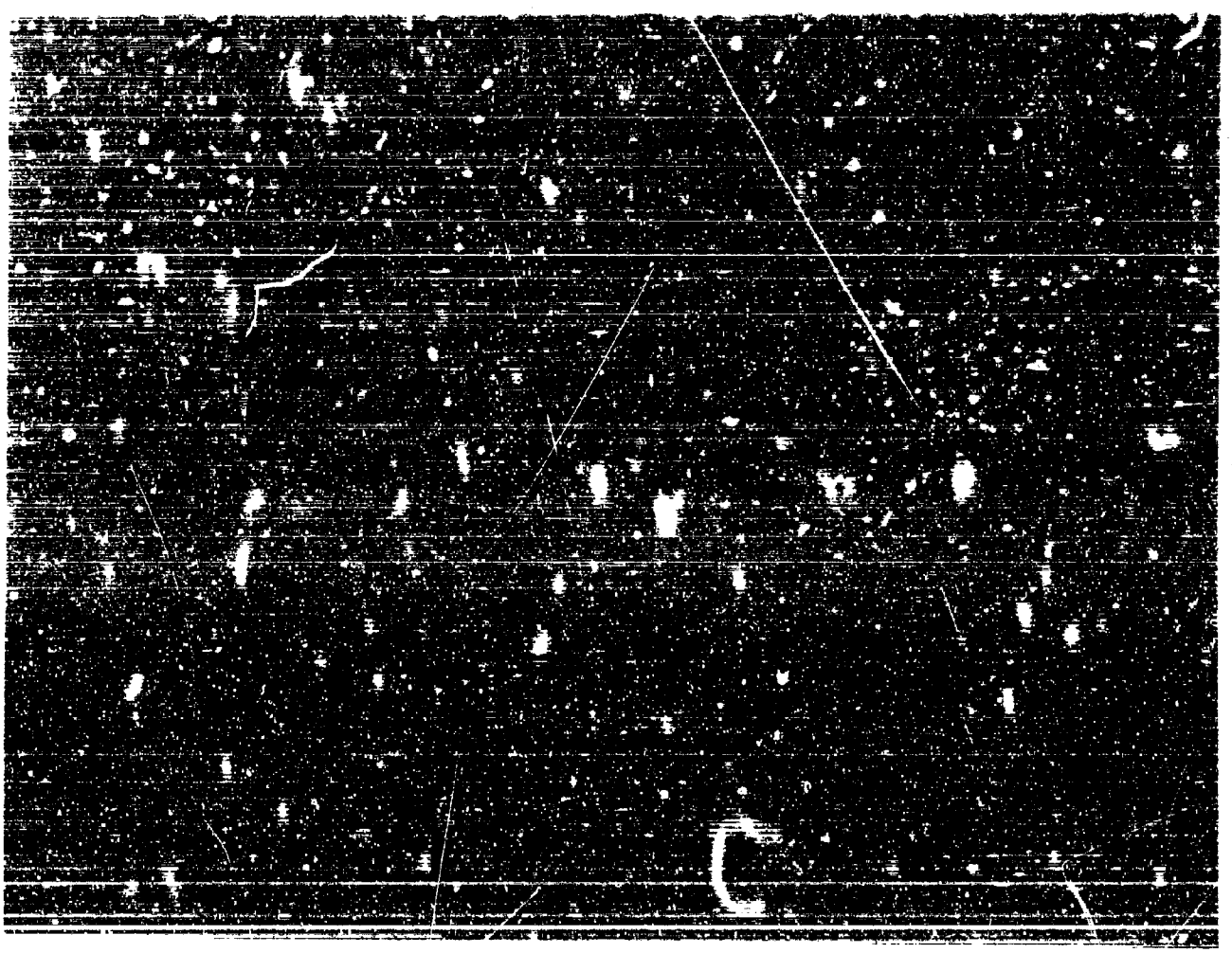

BLANK PAGE

DEPARTMENT OF THE NAVY
NAVAL SHIP RESEARCH AND DEVELOPMENT CENTER
WASHINGTON, D. C. 20007

INVESTIGATION OF IMPACT OF RIGID AND ELASTIC BODIES WITH WATER

by

Sheng-Lun Chuang

February 1970

Report 3248

TABLE OF CONTENTS

LIST OF FIGURES

Page

LIST OF TABLES

NOTATION

A	Impact area of fluid or impact body
A	Cross sectional area in general
A_n	Peak displacement of transverse vibration at n^{th} cycle
A_{n+q}	Peak displacement of transverse vibration at $(n+q)^{th}$ cycle
a	Acceleration in general
a, l	Length and width of rectangular plate
B	Arbitrary constant
b	See a, b
c	Speed of sound in fluid
c_a	Speed of sound in atmosphere at p_a
c_{air}	Speed of sound in air
c_b	Damping constant of backing material
c_c	Critical damping constant
c_p	Structural damping constant
c_v	Viscous damping constant = $c_p + c_{zz}$
c_{zz}	Damping constant of fluid
D	Flexural rigidity of isotropic plate = $\frac{E\,h^3}{12(1-\nu^2)}$
$D_1(t)$	Dynamic load factor for fundamental mode
D_x	$= \frac{E_x\,h^3}{12\,(1-\nu_{xy}\,\nu_{yx})}$
D_y	$= \frac{E_y\,h^3}{12\,(1-\nu_{xy}\,\nu_{yx})}$
D_{xy}	$= \frac{G_{xy}\,h^3}{12}$
D_1	$= \frac{\nu_{xy}\,E_y\,h^3}{12\,(1-\nu_{xy}\,\nu_{yx})}$

D_x, D_y, D_{xy}, D_1: Flexural rigidity constants of orthotropic plate

d	Distance in general

E	Modulus of elasticity of isotropic material in tension and compression
E_x, E_y	Modulus of elasticity of orthotropic material in x-, y-directions in tension and compression
F	Force acting upon falling body or force in general
$f(t)$, $f(\tau)$	Time dependent variable of $p(x,y,t)$
$f_{m/n}$	Vibratory frequency at $(m/n)^{th}$ mode
G_{xy}	Shear modulus of orthotropic plate
g	Acceleration due to gravity
H	$= D_1 + 2 D_{xy}$
h	Thickness of plate
I	Moment of inertia in general
I	Impulse in general
I_o	Moment of inertia about neutral axis
I_x, I_y	Moment of inertia of structural member in x-, y-directions
k	Spring constant in general
k_f	Spring constant of structure with fixed ends
k_s	Spring constant of structure with hinged ends
$k_{m/n}$	Spring constant at $(m/n)^{th}$ mode
k_{zz}	Spring constant of fluid
L	Half wetted breadth of wedge measured horizontally ($L = \pi/2$ of half breadth of wedge at undisturbed water level) or half breadth of flat bottom
M_o	Mass of falling body
m	Mass in general
m_b	Mass of backing material
m_f	Mass of fluid
m_p	Mass of plate $= \rho_p h$
m_s	Mass of structure
m_{zz}	Added mass of fluid
m/n	m^{th} and n^{th} mode numbers in orthogonal direction ($m, n = 0, 1, 2, \ldots$)
n	Arbitrary constant with limits $1 \leq n \leq 2$
P	Total impact pressure in general

P	Maximum pressure or force applied to a single degree of freedom system
p	Impact pressure in general
p_a	Atmospheric pressure
p_i	Interacting pressure between elastic body and fluid
p_{max}	Maximum impact pressure
p_{keel}	Impact pressure at keel
p_r	Rigid body impact pressure
p_t	Total impact pressure = $p_r + p_i$
q	$= \frac{p_{max}}{m} = \frac{P}{\rho_p h + m_{zz}}$
q	Number of vibratory cycles
s_x, s_y	Space between two adjacent supporting members in x-, y-directions
T	Half period or duration of first positive pulse of impact pressure, i.e., duration of pulse
$T_{m/n}$	Vibratory period at $(m/n)^{th}$ mode
t, τ	Time in general
t_o	Time at instant of impact
V	Velocity in general at time t
V_o	Impact velocity at instant of impact t_o
W	Total weight in general
w	Transverse displacement of plate in z-direction (i.e., plate deflection)
$w_{m/n}$	w at $(m/n)^{th}$ mode
w_{st}	Plate deflection due to maximum static load which is also p_{max}
$\cancel{w}$	Weight in general
$\dot{w}$	$= \frac{dw}{dt}$
$\ddot{w}$	$= \frac{d^2w}{dt^2}$
x, y	Horizontal coordinates in x-, y-, z-coordinate system
x_1, y_1, w	Coordinates on isotropic and orthotropic plates

Z	Mechanical impedance
$\dot{z}$	$= \frac{dz}{dt}$
$\ddot{z}$	$= \frac{d^2z}{dt^2}$
β	Deadrise angle, radian
γ	Ratio between specific heat at constant pressure and that at constant volume
δ	Logarithmic decrement defined by Equation [5.2]
ε	Strain in inches per inch
ν	Poisson's ratio of isotropic material
ν_{xy}, ν_{yx}	Poisson's ratios of orthotropic material
ρ	Mass density of fluid (= weight per unit volume/g = 1.94 lb-sec^2/ft^4 for fresh water)
ρ_a	Mass density of air at p_a
ρ_l	Mass density of air at p
ρ_p	Mass density of plate
$\rho_{\text{fresh water}}$	Mass density of fresh water
$\rho_{\text{sea water}}$	Mass density of sea water
σ	Stress in pounds per square inch
τ	See t, τ (usually τ is used as dummy variable for t)
ω	Circular frequency in general
$\omega_{m/n}$	ω at $(m/n)^{th}$ mode
∇^4	Operator, e.g., $\left[\frac{\partial^4}{\partial x^4} + 2\frac{\partial^4}{\partial x^2 \partial y^2} + \frac{\partial^4}{\partial y^4}\right]$ in rectangular coordinate system

ABSTRACT

Impact tests of rigid flat-bottom models indicated that the maximum impact pressure is nowhere near the theoretical infinitely large hydrodynamic pressure nor near the theoretical acoustic pressure. The cushioning effect of the compressible air trapped between the impact body and the water surface reduces the maximum impact pressure to about one-tenth of the acoustic pressure. However, the nature of the trapped air phenomenon is not very stable. Much more air was trapped for the impact of a flat bottom and a 1-deg wedge than for a wedge with deadrise angles of 3 deg or higher. Tests of elastic models verified the fact that the pressure generated by the impact is affected by the vibratory movement of the impact surface and that it can be separated into rigid body impact pressure and interacting pressure. This dynamic interaction is closely related to the hydrodynamic phenomenon rather than to the acoustic phenomenon. In summary, the present study demonstrates that for the impact of rigid and elastic bodies, (1) water can be treated as an incompressible fluid regardless of the size of the deadrise angle, (2) trapped air must be taken into consideration for small deadrise angles, and (3) the structural response to impact can be treated as the impact of a deformable body on an incompressible fluid, with or without trapped air.

ADMINISTRATIVE INFORMATION

The work presented in this report was originally offered as a dissertation in partial fulfillment of the requirements for the Ph.D. degree in Structural Mechanics, Catholic University of America, June 1969. The work was funded by Subproject Z-R011 01 01, Task 0401 and the publication of this report by Subproject S46-06X, Task 1707 (Hydrofoil Hull).

I. INTRODUCTION

In recent years, speed has become an increasingly important factor in ship operations for reasons of economy, tactics, etc. While attempting to maintain high speed during heavy weather, a ship inevitably experiences the impact force of the surface wave of the sea at the bow or elsewhere. This type of impact force may easily damage the local hull structure or cause the entire ship to vibrate.

There are three categories of ship response to this type of impact load: localized, transitional, and overall.[1] The present study is concerned only with the localized response of the structure where the impact occurs, namely, the impact load and the local structural response of ship bottom.

A. BACKGROUND

At the present time, the impact of a ship with large deadrise angle (say, 15 deg and above) is generally considered to be an unsteady hydrodynamic phenomenon whereas that with zero deadrise angle is considered to be a combined acoustic and unsteady hydrodynamic phenomenon.[2] (Deadrise angle is defined as the angle between the tangent at the impact surface of a falling body and the horizontal line of the fluid which the body strikes; a flat bottom has zero deadrise angle.) However, the phenomenon has never been clearly defined for the impact of a ship bottom with small deadrise angles (say, below 15 deg and above 0 deg).

The rationale for the distinction is as follows. At large deadrise angles, water is considered incompressible and nonviscous. At zero deadrise angle, it is assumed that all intervening air is completely forced out from underneath the impact surface. Traditionally, then, computing the maximum impact pressure for zero deadrise angle has necessitated considerations of fluid compressibility. The basis for the related analysis is as follows.

With the assumption of no trapped air and compressible fluid, an approximate value for the maximum impact pressure of a flat bottom is:[3]

$$p_{max} = \rho c V_o$$

where p is the pressure,

ρ is the mass density of the fluid,

c is the speed of sound in the fluid, and

V_o is the impact velocity.

---

[1]References are listed on page 108.

In his study on the compressibility effects of water in ship slamming,[4] Ogilvie indicated that the duration of the compression phase is 2 L/c, where L is the half-width of the flat bottom.

Following the termination of the compression phase in the fluid beneath the flat bottom and return to normal mass density of the fluid, the energy delivered by the flat bottom (which is still falling) is expended in setting up an unsteady flow.[2] This may be called the fluid-displacement phase. The flow characteristics change during this phase even though its duration is only a small fraction of a second. However, it is still much longer than the duration of the compression phase.

Since the acoustic pressure ρcV_o occurs in flat-bottom impact only at the instant of impact Δt, an elastic body does not deform until the maximum pulse of this ρcV_o pressure is over. In principle, therefore, the initial pressure is always equal to ρcV_o regardless of the elastic properties of the impact body.[5,6] So far, experiments have failed to measure this ρcV_o pressure. Several researchers have suggested that a layer of air may be trapped between the impact body and the water surface,[7,8] but this hypothesis has not been substantiated. Possibly this can be attributed to insufficient capability of the recording system used in experimental work.

B. PURPOSE AND ORGANIZATION OF THE PRESENT STUDY

The objectives of the present study are:

1. To clarify the controversial nature of the impact phenomenon for flat-bottom ships.

2. To demonstrate experimentally that the impact pressure for ship bottoms at small deadrise angles is substantially smaller than the corresponding initial acoustic pressure ρcV_o as well as the hydrodynamic pressure derived by Von Karman[3] or Wagner.[9]

3. To demonstrate that the structural response phenomenon resulting from ship bottom impact can be treated as the impact of an elastic body on an incompressible fluid irrespective of the presence of trapped air between the impact body and the fluid.

More specifically, realistic solutions were sought to the following questions:

1. Is flat bottom impact an acoustic or a hydrodynamic phenomenon?

A basic experiment was conducted with a rigid flat model (Section II). The principal purpose of this test required devising a special recording technique and particular attention to the instrumentation selected.

Evidence resulting from this investigation supports the thesis that the impact of a flat bottom with water is cushioned by the presence of trapped air between the falling body and the water. In that case, water may be considered incompressible.

2. Can the Wagner hydrodynamic impact theory provide with reasonable accuracy the impact pressure distribution on a falling wedge of small deadrise angle?

Several wedge-shaped models with small deadrise angles varying from 0 to 15 deg were dropped from various heights to establish the impact pressure as a function of impact velocity (Section III).

Evidence resulting from this investigation supports the thesis that the Wagner hydrodynamic impact theory does not apply to the impact of a wedge-shaped body with small deadrise angle. This is because, as for the flat-bottom impact, the cushioning effect of trapped air must be taken into consideration.

3. Does the deformability of the ship bottom relieve a certain percentage of the impact loads?

Two hull-shaped inflatable models of a sealed rubber fabric (Airmat) were tested to provide a deformable body that would permit easier measurements of the relief from impact loads (Section IV).

Evidence resulting from this investigation supports the thesis that a deformable body affords considerable relief from the impact load. However, because a slow recorder speed was used during this part of the investigation, the recorded pressure time histories showed only a line of pulse with large magnitude at the instant of impact, and it was not possible to analyze and compare the test record with the interaction theory given in Section IV-A. This raised the following question.

4. How does a ship bottom respond to impact loads, and how can these experimental results be compared with the interaction theory given in Section IV-A?

Theories for determining the structural response caused by the ship bottom impact have been treated in two different ways: as impact on an

incompressible fluid and as impact on a compressible fluid.[6,10,11] Since these theories have not been rigorously verified by experiment, an experimental procedure was developed to provide the basis for a valid theory.

In the subsequent study, the effect of trapped air on the dynamic structural response was taken into consideration for an elastic plate model (Section V) and for two ship flat-bottom structural models (Section VI).

Evidence resulting from this investigation supports the thesis that a hydroelastic vibration theory can be used to solve the ship bottom impact problem, with or without the trapped air.

5. How do severe impact loads damage a ship bottom and can backing material reduce this damage?

This question was investigated by testing eight ship structural models with deadrise angles of 10 deg. Some of these models were tested with various kinds of backing material (Section VII) as part of a damage reduction study.

These test results were also used to verify findings developed during the course of the complete study. Unfortunately, they indicated that backing materials are not very effective in reducing impact damage to a ship bottom structure. This deficiency can also be explained by the interaction theory given in Section IV-A.

In summary, the present study attempts to demonstrate (1) that water can be treated as an incompressible fluid regardless of the size of the deadrise angle, (2) that trapped air must be taken into consideration for small deadrise angles, and (3) that the structural response to an impact load can be treated as the impact of an elastic body on an incompressible fluid, with or without trapped air. Sections II and III concern the impact of rigid bodies with water, and Sections IV through VII concern the impact of deformable and elastic bodies with water. Each section presents the models, instrumentation, test results, analyses, and discussions relevant to it. The essential findings of the complete study are given in Section VIII.

II. RIGID FLAT-BOTTOM IMPACT

This section attempts to resolve whether the flat-bottom impact is an acoustic or a hydrodynamic phenomenon. At the beginning of the section, model and tests are described. Then, the development and calibration of instrumentation are discussed because if acoustic pressure is present, its measurement requires instrumentation of a specialized nature. Next, the test results are presented, checked, and discussed. Since the trapped air has considerable effects on the impact pressure of a flat bottom, detection of trapped air is also presented. Finally, a short summary is included at the end of the section.

A. DESCRIPTION OF MODEL AND TESTS

The model, shown in Figure 1, consisted of a 20- x 26.5- x 0.5-in. steel plate welded to a steel box. The plate was stiffened with four 0.5- x 3-in. steel flat bars inside the box so that for drop heights of 7.5 in. and below, the model may be considered as a rigid flat bottom. The total drop weight, which included the guided sliding beam and other attachments, was 255 lb.

Essentially, the test consisted of dropping the flat-plate model from various elevated positions in such a way that it remained parallel to the water surface, and of recording pressures and accelerations. Two positions, one just below the hanging position of the model and one just above the water surface, were recorded with respect to time for checking the velocity of the falling body. The drop heights were 3.0, 4.5, 6.0, 6.5, and 7.5 in., but most drops were from 6 in. High-speed movies, both underwater and surface, were taken during drops to study water flow, piled-up water, and trapped air. The speed of the movie varied up to about 5000 frames/sec.

The tests were conducted in a large rectangular tank, 25 x 15 ft, filled with water to a depth of 8.5 ft.[12] To ensure two-dimensional flow conditions, two rigid walls were constructed to span the length of the tank and to extend from 18 in. above the water surface to the full tank depth. The two walls, which were parallel to each other, were rigidly connected to the tank floor and sides and were separated by a distance equal to the

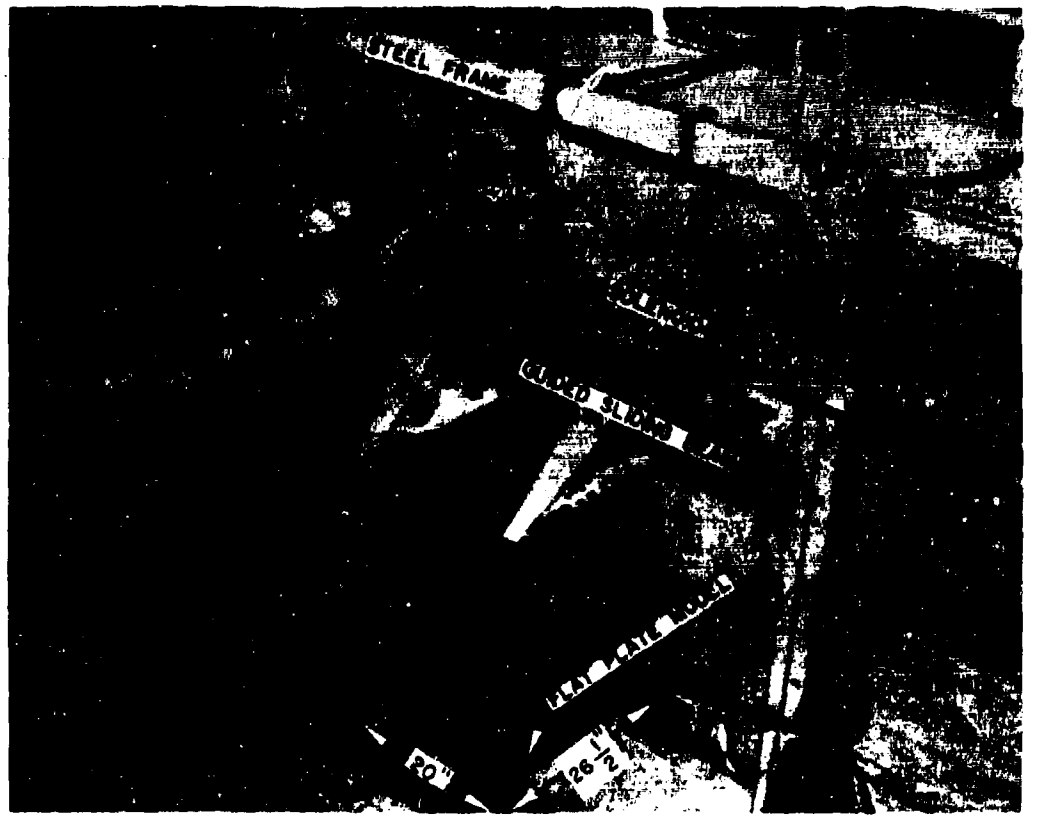

Figure 1 - Installation of Test Model

model length plus a small amount of clearance. The parallel walls had open ends to permit free flow of the surface wave around the tank during the drop test.

The desired impact velocity was obtained by proper positioning of the sliding beam above the surface; see Figure 1. The beam was guided so that maximum rotation of the model in any direction was limited to 0.25 deg during the drop.

B. INSTRUMENTATION

The instrumentation system developed for this experimental investigation consisted essentially of quartz-crystal transducers, charge amplifiers, a dual-beam oscilloscope, and a high-speed streak camera. The Kistler Model 568 charge amplifiers were able to pick up the 200-kHz signal without noticeable error. The oscilloscope was Tektronix Type 551, with a frequency range from 0 to $25(10)^6$ Hz. The streak camera was a General Radio Type 651-A, with speeds up to 1000 in./sec; it was fitted with suitable optics to view the screen of the dual beam oscilloscope.

Two pressure gages were installed, one at the center of the model and the other 3 5/16 in. from the edge at the middle of the longer side of the plate. These Kistler Model 603 quartz-crystal-type gages were rated to have a natural frequency of 200 kHz and a rise time of 1 μsec.

The complete recording system was tested and evaluated in the laboratory before being moved to the drop-test facility. The system, exclusive of the transducer, was found satisfactory to pick up and record a 200-kHz input signal. This 200-kHz frequency response can certainly pick up ρcV_o acoustic pressure at the center of the flat plate. According to the steady supersonic flow theory,[4] this ρcV_o pressure lasts L/c sec or 167 μsec for the 20-in. flat plate.

To eliminate any doubts about the test results, the entire recording system including the transducer was also calibrated mechanically by dynamically applying various known oil pressures to the pressure gage and reading the results shown on the oscilloscope.

A piezoelectric accelerometer, Endevco Model 2225, was used to measure plate acceleration near the center of the model. The gage had a natural frequency of 80 kHz, and it was considered adequate for the test.

C. RELATION OF PRESSURE TO IMPACT VELOCITY

The maximum impact pressures measured at the center of the flat bottom at various impact velocities are plotted on the log-log chart shown in Figure 2. These test results have been used by others for comparisons and showed general agreement.[13-16]

As can be seen in the figure, the pressure is approximately proportional to the square of the impact velocity; it may be expressed as

$$p_{max} = 0.68\ V_o^2 \qquad [2.1]$$

where p_{max} is the maximum impact pressure of the flat bottom in pounds per square inch and V_o is the impact velocity in feet per second.

The impact pressure at the edge of the flat bottom was also measured for several drop tests. In general, the edge impact pressure is somewhat lower than the center pressure. However, as shown in Figure 3, the edge impact pressure was somewhat higher than the center impact pressure. This could be caused by the imperfect impact of flat bottom.

Figure 3 shows two typical pressure-time history curves recorded on 35-mm film during a 6-in. drop. As indicated in the figure, one of these two curves is for the center pressure and one is for the edge pressure of the flat bottom. The polarities of the reading were set so that the positive pressures moved towards the middle of the film and the negative pressure towards the edge of the film. (Positive pressure is defined as the pressure above atmospheric pressure and negative pressure, as the pressure below atmospheric pressure.) The 0-msec value is chosen as an arbitrary time and is by no means the time at which the impact occurred, since there is no way to pinpoint this occurrence.

Acceleration of the plate near the center was also recorded for a selected number of tests. Acceleration measurements during the impact were taken for two purposes:

1. Because the pressure gages are sensitive to acceleration, the acceleration measurements indicate whether corrections are necessary for the pressure readings. The acceleration readings indicated that the corrections for the pressure reading were negligibly small and were therefore unnecessary.

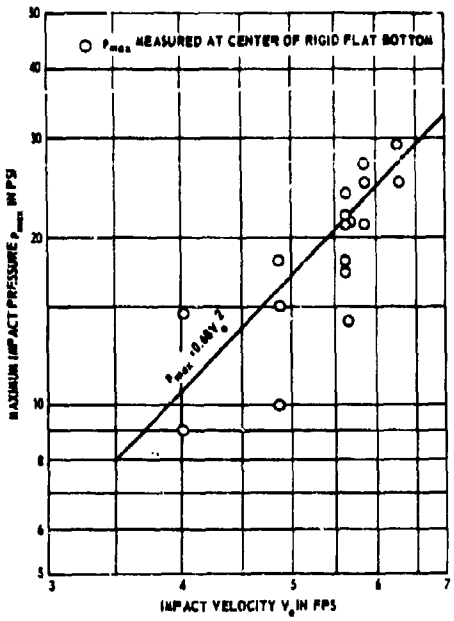

Figure 2 - Experimental Results of Maximum Impact Pressure due to Rigid Flat-Bottom Impact

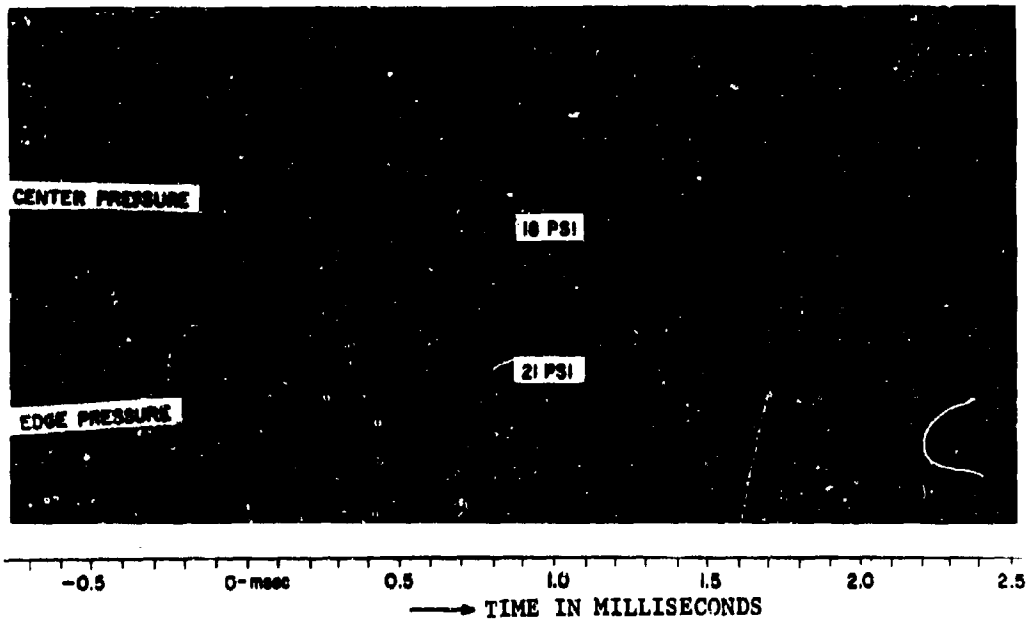

Figure 3 - Sample of Impact Pressure Record for a Test of Rigid Flat-Bottom Model with Initial Drop Height of 6 Inches

2. The acceleration data enable a rough check on the impact pressure reading since the resulting impulse I is measured by the change of momentum produced in the system, i.e.,

$$I = \int_{t_o}^{t} p \, dt$$

$$= M_o (V - V_o)$$

$$= M_o \int_{t_o}^{t} \frac{dV}{dt} dt \qquad [2.2]$$

where M_o is the mass of falling body,

$\int_{t_o}^{t} p \, dt$ is the area of the pressure history curve, and

$\int_{t_o}^{t} \frac{dV}{dt} dt$ is the area of the acceleration history curve.

A typical example is shown in Figure 4. By means of Equation [2.2], the impact pressure checks reasonably well with the measured impact acceleration. This is shown in the last part of Figure 4.

D. TRAPPED-AIR PHENOMENON

If all the air is to be forced out during a flat-bottom drop, it is necessary for the escape velocity of air to become infinite just before impact occurs. Therefore, it appears that some air remains trapped between the water and the plate. The air may deform the water surface and be forced into the water. In any event, this causes the impact pressure to be reduced. Examination of underwater photographs taken during and after impact indicated the presence of bubbles which help to substantiate the assumption that air is forced into the water. The underwater photographs will be presented later in Section III.

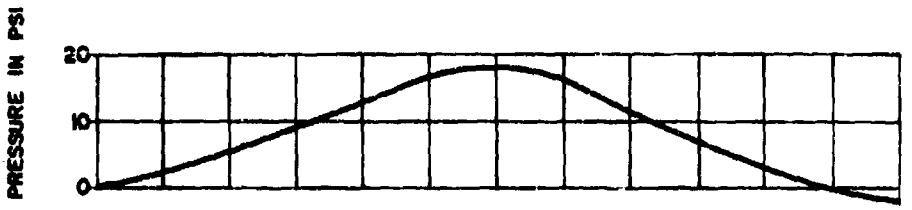

Figure 4a – Impact Pressure History

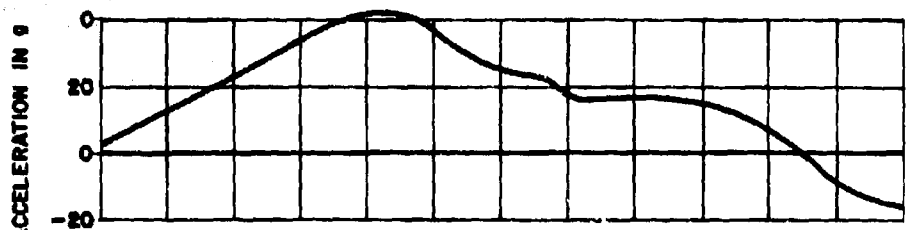

Figure 4b – Impact Acceleration History

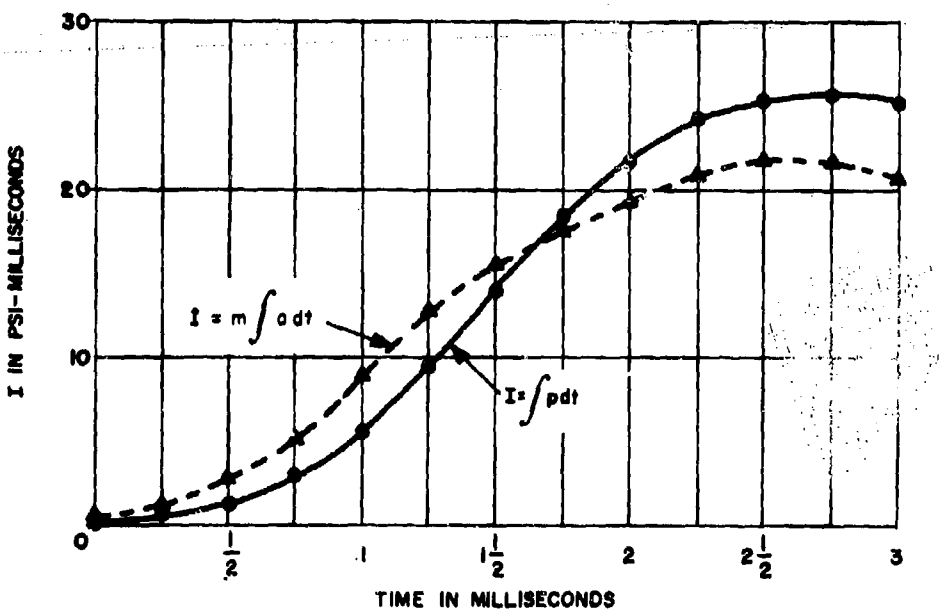

Figure 4c – $\int p\,dt$ versus $m \int a\,dt$

Figure 4 - Comparison of Resulting Impulse and Change of Momentum for a 6-Inch Drop of Rigid Flat-Bottom Model

In addition, the electronic detection method was used in an experimental attempt to detect the air trapped between the falling impact surface of the rigid flat-bottom model and the water surface. Two electrically isolated probes of very thin copper sheet metal were firmly attached to the impact surface of the model. If two probes are not connected by a mass of water, the resistance across them is practically infinite, even if they are independently wet. The output voltage signal equals the input voltage because the probes are electrically isolated from each other at that time. At the instant a mass of water is in contact with the impact surface of the falling body, the two probes are no longer separated electrically, and the electrical resistance between them will be about 3000 ohm depending on the distance between the two probes. At this instant, the output voltage signal will be reduced to a small fraction of the input voltage.

The sample record given as Figure 5 shows the time relationship between the occurrence of the first positive pulse of the impact pressure and the actual contact of water with the impact surface of the flat-bottom body. The trace with a 10-kHz signal is used to indicate whether or not a mass of water is actually in contact with the impact surface of the model. A large 10-kHz signal indicates that a layer of air is trapped between the model and the water surface. A very small 10-kHz signal means that at that moment the water is actually in contact with the impact surface of the model.

The other trace of the record shown in Figure 5 is the time-history curve of the impact pressure measured at the center of the rigid flat-bottom model. The curve indicates the instant of time when the maximum impact pressure occurs. For this particular record, the drop height was 6.5 in. The maximum impact pressure measured from the record was 27 psi, and this point is also included in Figure 2. The maximum pressure occurred about 13 msec before the water came in contact with the impact surface of the flat bottom. In other words, it was only after the first positive pulse of the impact pressure was completely over that the trapped air appeared partly to have escaped and partly to have been pushed into the water surface layer.

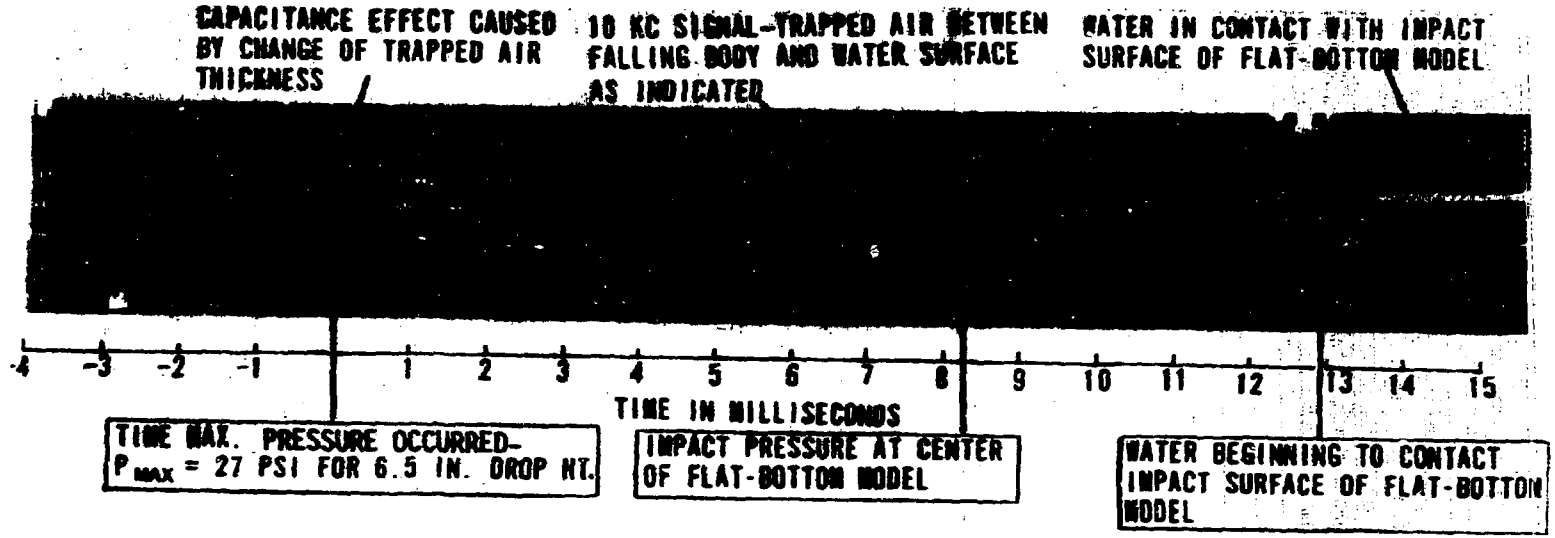

Figure 5 - Sample Record Showing Time Lag between Pulse of Maximum Impact Pressure and Escape of Trapped Air for Rigid Flat-Bottom Impact

From the observations and the analyzed data of the trapped-air detection tests, it is reasonable to conclude that during the impact of a rigid flat-bottom body with the water surface, the first positive pulse of the impact pressure occurs when the air is trapped momentarily between the falling body and the water surface.

E. THEORETICAL INVESTIGATION OF FLAT-BOTTOM IMPACT

Observations made during the two-dimensional rigid flat-bottom impact test indicated that the maximum impact pressure was considerably lower than that calculated from the acoustic theory ($\rho c V_o$). In view of this finding, it seems reasonable to assume that the rise and decay times of the impact pressure are increased greatly by the presence of the air which exists between the falling body and the fluid. These observations led to the formulation of the theory developed in the Appendix.

Figure 6 compares experimental results with the theoretical maximum impact pressure given in the Appendix (Equation [A.16]). The rigid 20- x 26.5-in. flat-bottom data are obtained from Figure 2. The elastic-plate model has a 20- x 26.5-in. flat surface (see Section V). The two UERD (Underwater Explosions Research Division of the Naval Ship Research and Development Center) structural flat-bottom models have 80- : 90-in. flat surfaces and are composed of 1/8-in. shell plating stiffened with keel, floors, longitudinals, and bulkheads to simulate a 1/4-scale ship hull bottom (see Section VI). The UERD 10-deg deadrise ship hull-bottom models have a 2-in. flat surface along the keel (see Section VII). These UERD models were dropped onto salt water. Comparisons between the experimental and the theoretical results generally show agreement.

F. SHORT SUMMARY

To resolve the controversy as to whether the pressure produced by the impact of a flat bottom is an acoustic or a hydrodynamic phenomenon, a test program was conducted with a rigid flat-bottom model. It is concluded that:

1. During rigid-body impact of the flat bottom, the first positive pulse of the impact pressure occurs at the instant when the air is trapped momentarily between the falling body and the fluid.

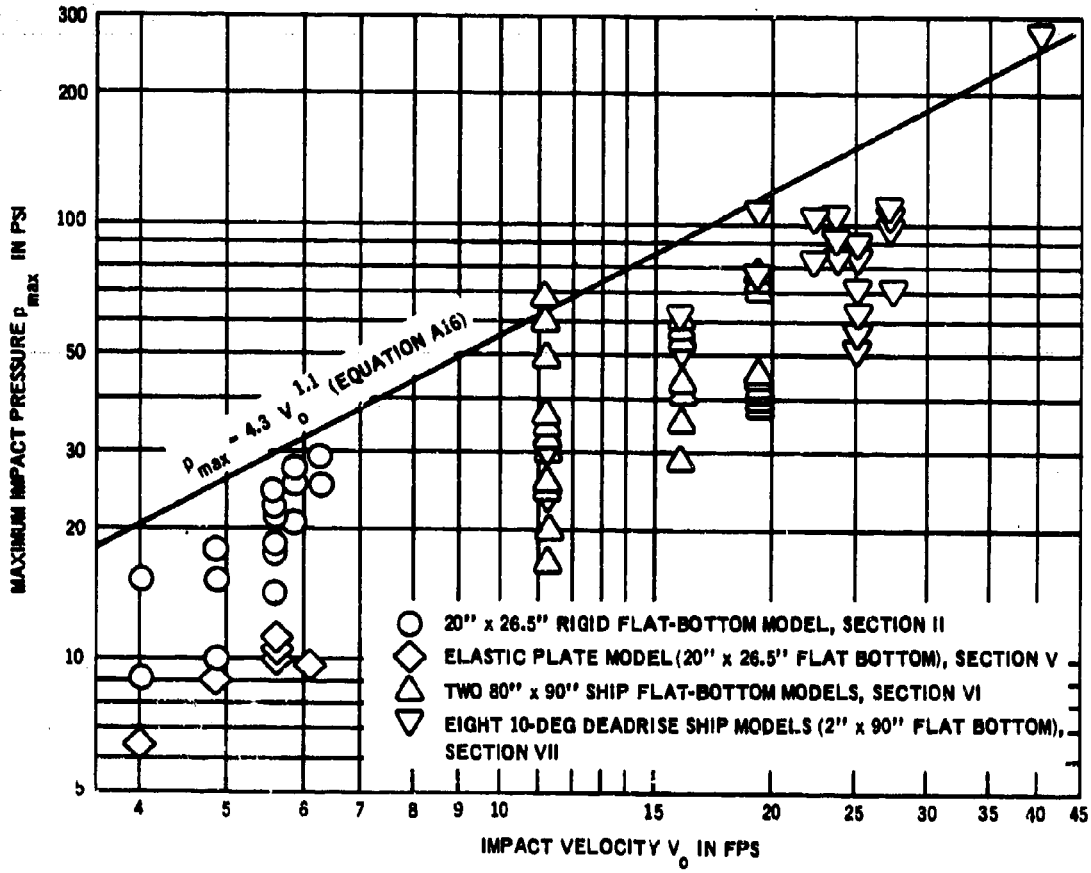

Figure 6 - Comparison of Theoretical and Experimental Flat-Bottom Impact Pressures

2. Test results show that the impact pressure measured at the center of a flat-bottom model is somewhat higher than those measured near the edge of the model but not very much. This is because the existence of trapped air acts as a cushioning medium and causes the impact load to be distributed more evenly over the entire area of the flat bottom.

3. No acoustic pressure $\rho c V_o$ was detected from the test; therefore, water may be considered incompressible.

III. IMPACT OF RIGID WEDGE-SHAPED BODIES WITH SMALL DEADRISE ANGLES

This section attempts to resolve whether the Wagner impact theory is reasonably accurate for determining the pressure on a falling wedge of small deadrise angle. At the beginning of the section, some theoretical background is provided. Then models and tests are described. Since the trapped air has considerable influence on the impact pressure, these effects are examined together with test results. Finally, a short summary is presented at the end of the section.

A. THEORETICAL BACKGROUND ON IMPACT OF RIGID BODIES WITH WATER

When a rigid wedge-shaped body penetrates a water surface, the distribution of the unsteady hydrodynamic impact pressure p acting on the impact surface of the falling body is given by Wagner[9] as

$$p(x) = \frac{1}{2}\rho V^2 \left[\frac{\pi \cot \beta}{\left(1 - \frac{x^2}{L^2}\right)^{\frac{1}{2}}} - \frac{\frac{x^2}{L^2}}{1 - \frac{x^2}{L^2}} \right] + \ddot{z}\,\rho\,(L^2 - x^2)^{\frac{1}{2}} \qquad [3.1]$$

The symbols L, x, z, and β are given in the sketch below.

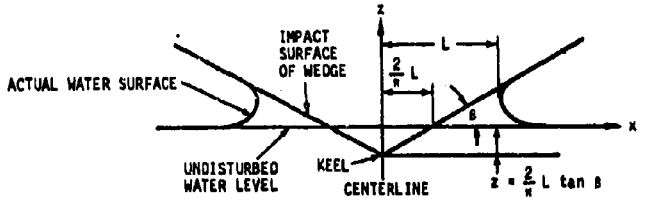

The maximum impact pressure p_{max} is obtained by putting

$$\frac{dp}{dx} = 0$$

and by assuming the acceleration of the falling body $\ddot{z}$ to be negligibly small. This gives

$$p_{max} = \frac{1}{2} \rho V^2 \left[1 + \frac{\pi^2}{4} \cot^2 \beta\right] \qquad [3.2]$$

which occurs at the point where

$$x = L \left[1 - \frac{4 \tan^2 \beta}{\pi^2}\right]^{\frac{1}{2}} \qquad [3.3]$$

Since p_{max} occurs some time t after the instant of impact t_o, V is used in Equation [3.2] since it may not be the impact velocity V_o.

At the keel of the wedge, x = 0. From Equation [3.1], the impact pressure at that point is

$$p_{keel} = \frac{1}{2} \rho V^2 \pi \cot \beta + \ddot{z} \rho L \qquad [3.4]$$

If z can be neglected,

$$p_{keel} = \frac{1}{2} \rho V^2 \pi \cot \beta \qquad [3.5]$$

As derived by Von Karman,[3] the maximum impact pressure occurs at the moment when the keel of the wedge first contacts the water surface, i.e.,

$$p_{keel} = \frac{1}{2} \rho V_o^2 \pi \cot \beta \qquad [3.6]$$

which is identical to Equation [3.5]. However, Equation [3.6] applies only at the instant of impact t_o.

In the case of flat-bottom impact, the deadrise angle β is zero. This means that the impact pressure p is infinitely large if Equations [3.1] to [3.6] are applied. Therefore, these equations cannot be used. Instead, Equation [2.1] of Section II may be used. This equation is based on the experimental evidence that air is trapped between the falling flat-bottom body and the water surface. The trapped air has a great effect on the magnitude of peak impact pressure.

Because the flat-bottom impact causes the air to be trapped, it is quite possible that a certain amount of air is trapped during the impact of a wedge-shaped body with very small deadrise angle β. Accordingly, experiments were performed to confirm this possibility. Wedge-shaped models with deadrise angles varying from 1 to 15 deg were dropped from various heights to establish the effects and relationship of the impact pressure, the deadrise angle, and the trapped-air phenomenon.

B. DESCRIPTION OF MODELS AND TESTS

The wedge-shaped models were essentially similar to the flat-bottom model described in Section II except that the 20-in. side of the test plate of each model was cut into two equal widths, and then the two pieces were welded together to form a V-shaped wedge. There were five models, with respective deadrise angles of 1, 3, 6, 10, and 15 deg. The total drop weight, including the guided sliding beam and other attachments, was 255 lb for each wedge-shaped model. This 255-lb total drop weight is identical to that for the flat-bottom model.

The same test facility, described in Section II and shown in Figure 1, was used for this series of tests. The tests and the instrumentation were identical to those used for the flat-bottom impact tests. The drop height (defined as the distance between the keel of the model and the water surface) also varied from 3 to 7.5 in. at 1.5-in. increments.

C. EFFECT OF DEADRISE ANGLE ON TRAPPED AIR

High-speed, 16-mm underwater movies were taken during the drops of the models to determine how the deadrise angles of the wedges affected the amount of air trapped between the impact surface of the falling body and the water surface. The film speed varied up to about 5000 frames/sec, and all movies were taken at the 6-in. drop height.

These underwater photographs (Figure 7) revealed that only the flat-bottom and the 1-deg-deadrise models trapped a considerable amount of air and pushed some of it into the surface layer of water. Most of the air had not been trapped at the instant of impact by models with deadrise angles of 3 deg and higher. During the impact, the higher the deadrise

Flat-Bottom Model

6 Degree Deadrise Model

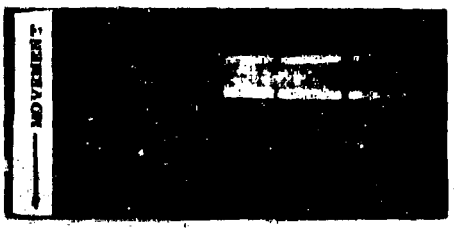

1 Degree Deadrise Model

10 Degree Deadrise Model

3 Degree Deadrise Model

15 Degree Deadrise Model

Figure 7 - Underwater Views Taken during 6-Inch Drop Tests of Rigid Wedge-Shaped Models

angle of the wedge, the clearer and cleaner was the view of the impact surface. Since a 3-deg angle is not much of a deadrise and since the air is trapped for a very short period, the trapped-air phenomenon can be considered to be highly unstable with respect to time duration and the deadrise angle of impact. Thus the test results are sufficient to make a general conclusion, namely, that during the impact of a wedge with a deadrise angle of 3 deg or greater, most of the air is pushed aside by the wedge before the keel pierces the water surface.

D. EFFECT OF DEADRISE ANGLE ON IMPACT PRESSURE

The cushioning effect of the trapped air may play an important role in the impact wedges with small deadrise angles (say 0 deg < $\beta \leq$ 3 deg). Since this effect has been completely ignored in deriving Equations [3.1] to [3.6], models with low deadrise angles were tested to resolve some of the uncertainties in this region.

Sample records, Figure 8, show that the impact-pressure time histories at the keel were quite different from those away from it. The impact pressure at the keel began with a pulse of short duration (less than 0.05 msec) and was followed by the so-called hydrodynamic pressure. The pulse pressure at the keel was not pronounced for the 1-deg model since the impact pressure was affected by the trapped-air cushioning effect; see Figures 7b and 8a. With the exception of the 1-deg model, the impact pressure away from the keel stepped up rapidly with a rise time about 0.1 msec, then died out slowly. The impact-pressure time histories of the 1-deg model closely resemble those of the flat-bottom model (as compared with Figures 3 and 5) with time delay since the pressure was measured farther away from the keel.

The maximum impact pressures at and away from the keel are plotted on the log-log charts shown in Figure 9. The pressure-velocity relations (or pressure-drop height relations) may be obtained empirically from the test data by fitting straight lines on the charts since Equations [3.2], [3.5], and [3.6] may be written in a general form as

$$p = B\, V^n \qquad [3.7]$$

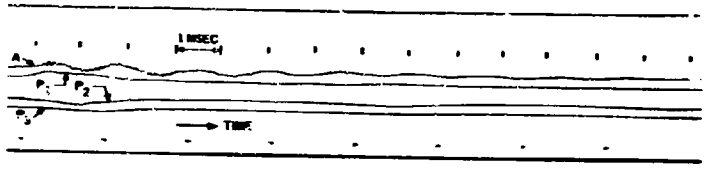

Figure 8a — 1-Degree Deadrise Model

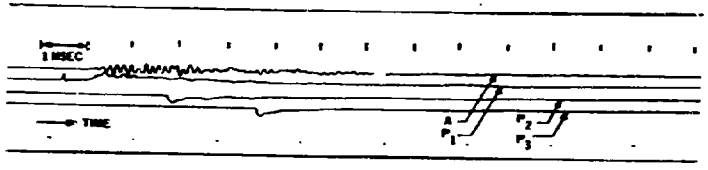

Figure 8b — 3-Degree Deadrise Model

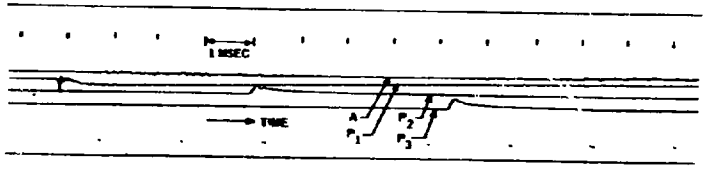

Figure 8c — 6-Degree Deadrise Model

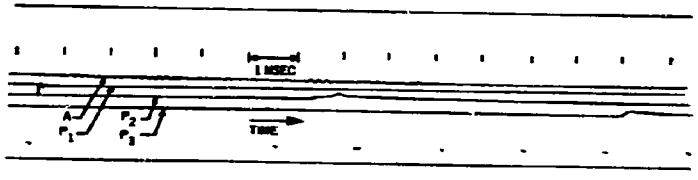

Figure 8d — 10-Degree Deadrise Model

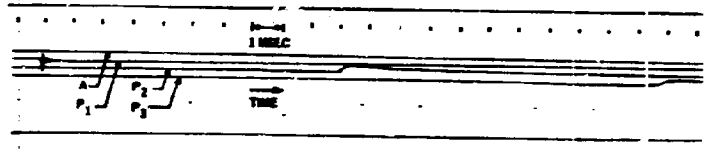

Figure 8e — 15-Degree Deadrise Model

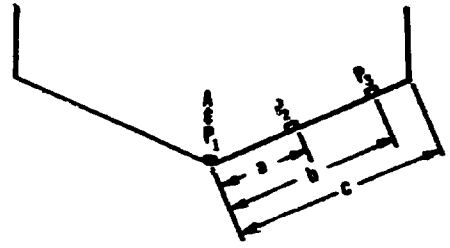

Figure 8f — Gage Locations

MODEL DEADRISE ANGLE, DEG	1	3	6	10	15
RUN NUMBER	86-78	86-80	86-84	86-88	86-100
DIMENSIONS a - b - c IN.	3 29/32 - 7 15/16 - 10	3 29/32 - 7 13/16 - 10	4 - 7 29/32 - 9 31/32	3 7/8 - 7 29/32 - 10	3 29/32 - 7 27/32 - 10 1/32
A - ACCELERATION AT KEEL, G	64 MAX.	135 PEAK/PEAK	11 P/P	1.5 P/P	MIN.
P - MAXIMUM PRESSURE A: KEEL, PSI (-*PULSE/HYDRO)	8/33	13/11.2	15.3/5.5	20.5/3.8	23.4/2.1
P - MAXIMUM PRESSURE b-IN. OFF KEEL, PSI	33	46	36.4	12.8	6.0
P - MAXIMUM PRESSURE b-IN. OFF KEEL, PSI	20	46	25	11.8	5.5

Figure 8 - Sample Records Taken during 6-Inch Drop Tests of Rigid Wedge-Shaped Models

Figure 9 - Experimental Results of Maximum Impact Pressure due to Impact of Rigid Wedge-Shaped Models

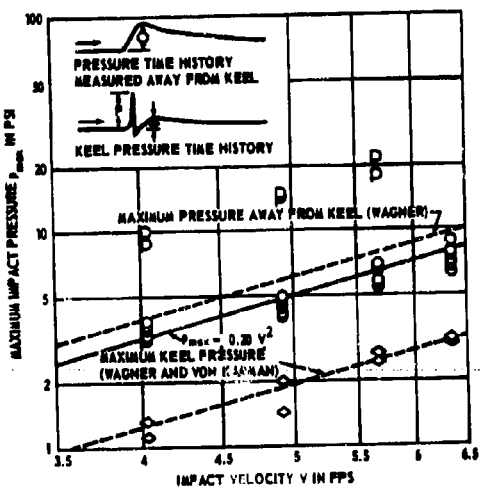

Figure 9a — Model With 15-Degree Deadrise Angle

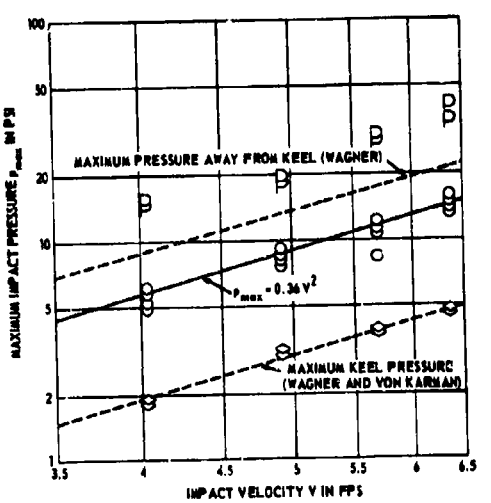

Figure 9b — Model With 10-Degree Deadrise Angle

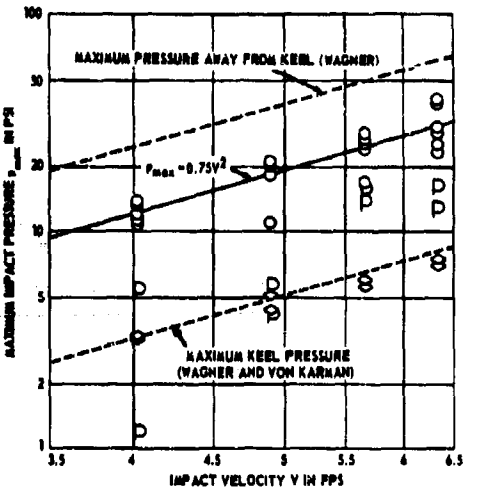

Figure 9c – Model With 6-Degree Deadrise Angle

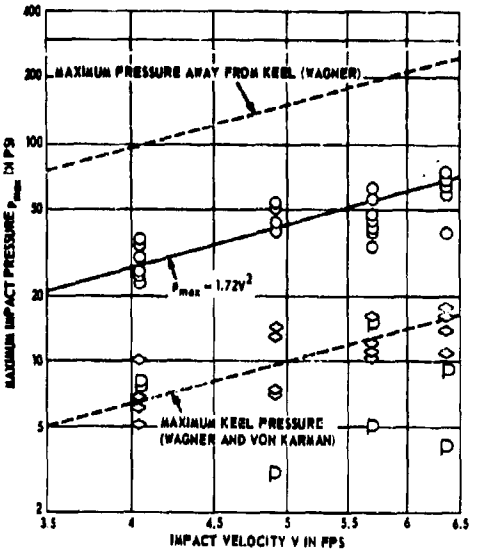

Figure 9d – Model With 3- Degree Deadrise Angle

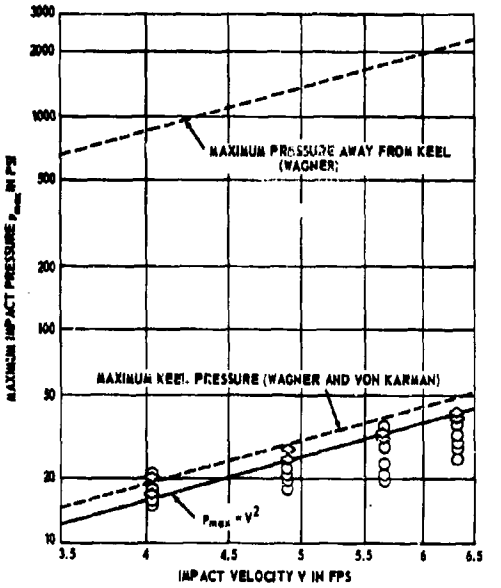

Figure 9e – Model With 1-Degree Deadrise Angle

(Pulse pressure (P) at keel not noted from test records.)

which is a straight line on a log-log chart. B and n are the arbitrary constants and n has limits of $1 \leq n \leq 2$.

The method just described provides equations for estimating the maximum impact pressure of a wedge penetrating a fresh-water surface; they are summarized as follows:

1. Flat bottom - see Figure 2:
   At and away from keel - - - - - $p_{max} = 0.68\ V_o^2$
2. 1-deg deadrise angle - see Figure 9e:
   At keel - - - - - - - - - - - - $p_{keel} = 1.00\ V_o^2$
   Away from keel - - - - - - - - $p_{max} = 1.00\ V^2$
3. 3-deg deadrise angle - see Figure 9d:
   At keel - - - - - - - - - - - - Use Equation [3.5]
   Away from keel - - - - - - - - $p_{max} = 1.72\ V^2$
4. 6-deg deadrise angle - see Figure 9c:
   At keel - - - - - - - - - - - - Use Equation [3.5]
   Away from keel - - - - - - - - $p_{max} = 0.75\ V^2$
5. 10-deg deadrise angle - see Figure 9d:
   At keel - - - - - - - - - - - - Use Equation [3.5]
   Away from keel - - - - - - - - $p_{max} = 0.36\ V^2$
6. 15-deg deadrise angle - see Figure 9a:
   At keel - - - - - - - - - - - - Use Equation [3.5]
   Away from keel - - - - - - - - $p_{max} = 0.20\ V^2$
7. 18-deg deadrise angle and above:
   At keel - - - - - - - - - - - - Use Equation [3.5]
   Away from keel - - - - - - - - Use Equation [3.2]

[3.8]

In the above equation, V and V_o are given in feet per second and p in pounds per square inch. A conversion factor (1/144) is required for using Equations [3.2] and [3.5] if p is in pounds per square inch, ρ in pound-second square per foot fourth power, V and V_o in feet per second, and β in radians. For the sea-water impact problem, a correction factor of $(\rho_{\text{sea water}}/\rho_{\text{fresh water}})$ should be applied for the empirical formulas in Equation [3.8]. Furthermore, note that at the keel, V_o is used in

Equation [3.8] because the maximum impact pressure of the flat bottom and the keel impact pressure of wedge occur at the instant of impact t_o. Away from the keel, however, V is used because there the maximum impact pressure of wedge occurs at some time t after the instant of impact t_o. The relation between V and V_o depends on the deadrise angle of the impact body, the time t, and the drop weight.[13] This relationship has not yet formulated.

Figures 10 and 11 are plotted from Equation [3.8], and Figures 12 and 13 are the cross plots of Figures 10 and 11. Since the pressure gages are located not far off the keels of the models, the relation $V = V_o$ is assumed in applying the equation for the plots.

No formula or plot is formulated for the pulse pressures (marked as P in Figure 9) at the keel because they are scattered. Therefore, further investigations are required.

This completes the investigation of the rigid-body impact from tests of two-dimensional models. However, data available from the test of three-dimensional ship models showed that the impact pressures obtained from the three-dimensional ship models were considerably lower than those obtained from the two-dimensional models. Reasons for this discrepancy have not been determined.[17]

E. SHORT SUMMARY

Several wedge-shaped models with small deadrise angles varying from 0 to 15 deg were dropped from various heights up to 7.5 in. It is concluded from the test that:

1. At the instant of impact, only the flat-bottom and 1-deg wedge trap a considerable amount of air; in contrast, wedges with deadrise angles of 3 deg or higher do not trap very much air.

2. Because of the trapped-air phenomenon, the Wagner hydrodynamic theory does not apply very well for the impact of wedges with small deadrise angle.

3. Because no impact theory is applicable in the region of small deadrise angle of wedge, Equation [3.8] and Figures 10 to 13 were developed for the purpose of estimating the maximum impact pressure of a rigid wedge-shaped body of any deadrise angle from 0 to 45 deg.

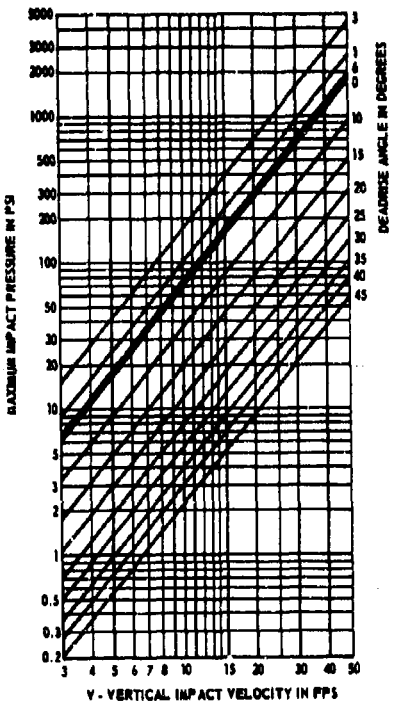

Figure 10 - Maximum Impact Pressure away from Keel due to Rigid- Body Impact of Wedges versus Impact Velocity

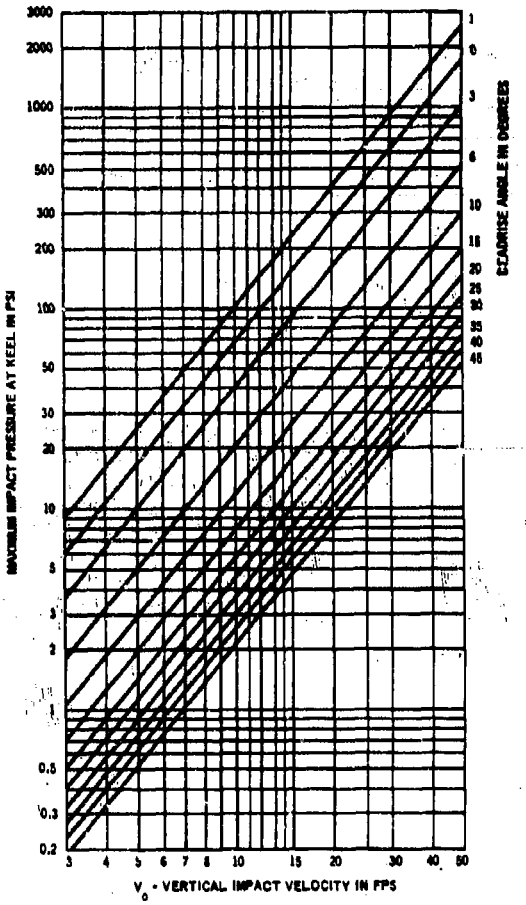

Figure 11 - Maximum Impact Pressure at Keel due to Rigid-Body Impact of Wedges versus Impact Velocity

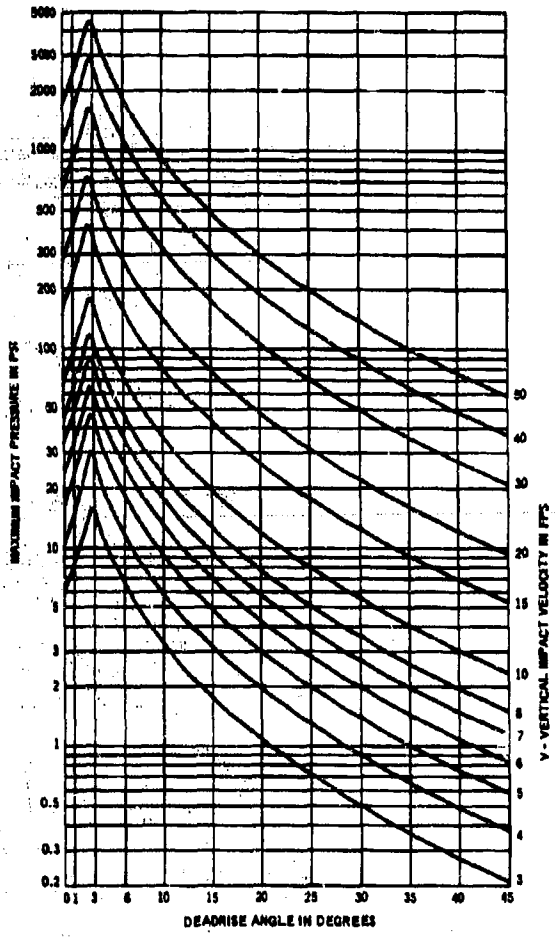

Figure 12 - Maximum Impact Pressure away from Keel due to Rigid-Body Impact of Wedges versus Deadrise Angle of Impact Body

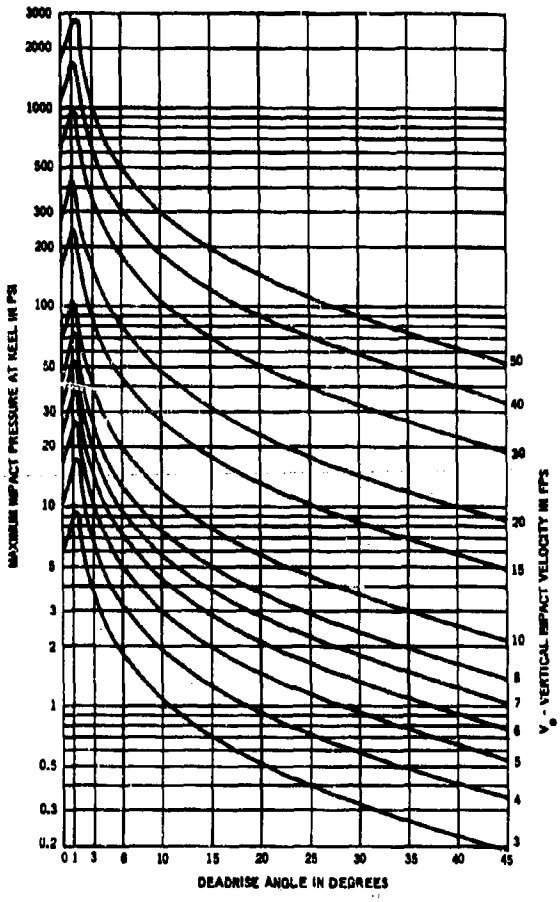

Figure 13 - Maximum Impact Pressure at Keel due to Rigid-Body Impact of Wedges versus Deadrise Angle of Impact Body

IV. IMPACT OF INFLATABLE FABRIC SHIP SECTIONS

This section resolves the question of whether a deformable body affords relief from the load caused by its impact with water. An elastic body is also classified as a deformable body.

The concept is that the impact pressure is related to the movement of the impact region with respect to the sea wave. At the time of impact, if the relative velocity of the shell plating in the impact area can be reduced by deforming instantaneously and locally, then the impact body will feel a smaller impact load. Inflatable fabrics are considered to have this kind of property. They sustain temporary high pressure by deforming locally without transmitting this load through the entire structure, and they will return to their original shape when the load is released.

Airmat, a form of inflatable fabric developed by Goodyear Tire and Rubber Company, appears to be practicable for use in certain parts of weight-critical vehicles or ships. Therefore, Airmat was selected for use in models of a Mariner ship section to investigate the merits of an inflatable fabric as an impact-relief mechanism.

This section presents the theoretical background on dynamic interaction during impact of deformable and elastic bodies with water, describes the models and the tests, and presents and discusses the test results. A short summary is included at the end of the section.

A. THEORETICAL BACKGROUND ON DYNAMIC INTERACTION DURING IMPACT OF DEFORMABLE AND ELASTIC BODIES WITH WATER

Equations have been developed for determining the response of ship bottom to impact loads.[18,19*] Three types of bottom were considered: plate, grillage, and ship hull.

On the basis of the experimental results given in the previous sections, it is reasonable to assume that water is incompressible during the entire period of impact. Let p_t be the total impact pressure

---

*Also by S.L. Chuang as reported informally in NSRDC Technical Note SML 760-89 (Dec 1966).

generated by the deformable body falling upon the water surface. This p_t can be separated into two types of pressure. The first may be called the rigid body impact pressure p_r generated by the impact of a deformable body as if it were held rigid during impact. The second may be called the interacting pressure p_i caused by the interaction between the vibrating surface of the deformable body and the surrounding water with or without a thin layer of trapped air between them.

The interacting pressure p_i may be subdivided into pressures due to the effects of the inertial, the damping, and the spring forces of trapped air and water. However, the effects of these forces of trapped air are small compared with those of water and can be neglected. Therefore,

$$\begin{aligned} p_t &= p_r + p_i \\ &= p_r - (m_{zz}\ddot{w} + c_{zz}\dot{w} + k_{zz}w) \end{aligned} \qquad [4.1]$$

The negative sign is used at the right side of the equation because the interacting pressure is always acting against the movement of the impact surface.

When an isotropic plate is subjected to any type of external dynamic load, the general expression of the motion of the plate is[18]

$$m_s\ddot{w} + c_p\dot{w} + D\,\nabla^4 w = p_t$$

Combine this equation with Equation [4.1], neglect k_{zz} because it is small, and set $c_v = c_p + c_{zz}$. This yields

$$(m_s + m_{zz})\ddot{w} + c_v\dot{w} + D\,\nabla^4 w = p_r \qquad [4.2]$$

Similarly, the equation for the grillage is

$$(m_s+m_{zz})\ddot{w} + c_v\dot{w} + \left[D_x \frac{\partial^4}{\partial x_1^4} + 2H \frac{\partial^4}{\partial x_1^2 \partial y_1^2} + D_y \frac{\partial^4}{\partial y_1^4}\right] w = p_r \qquad [4.3]$$

In Equations [4.1] to [4.3], $w = w(x_1,y_1,t)$ and $p = p(x_1,y_1,t)$.

In some cases, the fundamental mode which causes the largest deflection of ship bottom predominates. For that reason, the ship bottom

may be considered as a system with a single degree of freedom. By neglecting the damping term $c_v \dot{w}$, we may correct Equations [4.2] and [4.3] to

$$\left.\begin{aligned} (m_s + m_{zz})\,\ddot{w}(t) + k\,w(t) &= p(t) \\ \text{or} \qquad \ddot{w}(t) + \omega^2\,w(t) &= q \cdot f(t) \end{aligned}\right\} \qquad [4.4]$$

where $\omega^2 = \dfrac{k}{(m_s + m_{zz})}$

$$p(t) = P \cdot f(t)$$

$$q = \frac{P}{(m_s + m_{zz})}$$

Here P is a force that will cause a static deflection of a single degree of freedom system exactly equal to the static deflection at the center of the structure, caused by the application of the maximum pressure p_{max} to the structure.

The solution for Equation [4.4] is

$$\left.\begin{aligned} w(t) &= w_{st}\,D_1(t) \\ D_1(t) &= \omega \int_{t_o}^{t} f(\tau)\,\sin \omega(t - \tau)\,d\tau \end{aligned}\right\} \qquad [4.5]$$

Here τ is the dummy variable for time t, w_{st} denotes the maximum deflection of the structure as though it were loaded statically by the maximum load, and ω is the circular frequency depending on the boundary conditions of the structure. For the fundamental mode, ω may be approximated with reasonable accuracy by the Warburton method for the plate[20] and the grillage.[21]

Caution is necessary when using this approximation method because the stress produced in the structure by its own vibration does not always occur at the fundamental mode for all boundary conditions. Thus good engineering judgment and careful evaluation are required in solving this type of problem.

Equations [4.2] and [4.3] are basically used to solve the dynamic response of the structure in its elastic region. However, they can be applied equally well for the structure with backing material and for the structural response in its elastoplastic region.

Since the backing material functions as added mass and damping, the first two terms of Equations [4.2] and [4.3] have to be modified, and these two equations become

$$(m_s + m_{zz} + m_b)\ddot{w} + (c_v + c_b)\dot{w} + D\,\nabla^4 w = p_r \qquad [4.4]$$

for the plate response and

$$(m_s + m_{zz} + m_b)\ddot{w} + (c_v + c_b)\dot{w} + \left[D_x \frac{\partial^4}{\partial x_1^4} + 2H \frac{\partial^4}{\partial x_1^2\,\partial y_1^2} + D_y \frac{\partial^4}{\partial y_1^4}\right] w = p_r \qquad [4.5]$$

for the grillage response.

The third term of Equations [4.2] and [4.3] has to be modified for the dynamic response of a structure in its elastoplastic region. These two equations may be written as

$$(m_s + m_{zz})\ddot{w} + c_v\dot{w} + k[w]_{\substack{\text{corrected for} \\ \text{plastic flow}}} = p_r \qquad [4.6]$$

The method of calculating k in the above equation was shown in Reference 18 and is illustrated in Section IV.

B. DESCRIPTION OF MODELS AND TESTS

Two inflatable models were used for the test; one was a single-wall Airmat and the other a dual-wall Airmat. Both models were pressurized to have the same outside configuration and to represent a 1 to 20 scale of a Mariner ship section at 17.5 percent of the ship length aft of the forward perpendicular. They had a constant cross section and were 26.5 in. long, with a maximum beam of 34.4 in. and a height of 29.62 in. (see Figure 14). Each model was fitted with removable aluminum bulkheads at the ends and an aluminum plate at the top.

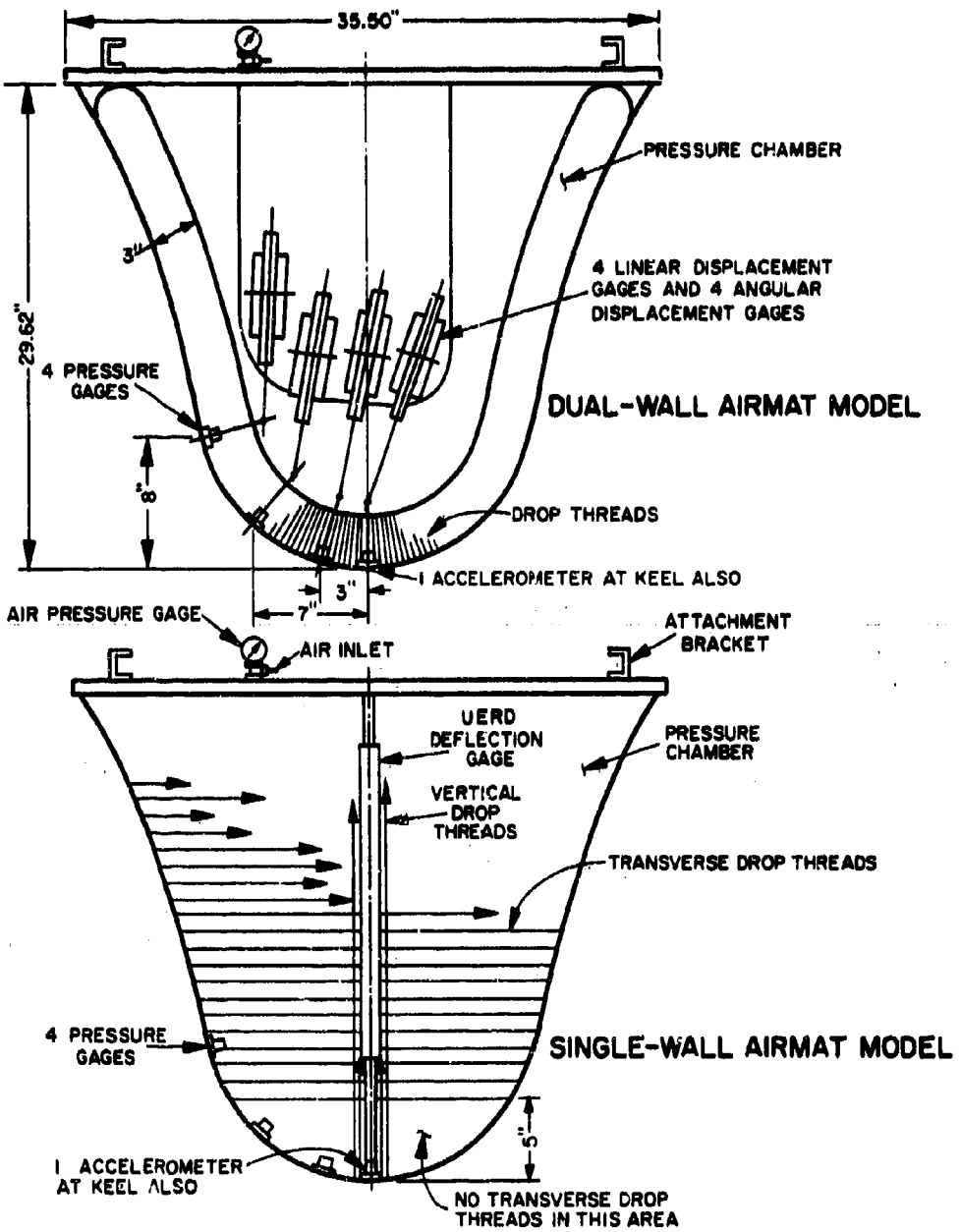

Figure 14 - Mariner Hull Inflatable Models

The facility used for the series of tests has been described in Section II and shown in Figure 1. The impact test consisted essentially of dropping the models vertically from various elevated positions and recording impact pressures, accelerations, and deformations of the model. The drop heights (defined as the distance between the keel of the model and the water surface) also varied from 3 to 7.5 in. in increments of 1.5 in. Both models were tested with and without the rigid bulkheads at the ends of models. The total drop weight varied from 197 to 400 lb, and the internal air pressure varied from 3 to 12 psi. For quick reference, the test schedule is listed in Table 1.

C. COMPARISON OF KEEL IMPACT PRESSURE ON RIGID BODY AND ON INFLATABLE DEFORMABLE BODY

Samples of records of the different models are shown in Figure 15. These records were obtained from tests using a drop height of 6 in. and a total drop weight of 300 lb. Both the single-wall and the dual-wall inflatable models had 3-psi pressure in the Airmat and were tested with and without the rigid bulkheads at the ends. The cross section of the rigid-body model was, of course, identical to that of the inflatable models.[13] The rigid-body model was fitted with the same type of pressure gage at the keel and was tested under the same drop conditions.

Although the external configurations of the models were identical, the records show that the differences in their internal construction, surface rigidity, internal air pressure, and material resulted in three different pressure-time histories, one for each type of construction. The rigid-body model had the highest pressure at the instant of impact, then the pressure died down quickly (within about 0.04 sec). The single- and dual-wall models, with and without rigid bulkheads, had much lower pressures at the instant of impact.

The reason why the maximum impact pressures of the inflatable models were less than that of the rigid-body model has been explained in the previous section (Section IV-A), namely because the impact pressure p_t of the inflatable model is a combination of the rigid-body impact pressure p_r and the interacting pressure p_i (where p_i is the relief pressure due to

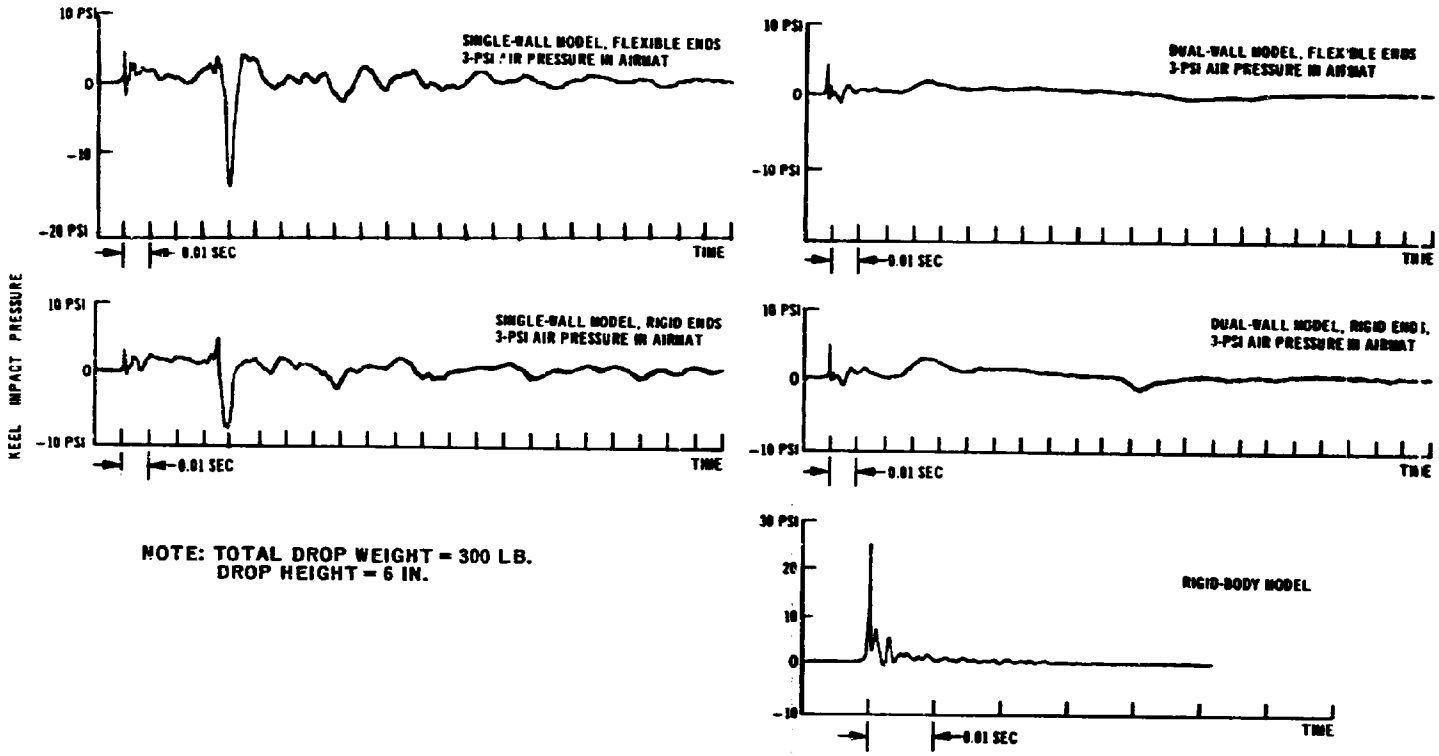

NOTE: TOTAL DROP WEIGHT = 300 LB.
DROP HEIGHT = 6 IN.

Figure 15 - Keel Impact Pressure of Inflatable and Rigid-Body Results

TABLE 1

Drop Test Schedule of Inflatable Airmat Models

Type of Airmat Model	Drop Height* in.	End Condition	Total Drop Weight lb	Chamber Air Pressure psi
Single Wall	3.0	With Rigid Bulkheads	197**	3
	4.5		223	6
	6.0	Without Rigid Bulkheads	300	9
	7.5		400	
Dual Wall	3.0	With Rigid Bulkheads	223	3
	4.5		300	6
	6.0	Without Rigid Bulkheads	400	9
	7.5			12

*Drop height is defined as the distance from the keel of the model to the water surface when the model is ready for the drop test.

The free-fall impact velocities for the drop heights used are:
4.01 fps for 3.0-in. drop height,
4.92 fps for 4.5-in. drop height,
5.68 fps for 6.0-in. drop height, and
6.34 fps for 7.5-in. drop height.

**Represents scaled weight of ship at 45-percent load.

surface movement at the point considered). However, because of the slow recorder speed, the recorded pressure time histories showed only a line of pulse at the instant of impact (see Figure 15) and it was not possible to analyze and compare the test record with the interaction theory given in Section IV-A; see also footnote to page 29.

The pressure-time history of the single-wall model was quite different from that of the dual-wall model. Because of fluid inertia and elastic overshoot, the pressure time history of the single-wall model showed a sudden drop in pressure about 0.04 sec after impact, and then oscillated for some time before it died out. The dual-wall model did not exhibit this phenomenon.

D. OTHER FINDINGS

Based on the experimental study performed for this series of tests, several other findings are listed below:

1. The air pressure in the Airmat of the models varies very little during impact. When the Airmat deforms during impact, the change in volume is so slight that the air pressure in the Airmat can be considered as constant.

2. Most of the data show that the maximum impact pressures at the keel are independent of drop weight. When the Airmat air pressure is low, i.e., 3 psi, model weight has some influence, but this is not very pronounced.

3. The Airmat air pressures have some influence on the maximum impact pressure at the keel, but they are not obviously indicated.

4. If the drop conditions are identical for both inflatable models, the deflection at the keel for the single-wall model is much less than that for the dual-wall model. When the air pressure in the Airmat is 3 psi, the keel deflection of the dual-wall model is definitely influenced by the various total drop weights.

5. The shape of piled-up water surface of the free falling models depends only on the degree of immersion during the drop. It is independent of impact velocity, total drop weight, air pressure in the Airmat, and the internal construction of the model. The ratio of the wetted width associated with the piled-up water surface to the width of the still waterline of the model is about 1.20. This value is about the same for the rigid-body model.[12]

E. SHORT SUMMARY

Two inflatable models of a Mariner ship section were dropped from various heights up to 7.5 in. It is concluded from the test that:

1. The impact pressure for the inflatable-fabric hull are considerably lower than those for the rigid-body hull. This is attributed to the fact that a deformable body affords relief from the impact load.

2. The maximum impact pressures are independent of drop weight for this case. However, this cannot be shown conclusively for all the cases.

V. IMPACT OF RECTANGULAR ELASTIC PLATE WITH TWO OPPOSITE EDGES HINGED AND TWO OTHER EDGES FREE

This section attempts to demonstrate that the structural response caused by the impact of a ship bottom with water can be treated as the elastic-body impact on an incompressible fluid, with trapped air. If this is so, it means that the hydroelastic vibration theory can be applied in solving the ship bottom impact problem.

In this section, the elastic response of the plate model is presented, and experimental results are discussed. But first, descriptions of model and tests are given. Because the trapped air has considerable effect on the impact pressure and plate response, tests to detect the presence of trapped air are presented next. Since the dynamic response of the plate is essentially a vibration problem, impedance tests to determine the plate vibratory frequencies and modes are also presented. Finally, the effect of damping is analyzed from drop tests of the plate model, and the interaction theory and the test results are compared. At the end of the section, a short summary is presented.

A. DESCRIPTION OF MODEL AND TESTS

One rectangular steel plate model was used for the study. The plate was 1/4 in. thick and was made of HY-80 steel with a yield stress of 80 ksi and a modulus of elasticity of $30(10)^6$ psi. The model was designed to simulate a rectangular isotropic plate with two opposite edges hinged and the other two edges free. Each hinged edge was 26 3/8 in. long and each free edge was 15 3/4 in. long (measured between centers of two hinges). Hinges were designed to provide the free lateral but not vertical movement of the plate at hinges. The plate was hinged to the relatively rigid frame of a steel box which had overall dimensions identical to the steel box of the rigid flat-bottom model shown in Figure 1. The gaps between the plate and the box were sealed with a thin piece of latex so that the box was watertight and yet provided flexibility to the free edges of the test plate. The combined weight of the steel box and the test plate was 290 lb, and the total drop weight for the test, including guide beam and hardware, was 333 lb.

The test facility described in Section II and shown in Figure 1 was used for this series of tests. The tests and the instrumentation were identical to those used for the flat-bottom impact tests.

Two Kistler Model 603 pressure gages were installed, one at the center of the plate model and the other on the rigid frame of the steel box, 1 in. inside the edge and at the middle of the longer edge of the box.

Two accelerometers, Endevco Model 2225, were used. One of the gages was used to measure the acceleration of the rigid frame of the steel box, and the other was located near the center of the plate model.

A linear potentiometer, Bourn Model 108, was used to measure the deflection of the plate model near its center. Although the gage was not rated for measuring the high-frequency dynamic response, the deflection records showed that data obtained were within reasonable accuracy.

B. DETECTION OF TRAPPED AIR

The method used to detect the trapped air between surfaces at impact of the plate model and the water was identical to that presented in Section II-D. Figure 16 is a typical record for measuring the time lag between the occurrence of the first positive pulse of the impact pressure and the actual contact of the elastic plate with the water surface.

As shown in the figure, a trace with a 10-kHz signal was used to indicate whether or not a mass of water was actually in contact with the impact surface of the plate model. (A large 10-kHz signal indicates the existence of a layer of trapped air between the plate model and the water surface. A 10-kHz signal with very small amplitude indicates that the water is actually in contact with the impact surface of the plate model.)

The other three traces in Figure 16 are the two time histories of the impact pressure (one measured at the center of the plate and one at the rigid frame of the steel box) and the time history of the transverse acceleration measured near the center of the plate.

It can be seen from the record that the water begins to contact the impact surface when the first positive pulse of the impact pressure tends to diminish. The acceleration of the plate damps out immediately after the water is completely in contact with the impact surface of the falling body.

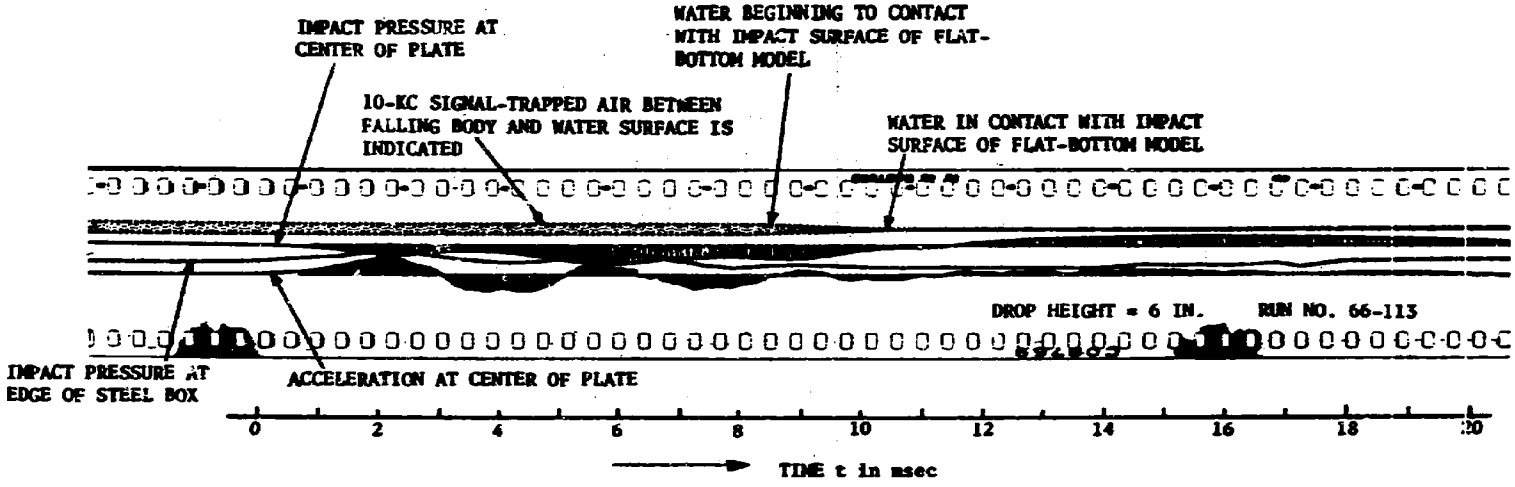

Figure 16 - A Typical Record to Show Time Relationship between the Occurrence of Maximum Impact Pressure and the Presence of Water in Contact with Impact Surface of Plate

A detailed evaluation of the record will be presented and discussed later. At present, it is reasonable to believe that during the impact of the elastic plate, the first positive pulse of the impact pressure occurs when the air is momentarily trapped between the falling body and the water. However, when this record is compared with that from the tests for rigid flat-bottom impact shown in Figure 5, it is obvious that the plate stiffness and boundary conditions affect the time required for the trapped air to escape.

C. MECHANICAL IMPEDANCE TEST

Prior to the drop test, the plate model was excited in air to determine its resonant frequencies by measuring the mechanical impedance (defined as the ratio of the driving force acting on a system to the resulting velocity of the system) of the plate. Since the test is conducted by attaching an impedance head to the point of concern which is at the center of the rectangular plate, the ratio of force to velocity at the point is the mechanical driving point impedance Z, i.e.,

$$Z = \frac{F}{V} \qquad [5.1]$$

where F is the applied force normal to the plate surface and V is the resultant velocity in the direction of the force.

If a plate vibrates at one of its resonant frequencies, a small amount of force will make the plate vibrate with large transverse displacement, producing higher transverse velocity of the plate than if the plate were vibrating at other than its resonance. This means that the impedance of the plate is lower at its resonant points than at other points. Thus as shown in Figure 17, the first five resonant frequencies of the plate tested are 102, 203, 530, 850, and 1100 Hz. These frequencies correspond to the first five even modes of the plate with the boundary conditions shown in Figure 18.

The mode frequencies may be determined by the Warburton method, which is explained in References 18 and 20. Using this method, the first even modes for the plate in air are calculated to be $f_{0/2}$ = 97 Hz, $f_{2/2}$ = 203 Hz, $f_{4/2}$ = 546 Hz, $f_{0/4}$ = 873 Hz, and $f_{6/2}$ = 1164 Hz. The ratio

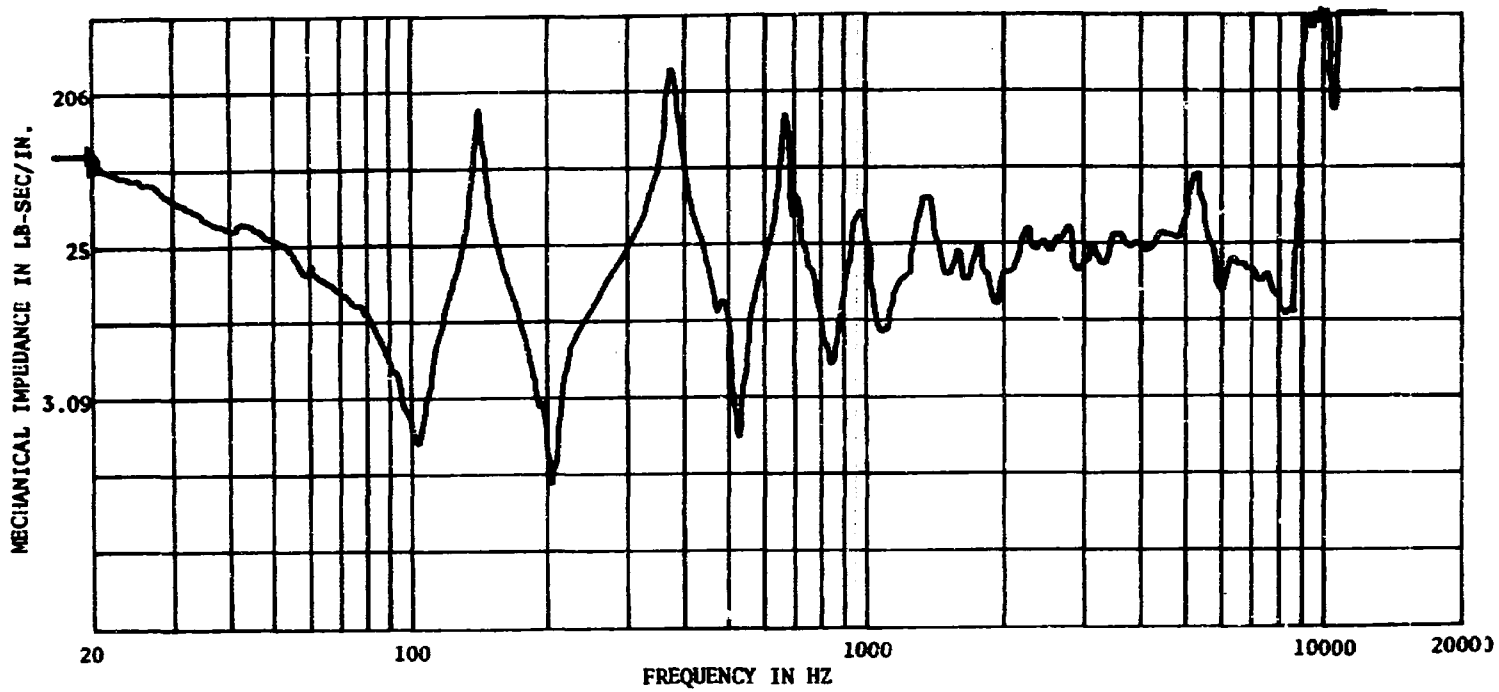

Figure 17 - A Sample of Record Obtained from Impedance Test of a Plate in Air

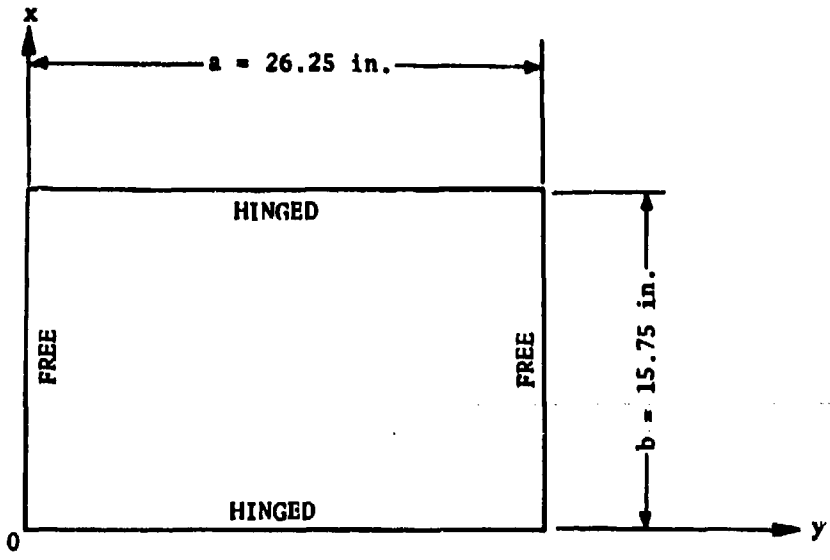

h = PLATE THICKNESS = 0.25 in.

Figure 18 - Dimensions and Boundary Conditions of the Rectangular Plate Model

among them is therefore 1 : 2.09 : 5.64 : 9 : 12. These values check with frequencies obtained from the impedance test within 6 percent. The first three even mode shapes ($f_{0/2}$, $f_{2/2}$, and $f_{4/2}$) are given in Figure 19.

The resonant frequencies of a plate with one side in contact with water and the other side in air have not been determined by the impedance test. They may be calculated from the concept of added mass of fluid by including the added mass m_{zz} with the mass of the plate ($\rho_p h$) in the frequency equation (Equation [C42] of Reference 18). Using the equation of added mass for flat bottom, $m_{zz} = \rho L^2 \pi/2$, with the frequency equation of Reference 18, the fundamental frequency of the plate model is calculated to be $f_{0/2} = 47.4$ Hz. The fundamental frequency of the plate model in water was found experimentally to be about 50 Hz; see Figure 20.

D. EFFECT OF DAMPING ON STRUCTURAL RESPONSE

A time trace of the plate deflection is shown in Figure 20. Note that the motion is damped out rapidly. Therefore, the effect of damping on the response must be investigated.

The damped frequency equals the undamped frequency times a damping factor

$$\sqrt{1 - \left[\frac{c_v}{c_c}\right]^2}$$

where c_v is the viscous damping coefficient and c_c is the critical damping coefficient. If c_v/c_c is small, damping has very little effect on the frequency response. The c_v/c_c can be calculated from Figure 20 (or Figure 21, which is a duplicate of Figure 20 with time extended) by using the relation of logarithmic decrement δ, namely

$$\delta = \frac{2\pi \frac{c_v}{c_c}}{\sqrt{1 - \left(\frac{c_v}{c_c}\right)^2}} = \frac{1}{q} \ln \frac{A_n}{A_{n+q}} \qquad [5.2]$$

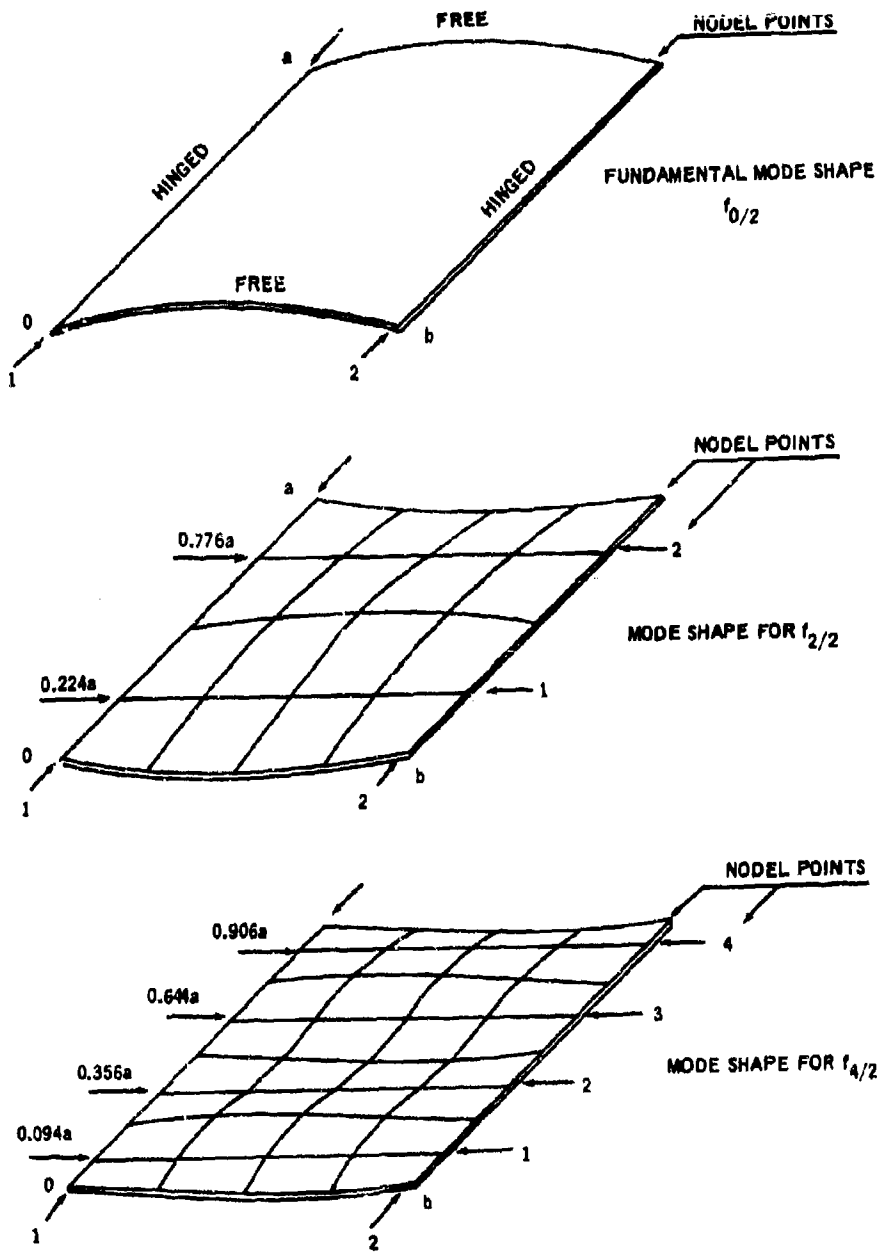

Figure 19 - First Three Even Mode Shapes of a Rectangular Plate with Two Opposite Edges Hinged and Two Others Free

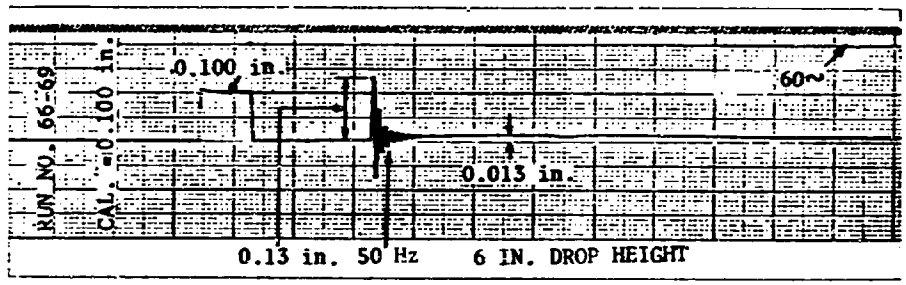

Figure 20 - Sample of Deflection Record Obtained by Sanborn Recorder during 6-Inch Drop Test of Elastic Plate Model

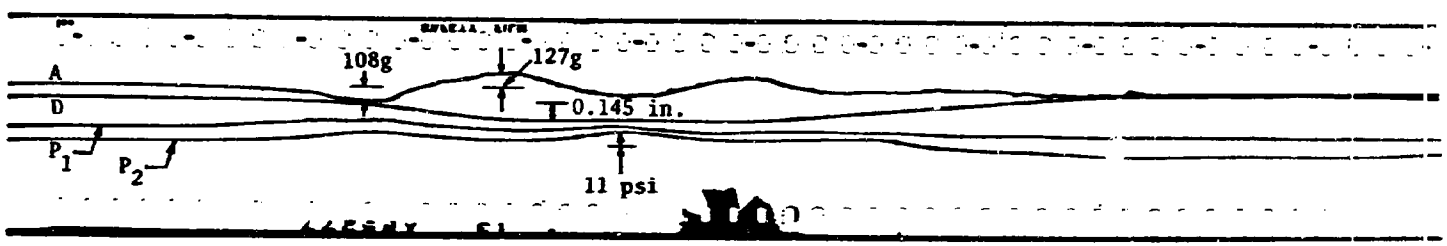

A - Acceleration at center of plate

D - Deflection at center of plate

P_1 - Impact pressure at rigid frame

P_2 - Impact pressure at center of plate

Figure 21 - Sample Record from 6-Inch Drop Test of Elastic Plate Model

This calculation produces a c_v/c_c of 0.057, which results in a damped frequency within 0.2 percent of the undamped frequency. Therefore, damping can be neglected in structural response for the usual ship bottom plating.

This is considered an important finding for although the fluid damping coefficients for ship bottom impact are generally low, they are usually not known precisely.

E. COMPARISONS OF INTERACTION THEORY AND TEST RESULTS

Data representing a typical drop test (see Figure 21) were chosen to compare the interaction theory given in Section IV-A with the test results. Figure 22 presents the complete time histories of the impact pressure $p_1(t)$ measured at the rigid frame of the steel box, the impact pressure $p_2(t)$ measured at the center of the plate, and the deflection $w(t)$ and acceleration $\ddot{w}(t)$ measured near the center of the plate model. The first few cycles of these data, except $p_1(t)$, are also plotted in Figure 23 for comparison.

The deflection time history $w(t)$ can be calculated by integrating acceleration time history $\ddot{w}(t)$ twice; the impact pressure time history $p_t(t)$ can be calculated from the acceleration history $\ddot{w}(t)$, the velocity time history $\dot{w}(t)$, and the deflection time history $w(t)$ as shown in Figure 23. The calculated and the recorded values of the deflection and the pressure for the first positive pulse of time histories are compared in the figure to confirm the accuracy of the recorded test results. Since the comparisons are good, the data are considered sufficiently accurate to use in the comparison with theory.

The equation of motion of the isotropic plate with interaction is given in Section IV-A by the equation

$$(m_s + m_{zz})\ddot{w} + c_v\dot{w} + D\,\nabla^4 w = p_r \qquad [4.2]$$

with $m_s = \rho_p h$, $w = w(x_1, y_1, t)$, and $p_r = p_r(x_1, y_1, t)$. For flat-bottom impact, except near its edge, Equations [A.8] of the Appendix and [2.1] of Section II apply, i.e.,

$$p(t) = 2\,p_{max}\,e^{-1.4\,\frac{t}{T}}\sin \pi \frac{t}{T} \qquad [A.8]$$

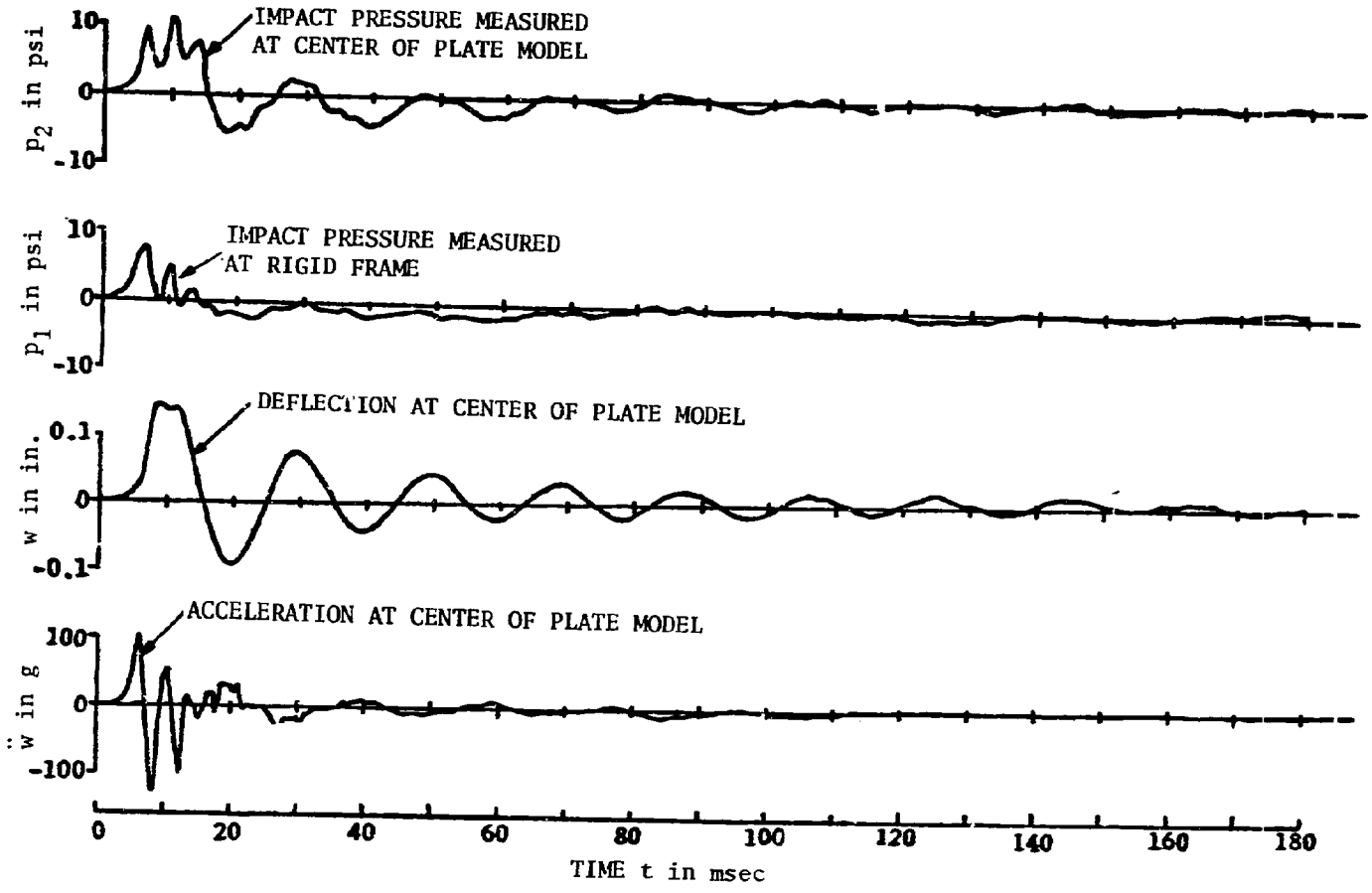

Figure 22 - Reduced Records of Figure 21

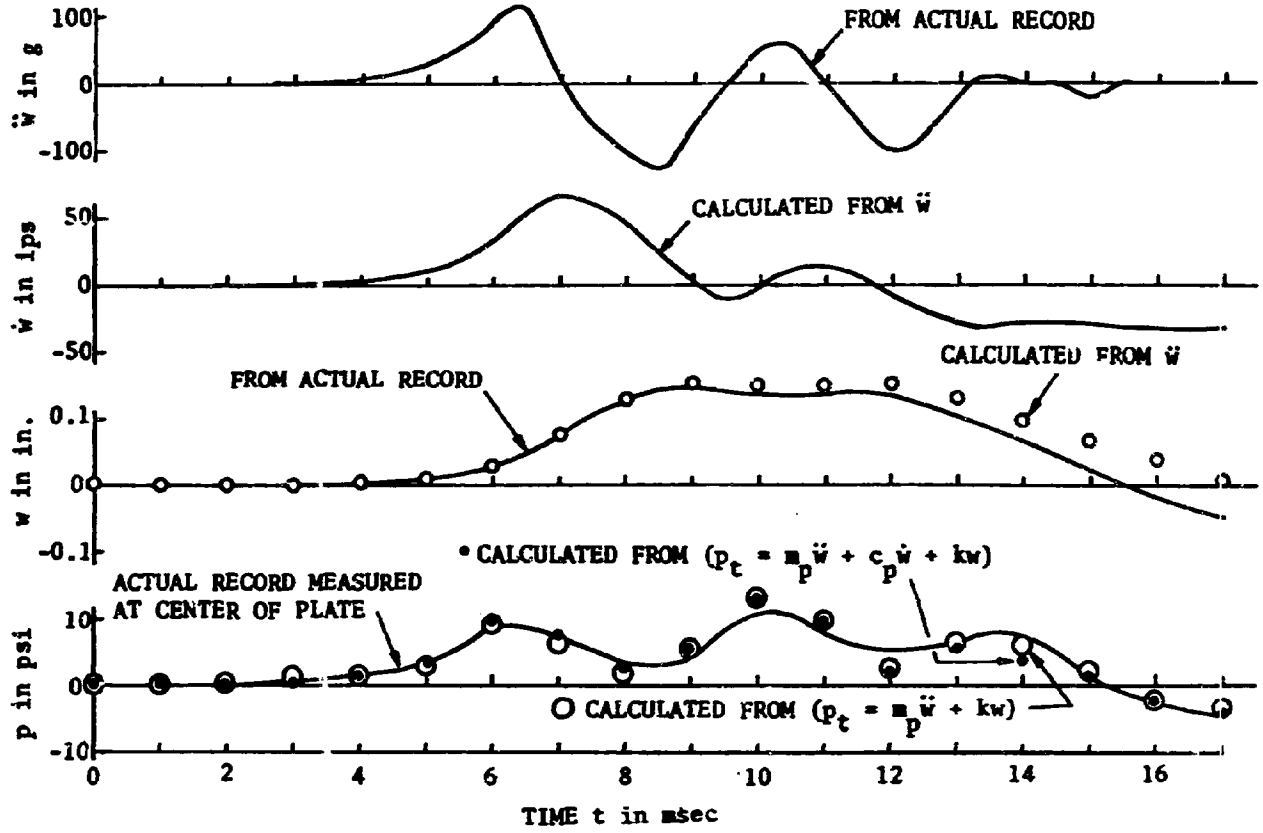

Figure 23 - Comparisons of Calculated and Recorded Values of Pressure and Deflection Time Histories

and

$$p_{max} = 0.68\ V_o^2 \qquad [2.1]$$

with $p(t) = p_r(x_1, y_1, t)$.

The solutions of Equation [4.2] may be obtained by using a set of appropriate boundary conditions, such as illustrated in Appendix C of Reference 18. Since only the deflection at the center of the plate was obtained from the drop test, the complete solutions of these equations are unnecessary. Instead, the following method of approximation is adopted for the spot checks between theory and the test results.

Experiments showed that the fundamental mode dominates the motion of the plate, and thus the first approximation for the problem is to consider it as an infinitely long two-dimensional plate. This assumption is made because boundary conditions of the plate include two opposite edges hinged and two other edges free. However, this may not be a legitimate assumption for the plate with other boundary conditions.

In Equation [4.2], w is then a function of x_1 and t only. The impact problem of the two-dimensional plate for Equation [4.2] with and without damping has been worked out by using a computer program similar to that given in Appendix A of Reference 18. The computer results for a 6-in. drop height (which corresponds to the height used in a typical test of Figure 21) are plotted in Figure 24. In solving the computer program, p_{max} is assumed to be 20 psi, which is the average rigid flat-bottom impact pressure given by Figure 2; ω is 330 rad/sec, determined from the actual test record shown in Figure 21.

The actual test results are also plotted in Figure 24; as shown, the maximum deflection from the test (0.145 in.) compares favorably with the computer results of 0.148 in. for damped or 0.158 in. for undamped. The computer results also indicate that the maximum dynamic load factors (max $D_1(t)$) for the fundamental mode are:

$$\text{Max } D_1(t) = 0.391 \text{ damped}$$
$$= 0.422 \text{ undamped}$$

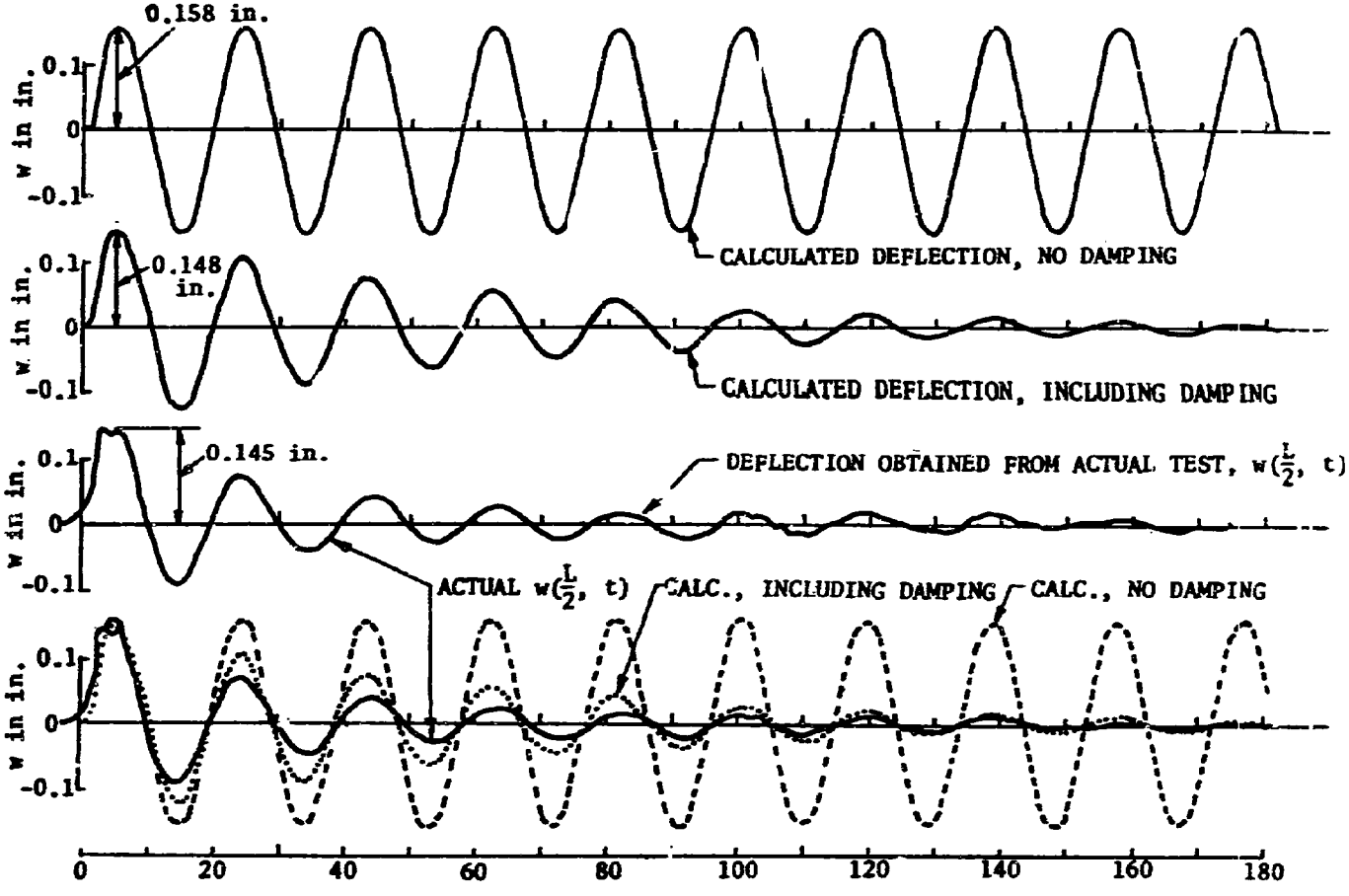

Figure 24 - Comparisons of Recorded Deflection Time History and Computer Calculated Fundamental Mode of Plate Deflection

For the problem of the two-dimensional plate, the computer results also showed that only the deflection due to the fundamental mode frequency $f_{0/2}$ is needed to evaluate an infinitely long hinged plate. The deflection caused by higher mode frequencies ($f_{0/4}$, $f_{0/6}$, ...) is very small and may be neglected without introducing noticeable error.

Examination of the test records indicates that only the first positive pulse of the deflection time history $w(\ell,t)$ was affected by the higher mode frequencies. As shown in Figure 19, these higher mode frequencies, $f_{2/2}$ and $f_{4/2}$, are excited in the orthogonal direction with the fundamental mode frequency $f_{0/2}$. If corrections for the higher mode frequencies are necessary, the following approach may be used. Since the ratio for the first five even mode frequencies is

$$f_{0/2} : f_{2/2} : f_{4/2} : f_{0/4} : f_{6/2} = 1 : 2.09 : 5.64 : 9 : 12$$

with

$$f_{0/2} = \frac{\omega}{2\pi} = \frac{330}{2\pi} = 52.52 \text{ Hz}$$

the periods for the first five even modes in this example are therefore $T_{0/2} = 19.0$, $T_{2/2} = 9.1$, $T_{4/2} = 3.38$, $T_{0/4} = 2.12$, and $T_{6/2} = 1.59$ msec, respectively. Since computer results indicated that the frequency $f_{0/4}$ has a small effect on the plate deflection, only $f_{0/2}$, $f_{2/2}$, and $f_{2/4}$ are needed for calculating the total dynamic response in terms of the plate deflection.

The plate deflection produced by the fundamental mode at the frequency $f_{0/2}$ is obtained from the computer program for the damped vibration; see Figure 24. The first positive pulse of the plate deflection is again plotted in Figure 25a.

The plate deflection produced by the frequencies $f_{2/2}$ and $f_{4/2}$ has not been evaluated mathematically since it requires tedious analysis; the deflection due to higher modes for boundary conditions of the present case are small when compared with the deflection produced by the fundamental mode. (This may not be true for boundary conditions other than those selected for the present case.) For that reason, assume arbitrarily that the maximum deflections due to higher modes are inversely proportional to the square of the frequency ratio, i.e.,

$$\text{Max } w_{2/2} = \max w_{0/2} \left[\frac{f_{0/2}}{f_{2/2}}\right]^2$$

$$\text{Max } w_{4/2} = \max w_{0/2} \left[\frac{f_{0/2}}{f_{4/2}}\right]^2$$

Deflections due to $f_{2/2}$ and $f_{4/2}$ are plotted in Figures 25b and 25c by assuming that damping effects are involved during the initial period of impact.

The deflections at the center of the plate model for the first positive pulse are plotted in Figure 25d and compared with records obtained from test data. The measured maximum impact pressure p_t is plotted in Figure 26. It is the resultant of the applied impact pressure p_r caused by the rigid body impact and the interacting pressure p_i between the vibrating plate and the fluid. The same figure also presents the maximum deflections of the plate model due to impact of the plate and the maximum impact pressure line obtained from Figure 2 for the rigid flat-bottom impact test. Because of the deformable impact surface of the plate, the measured maximum impact pressures are much lower than those for the rigid flat-bottom impact.

F. SHORT SUMMARY

On the basis of experimental work on the impact of a rectangular elastic plate with two opposite edges hinged and two other edges free, it is concluded that:

1. During the impact of the elastic plate, the first positive pulse of the impact pressure occurs when the air is momentarily trapped between the falling body and the water. However, as compared with the record from the rigid flat-bottom impact test, it is obvious that the plate stiffness and boundary conditions affect the time required for the trapped air to escape.

2. The equation of motion of plate given in Equation [4.2] of Section IV-A may represent the behavior of a ship-plate panel subjected to a ship bottom impact load (with any boundary conditions). In the equation, p_r is the impact pressure caused by the rigid body impact.

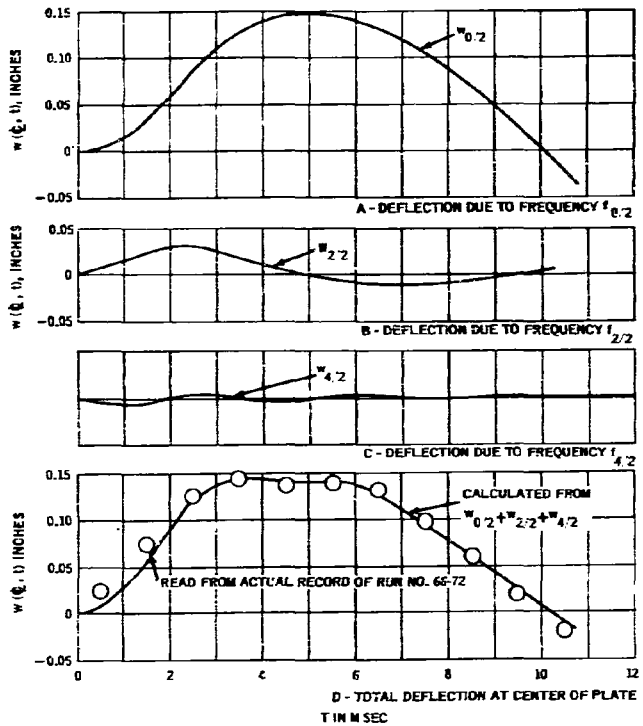

Figure 25 - Comparison of Measured and Calculated Deflection at Center of Plate Model Resulting from 6-Inch Drop Test

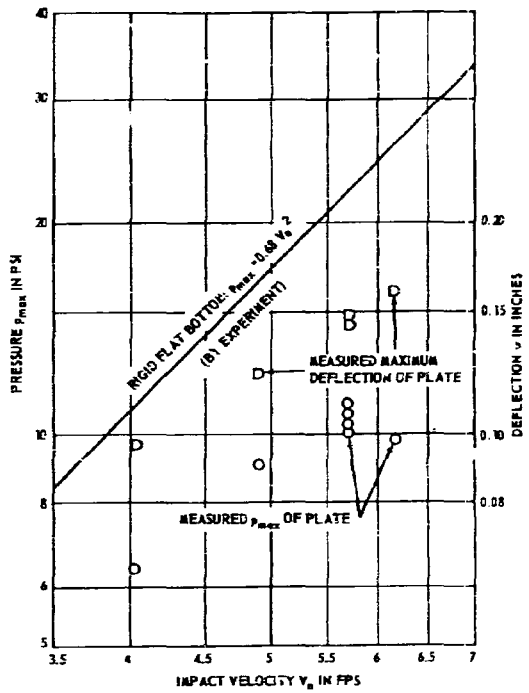

Figure 26 - Maximum Impact Pressure and Maximum Deflection Measured at Center of a Plate Model

3. From the practical point of view, the design of a ship bottom that will be subjected to bottom impact may omit the damping effect from the dynamic structural analysis without introducing noticeable error. This is because only the maximum values have primary importance in the design of local structures.

VI. IMPACT OF SHIP FLAT BOTTOM

This section attempts also to demonstrate that the structural response caused by the impact of a ship bottom with water can be treated as the impact of a deformable body on an incompressible fluid. The study in this section employed larger models than those previously used in the test programs. Their structural response was recorded for correlation with theory. The construction of models, the test facility and procedure, the instrumentation, the test results, and the important findings are given in the following paragraphs. A short summary is then provided at the end of the section.

A. DESCRIPTION OF MODELS AND TESTS

Two identical 1/4-scale models, designated as Models KG-3 and KG-4, were fabricated and scaled geometrically and structurally to represent a portion of the bottom of a seagoing vessel. The scantlings were selected from an area where bottom impact was likely to occur, i.e., between 15 and 25 percent of ship length aft of the forward perpendicular of the vessel.

The general arrangement and the scantlings of models are given in Figure 27. The overall dimensions of each model were 90 in. long by 80 in. wide and represent one-tenth the ship length and one-half the ship breadth. The bottom plating was fabricated from 1/8-in. high tensile steel plate and was welded to the bulkheads, the keel, the longitudinals, and the floors to divide the plate into 8- by 18-in. rectangular plate panels. The ends and the sides of each model were rigidly constructed to simulate the continuation of the vessel. The top of the model was welded with heavy flat bars (not shown in Figure 27) for bolting the model onto a relatively rigid carriage. Ballast weights were secured to the carriage

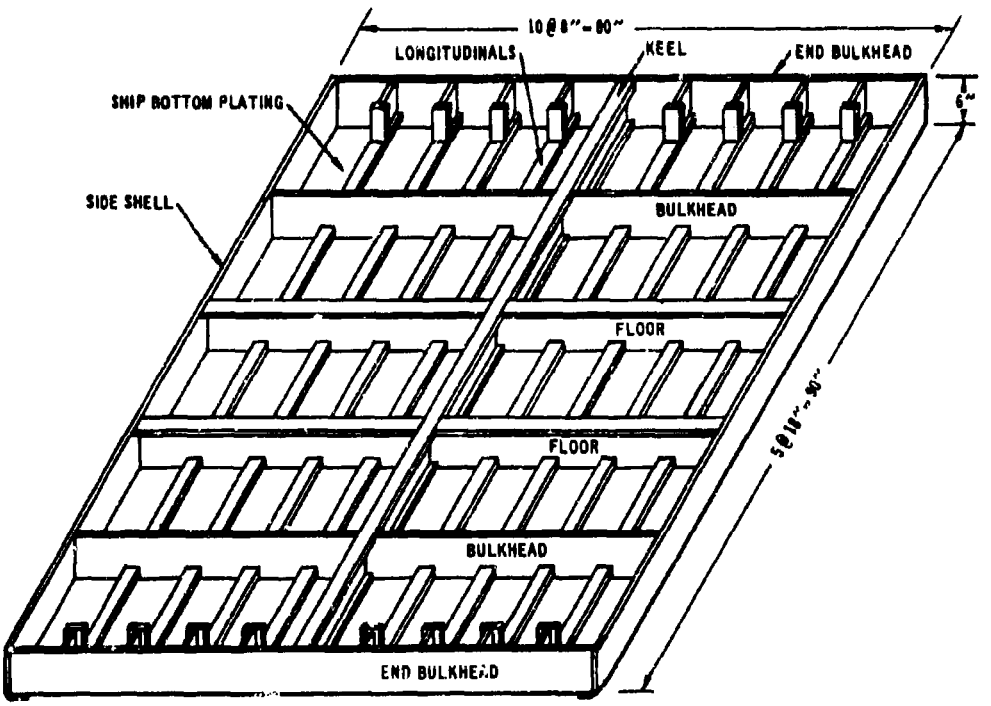

SCANTLINGS:

BOTTOM PLATING	-	1/8" HTS PLATE
BULKHEAD	-	1/4" MS PLATE
FLOOR	-	WEB = 14 GA × 6" HTS
		FLANGE = 1/8" × 1 1/8" HTS
LONGITUDINALS	-	WEB = 14 GA × 1 1/16" HTS
		FLANGE = 1/8" × 1 1/8" HTS
KEEL	-	1 7/8" × 6" × 4.4 LB, MS I-SECTION
SIDE SHELL	-	1/2" MS PLATE

Figure 27 - 1/4-Scale Structural Model of Flat Bottom

to make up the total drop weight of 8910 lb which simulated one-tenth the full load of the actual ship weight within the impact area. The selection of drop weight was arbitrary even though the length of each model was equivalent to one-tenth the ship length.

The test facility for the drop tests was a specially equipped barge outfitted with an instrumentation house and hoisting equipment capable of lifting heavy models. The test fixture (Figure 28) was built at one end of the barge. This fixture had guided tracks to ensure that under the controlled conditions of the tests, the models would impact on the water surface with a free fall. The releasing mechanism consisted of an explosive bolt for holding the carriage and the model in position at a prescribed drop height. When the explosive bolt was activated, the model and the carriage were released instantly.

The barge was located in an open but sheltered bay area at the time the tests were conducted. Since the test area was in open air, a perfectly calm water surface was difficult to accomplish even during good weather. The irregularity of the water surface illustrated in Figure 28 is typical of all test conditions.

Model KG-3 was tested at drop heights of 2, 4, and 6 ft and Model KG-4 at drop heights of 2 and 4 ft. No other drop was conducted because there was buckling, warping, and dishing at and near the ends of floors, bulkheads, and keels of the models during the 4-ft drop and thereafter. Thus, the bottom of each model could no longer be considered flat. The damaged models are shown in Figure 29.

Gage locations are shown in Figure 30. The complete instrumentation system was developed and designed to measure pressure, strain, velocity, and acceleration resulting from underwater explosion tests. Therefore, it was well suited to pick up response frequencies expected from the impact tests.

B. TEST RESULTS

The test records are presented as pressure histories in Figure 31, deflection histories in Figure 32, strain histories in Figure 33, and velocity histories in Figure 34. Underwater pressures were also recorded for Model KG-3 during the 6-ft drop test; the reduced data are given in Figure 35. These test results are used for the analyses presented in the following paragraphs.

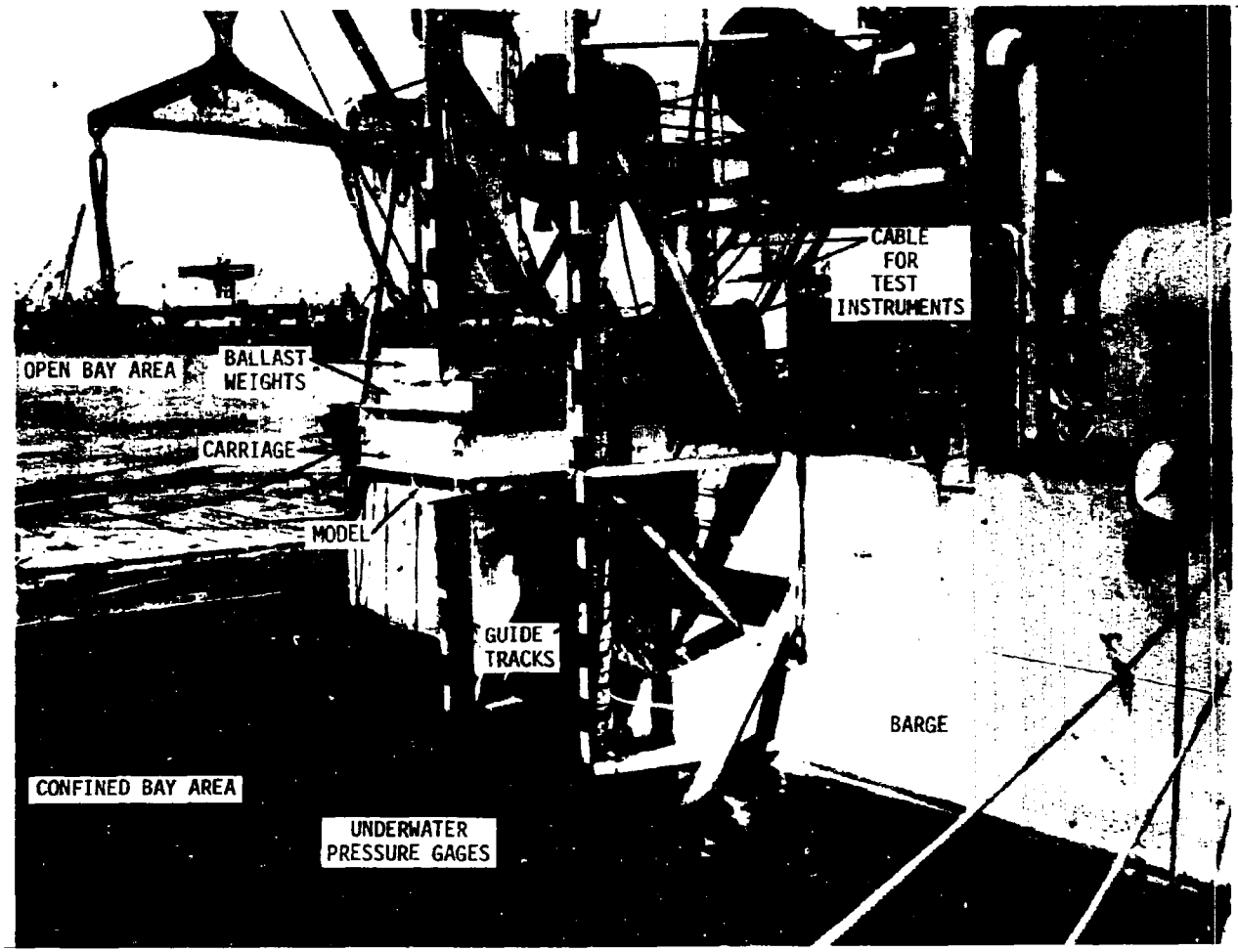

Figure 28 - Facility for Drop Tests of Large Models

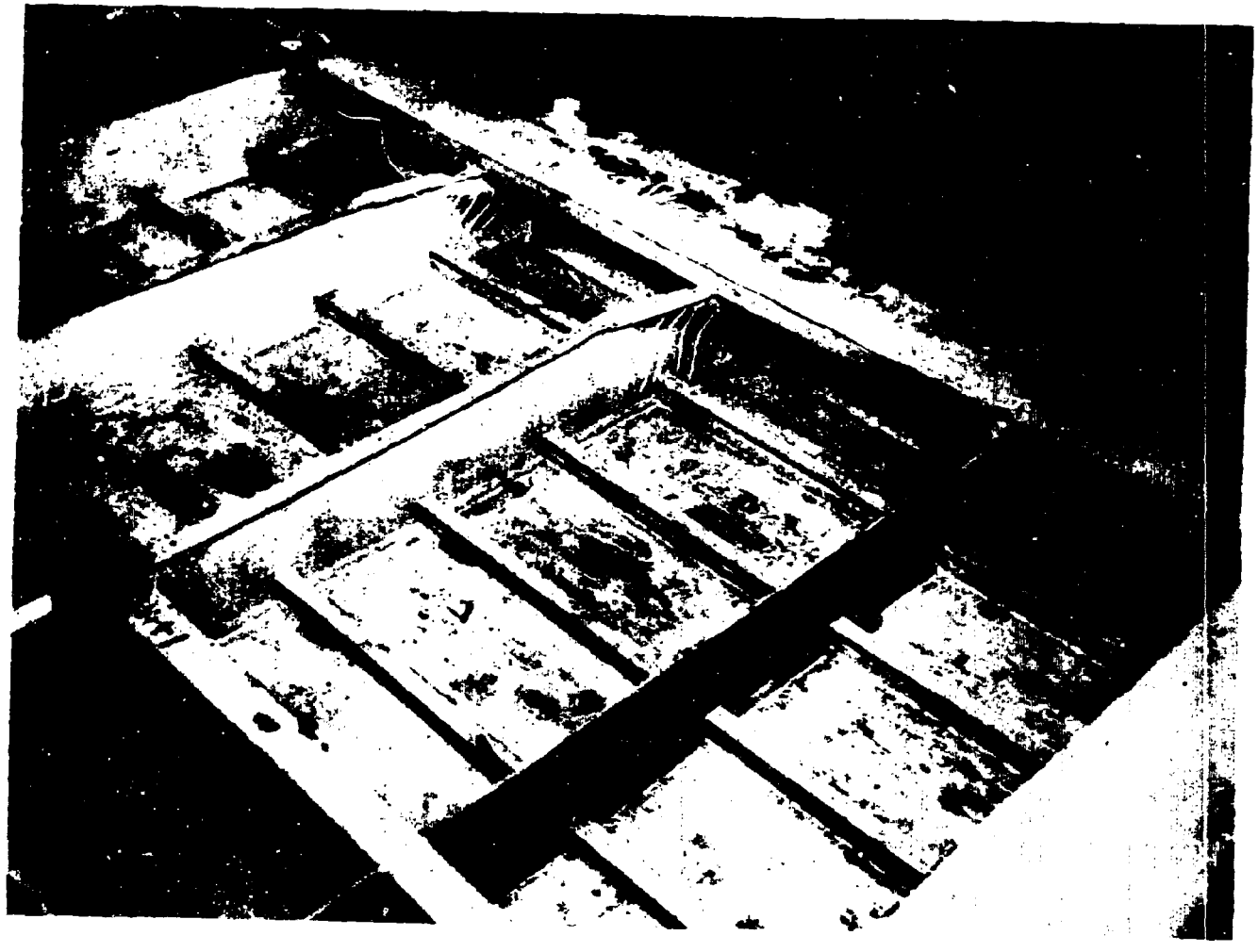

Figure 29 - Damaged Structural Model Following Drop Tests

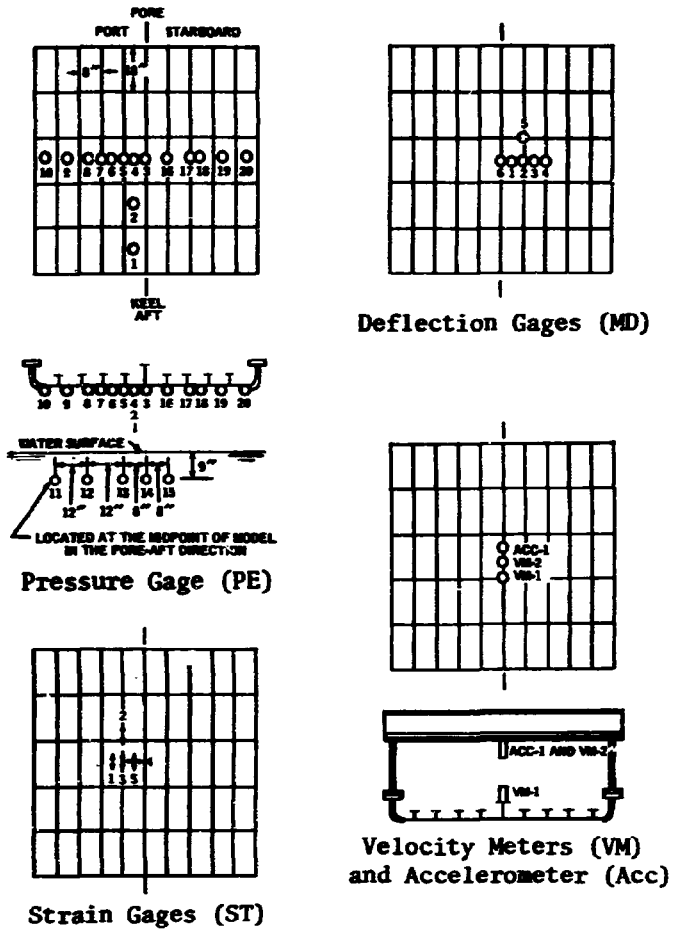

Figure 30a – Locations of Gages Mounted on Model KG-3

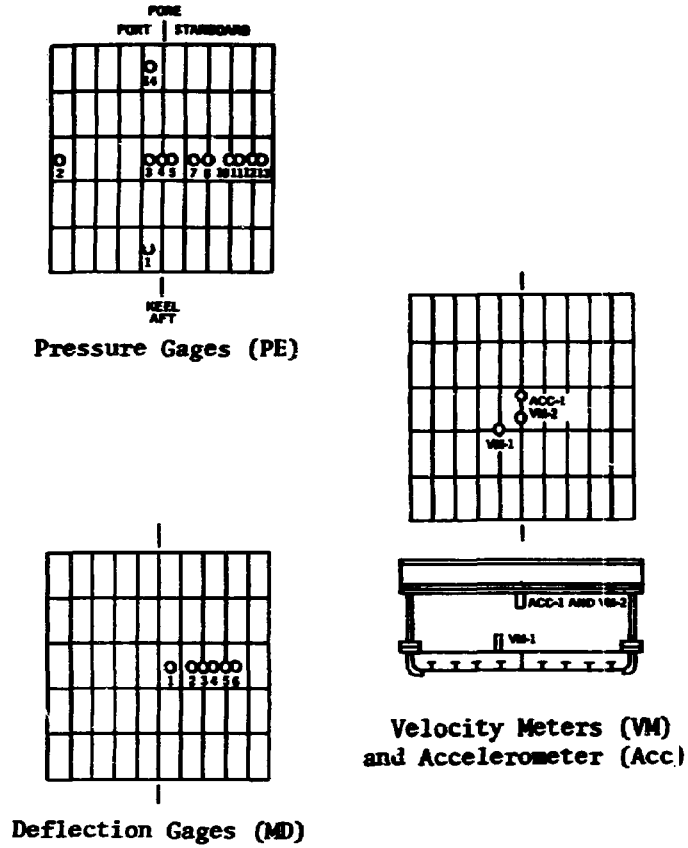

Figure 30b – Locations of Gages Mounted on Model KG-4

Figure 30 - Locations of Gages Mounted on Models KG-3 and KG-4

Figure 31 - Bottom Pressure Histories of Models KG-3 and KG-4

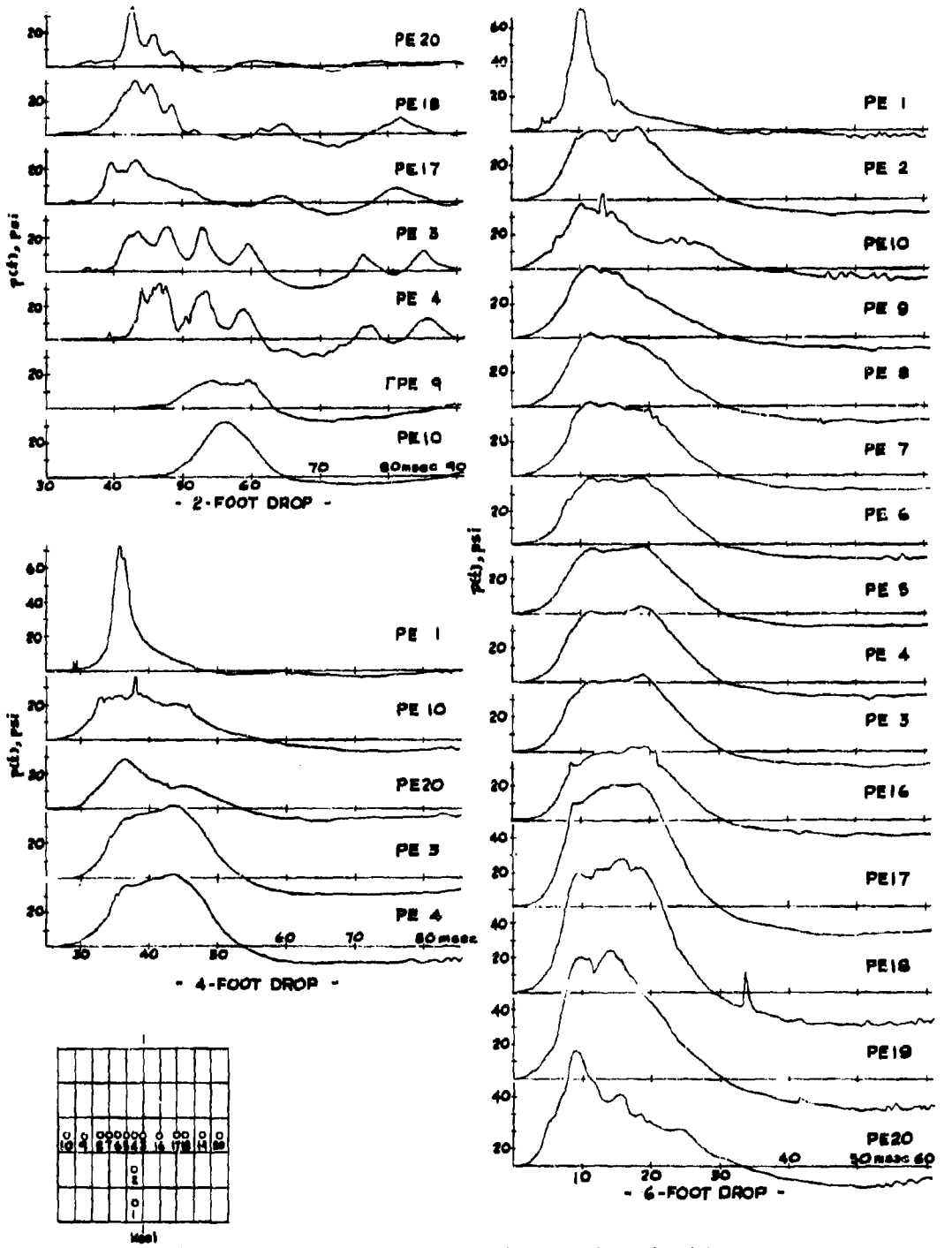

Figure 31a — Bottom Pressure Histories from Drop Tests of Model KG-3

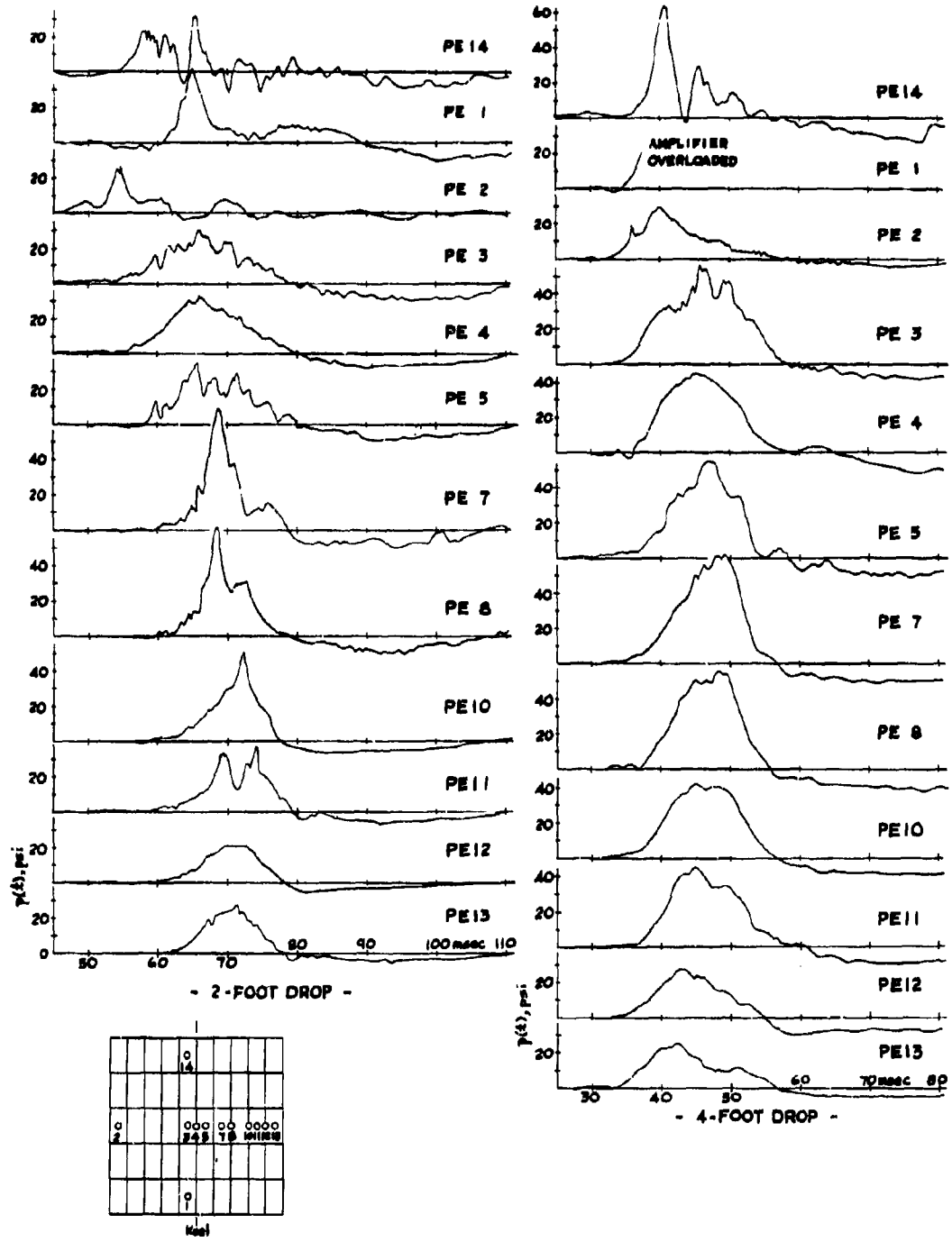

Figure 31b — Bottom Pressure Histories from Drop Tests of Model KG-4

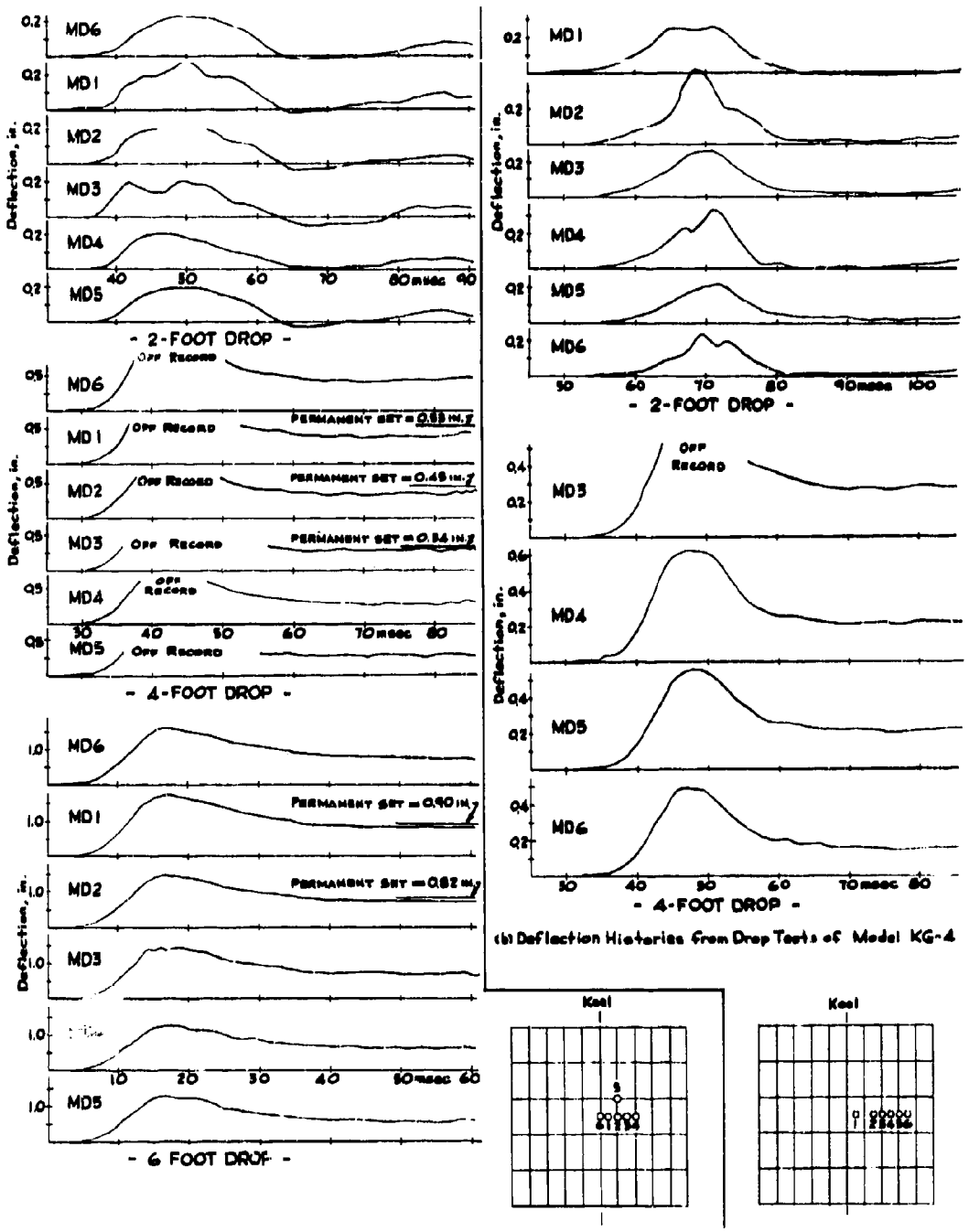

(b) Deflection Histories from Drop Tests of Model KG-4

Figure 32 - Deflection Histories of Models KG-3 and KG-4

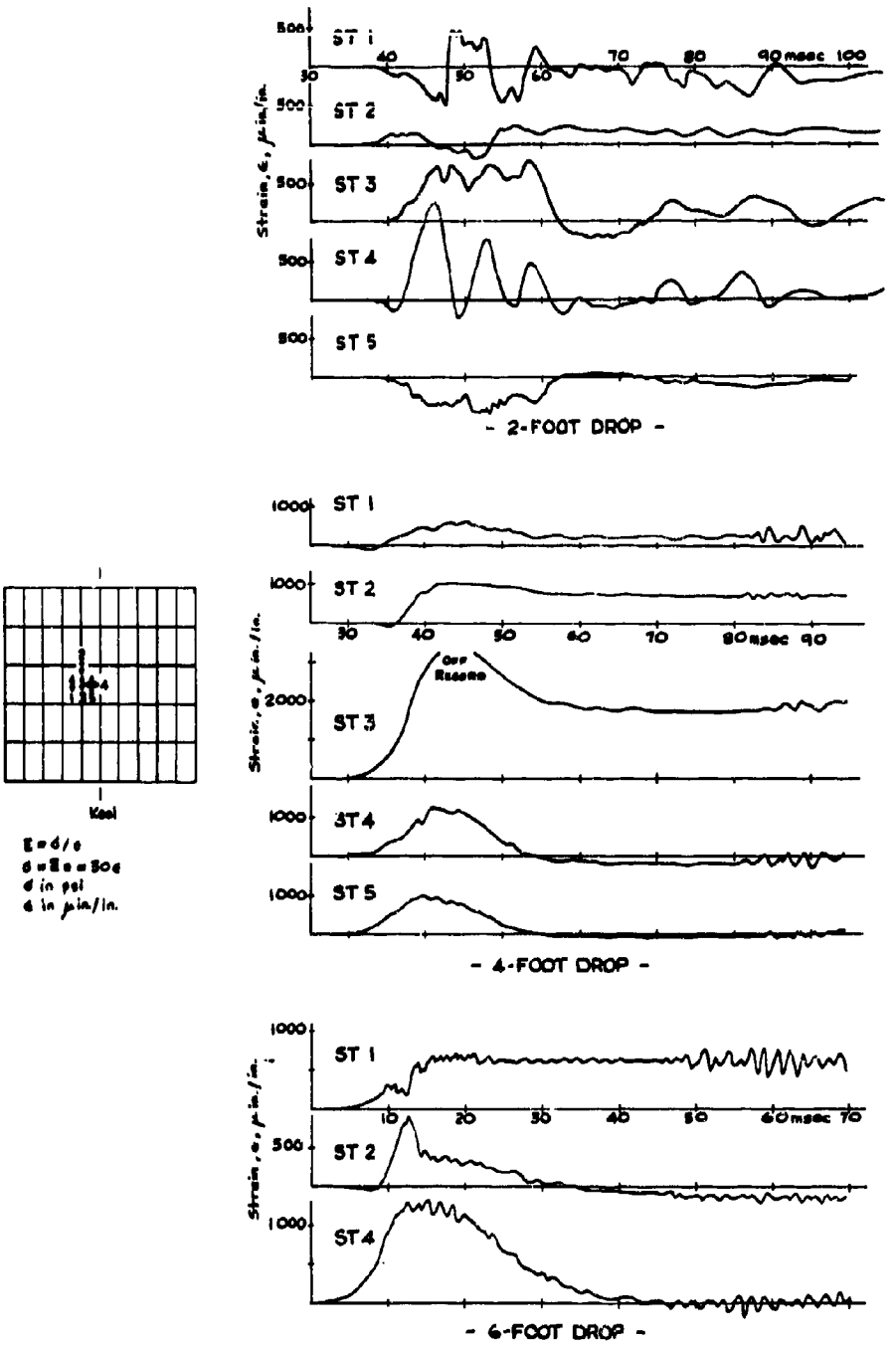

Figure 33 - Strain Histories of Model KG-3

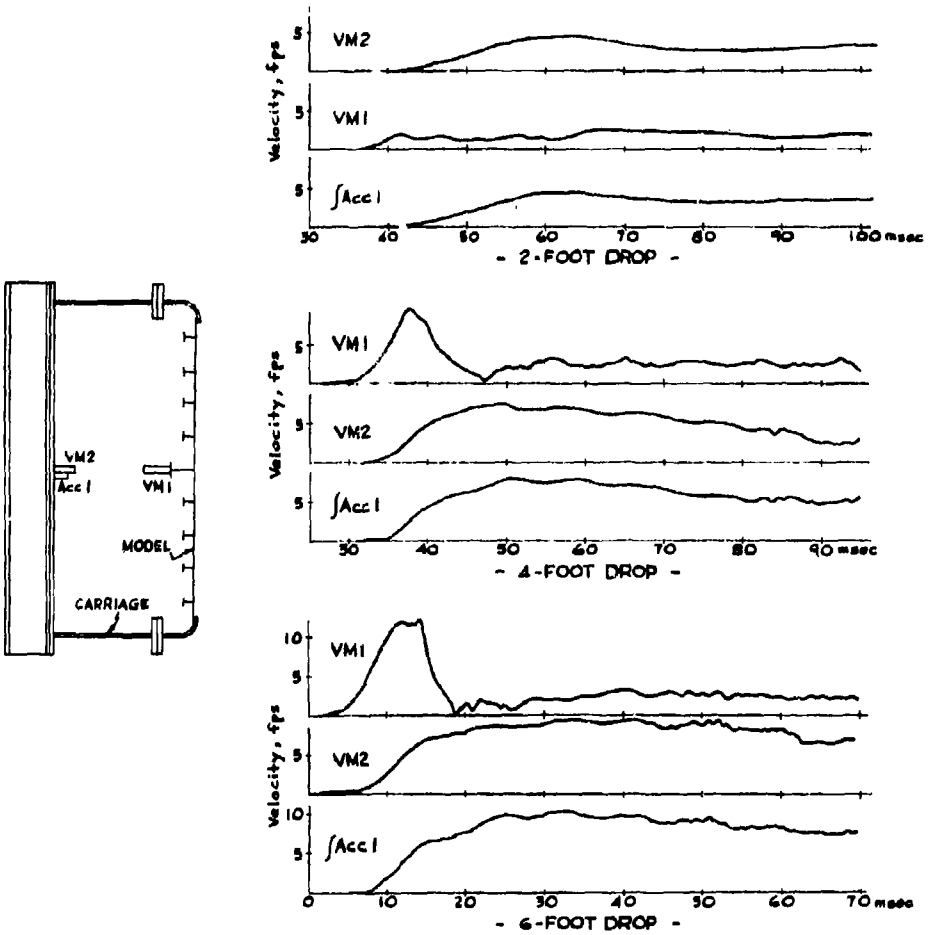

Figure 34a — Velocity Histories from Drop Tests of Model KG-3

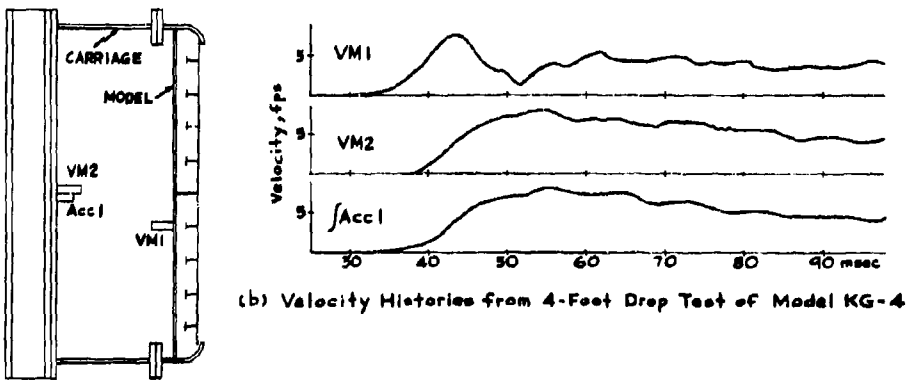

(b) Velocity Histories from 4-Foot Drop Test of Model KG-4

Figure 34b — Velocity Histories from 4-Foot Drop Test of Model KG-4

Figure 34 - Velocity Histories of Models KG-3 and KG-4

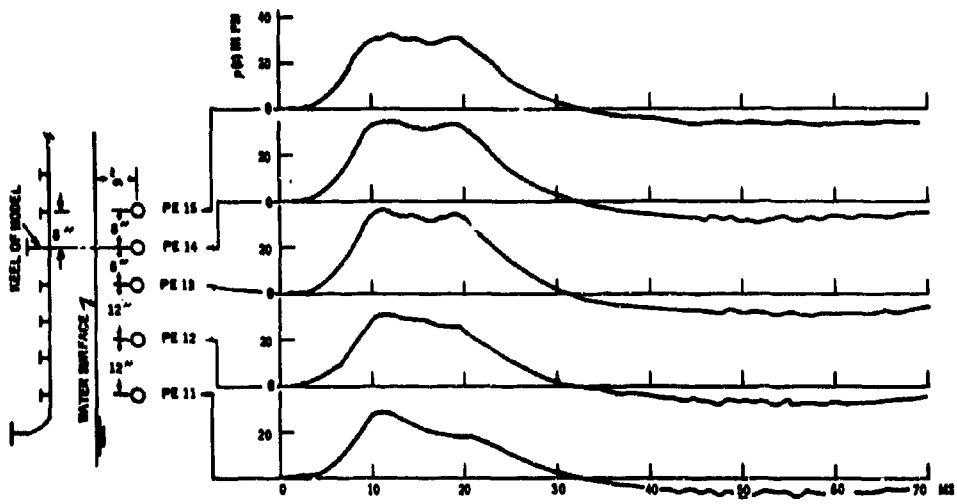

Figure 35 - Underwater Pressure Histories from 6-Foot Drop Test of Model KG-3

C. COMPARISONS BETWEEN RECORDED AND CALCULATED VALUES OF DEFLECTION TIME HISTORIES

To check the accuracy of the test records, the recorded and calculated values of the deflection time histories are compared in Figure 36. The calculated deflection (MD-5) was obtained by integration of the recorded plate velocity (VM-1) with respect to the rigid body motion (VM-2), i.e.,

$$(\text{MD-5}) = \int_0^t [(\text{VM-1}) - (\text{VM-2})]\, dt \qquad [6.1]$$

which is the difference between the area under the (VM-1) curve and the area under the (VM-2) curve from time t = 0 to t = t.

Since Gages VM-1, VM-2, and MD-5 were not located on the same vertical line, only a rough check was possible. However, comparisons between the recorded and calculated values of the deflection time histories showed reasonably good agreement.

D. COMPARISONS OF INTERACTION THEORY AND TEST RESULTS

The general expression for the dynamic interaction of a grillage-type ship bottom is given by Equation [4.3]. This equation can be written in another form as

$$m_s \ddot{w} + c_p \dot{w} + \left[D_x \frac{\partial^4}{\partial x_1^4} + 2H \frac{\partial^4}{\partial x_1^2 \partial y_1^2} + D_y \frac{\partial^4}{\partial y_1^4} \right] w = p_t \qquad [6.2]$$

where p_t is the actual load felt by the structure at its impact surface and is given by Equation [4.1]. At a particular location, Equation [6.2] is reduced to

$$m_s \frac{d}{dt} V + c_p V + k\, w(t) = p_t(w,t) \qquad [6.3]$$

Let us use the 6-ft drop test results of Model KG-3 to check the theoretical and experimental results. Equation [6.3] can then be rewritten as

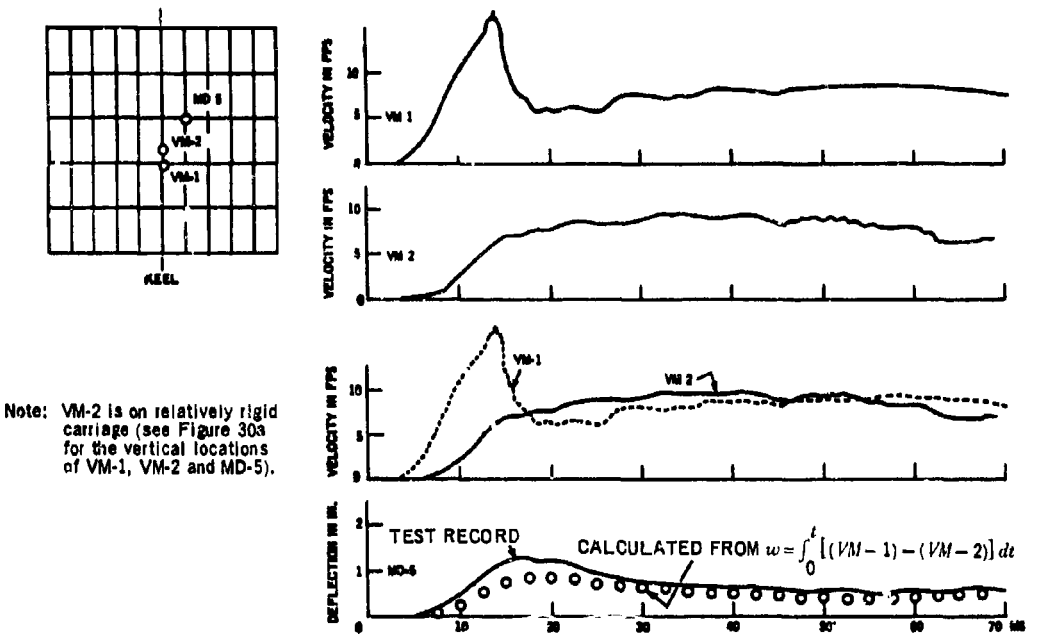

Note: VM-2 is on relatively rigid carriage (see Figure 30a for the vertical locations of VM-1, VM-2 and MD-5).

Figure 36 - Comparisons of Calculated and Recorded Values of Deflection Histories for 6-Foot Drop Test of Model KG-3

$$(PE\text{-}3) = m_s \frac{d}{dt}(VM\ 1) + c_p(VM\text{-}1) + k(MD\text{-}6) \qquad [6.3a]$$

where (PE-3) is the actual load felt by the structure at a given location and is a combined rigid body pressure p_r and interacting pressure p_i.

The method of calculating Equation [6.3a], which is reduced from Equation [6.2], is illustrated in the following manner. The response of the grillage-type ship bottom to impact is now treated as the transverse vibration of a homogenous orthotropic plate by Equation [4.3]. By neglecting damping, Equation [4.3] becomes

$$(m_s + m_{zz})\ddot{w} + \left[D_x \frac{\partial^4}{\partial x_1^4} + 2H \frac{\partial^4}{\partial x_1^2 \partial y_1^2} + D_y \frac{\partial^4}{\partial y_1^4}\right] w = p_r \qquad [4.3a]$$

For an orthotropic plate with simple support on all four boundaries, the circular frequency $\omega_{m/n}$ of Equation [4.3] is[22]

$$\omega_{m/n} = \pi^2 \sqrt{\frac{\frac{m^4}{a^4} D_x + 2H \frac{m^2 n^2}{a^2 b^2} + \frac{n^4}{b^4} D_y}{m_s + m_{zz}}} \qquad [6.4]$$

with m, n = 1, 2, 3 ...

As illustrated previously, the fundamental mode, which causes the largest deflection of the plate (isotropic or orthotropic), predominates any other higher modes. For that reason, the response of the orthotropic plate may be determined by considering the plate as a system with a single degree of freedom. The equation of motion for the single degree of freedom is given in Section IV-A by Equation [4.4], which is

$$\ddot{w}(t) + \omega^2 w(t) = q \cdot f(t)$$

with

$$\omega^2 = \frac{k}{m_s + m_{zz}} \qquad [6.5]$$

Compare Equation [6.4] with Equation [6.5], (see References 18 and 23 on method)

$$k_{m/n} = \left[\frac{m^4}{a^4} D_x + 2 H \frac{m^2 n^2}{a^2 b^2} + \frac{n^4}{b^4} D_y \right] \pi^4 \qquad [6.6]$$

For the fundamental mode, m = n = 1. Then

$$k_{1/1} = \left[\frac{D_x}{a^4} + \frac{2 H}{a^2 b^2} + \frac{D_y}{b^4} \right] \pi^4 \qquad [6.7]$$

with

$$\left.\begin{aligned} D_x &= \frac{E_x h^3}{12 (1 - \nu_{xy} \nu_{yx})} \\ D_y &= \frac{E_y h^3}{12 (1 - \nu_{xy} \nu_{yx})} \\ H &= D_1 + 2 D_{xy} \\ &= \frac{\nu_{xy} E_y h^3}{12 (1 - \nu_{xy} \nu_{yx})} + 2 \frac{G_{xy} h^3}{12} \end{aligned}\right\} \qquad [6.8]$$

For the grillage-type bottom, the following approximation may be made:

$$\left.\begin{aligned} D_x &\approx \frac{E h^3}{12} \\ &\approx \frac{E I_y}{s_y} \end{aligned}\right\} \qquad [6.9]$$

for $1 >> \nu_{xy}, \nu_{yx}$. And similarly,

$$D_y \approx \frac{E I_x}{s_x}$$

In these expressions, I_x, I_y represent the moment of inertia of the supporting member with an effective width of bottom plating about 30 times the thickness of the plate and s_x, s_y the space between two adjacent members.

Since ν_{xy}, ν_{yx} and G_{xy} are small (G_{xy} compared with E_x and E_y) for the grillage-type of structure,

$$H \to 0 \qquad [6.11]$$

To illustrate the use of the method outlined above, an example is given below for the test model shown in Figure 37:

1. Calculations of moment of inertia I_x and I_y:

a. Keel:

Size	I_o	A	d	Ad	A d^2	I
1 7/8 in. x 6 in. x 4.4 lb-I	7.3	1.3	3	3.9	11.7	19
1/8 in. x 4 in.	0	0.5	0	0	0	0
		1.8	2.165	3.9		19

$$I_x = I - Ad_o^2 = 19 - 1.8(2.165)^2 = 10.56 \text{ in.}^4$$

b. Longitudinals:

Size	I_o	A	d	Ad	A d^2	I
1/8 in. x 1 1/8 in.	0	0.141	1.0625	0.150	0.159	0.159
14 gage x 1 1/16 in.	0.007	0.080	0.531	0.042	0.0224	0.029
1/8 in. x 4 in.	0	0.500	0	0	0	0
		0.721	0.267	0.192		0.188

$$I_x = 0.188 - 0.721(0.267)^2 = 0.137 \text{ in.}^4$$

c. Bulkheads:

Size	I_o	A	d	Ad	A d^2	I
1/4 in. x 6 in.	9/2	3/2	3	9/2	27/2	18
1/8 in. x 4 in.	0	1/2	0	0	0	0
		2	9/4	9/2		18

$$I_y = 18 - 2(9/4)^2 = 7.9 \text{ in.}^4$$

d. Floors:

Size	I_o	A	d	Ad	A d^2	I
1/8 in. x 1 1/8 in.	0	0.141	6	0.846	5.076	5.076
14 gage x 6 in.	1.343	0.448	3	1.345	4.034	5.377
1/8 in. x 4 in.	0	0.500	0	0	0	0
		1.089	2	2.191		10.453

$$I_y = 10.453 - 1.089(4) = 6.1 \text{ in.}^4$$

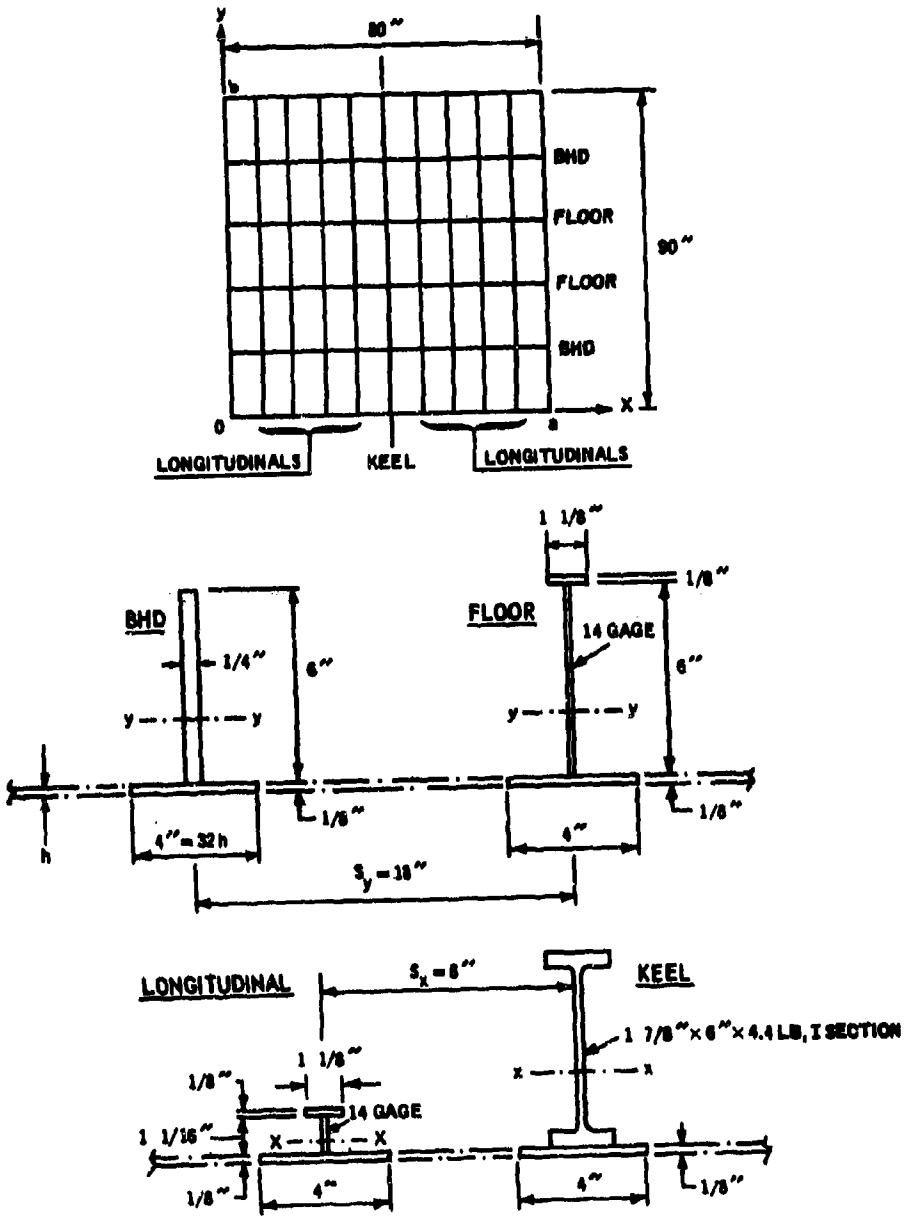

Figure 37 - Details of Supporting Members of Model KG-3

2. Calculations of flexural rigidities D_x and D_y:

a. Calculation of D_x:

$$(I_y)_{Bhd} = 7.9$$

$$(I_y)_{floor} = 6.1$$

$$\text{Ave } I_y = 7.0 \text{ in.}^4$$

$$D_x = \frac{E\, I_y}{s_y} = \frac{30(10)^6(7.0)}{18} = 11.67(10)^6 \text{ in.-lb}$$

b. Calculation of D_y:

$$(I_x)_{keel} = 10.56 \times 1 = 10.56$$

$$(I_x)_{longl} = 0.137 \times 8 = 1.10$$

$$9 \quad \boxed{11.66}$$

$$\text{Ave } I_x = 1.3 \text{ in.}^4$$

$$D_y = \frac{E\, I_x}{s_x} = \frac{30(10)^6(1.3)}{8} = 4.88(10)^6 \text{ in.-lb}$$

3. Calculation of spring constant k:

As given in Tables 7.4 and 7.5 of Reference 23, the spring constant for a simply supported two-way slab is $k_s = 271\ E\ I_a/a^2$ for a/b = 1 and that for a two-way slab with fixed edges is $k_f = 870\ E\ I_a/a^2$ for a/b = 1. For the test models, the edges simulate continuation of the ship bottom and are assumed to be somewhat halfway between fixed and simply supported. If we use values given for the two-way slab as a guide, then for the test models,

$$k = (k_s + k_f) \approx 2\ k_s$$

This modifies Equation [6.7] by:

$$k = 2\pi^4\left[\frac{D_x}{a^4} + \frac{2H}{a^2 b^2} + \frac{D_y}{b^4}\right] \qquad [6.12]$$

Thus, the spring constrant of the model is

$$k = 2\pi^4[11.67(10)^6/(80)^4 + 4.88(10)^6/(90)^4]$$
$$= 70 \text{ lb/in.}^3$$

4. Calculation of weight of model:

a. Bottom plate (1/8 in. x 80 in. x 90 in.):

$$w_1 = 5.1\left(\frac{80 \times 90}{144}\right) = 265 \text{ lb}$$

b. Keel (1 7/8 in. x 6 in. x 4.4 lb-I):

$$w_2 = 4.4\ (90/12) = 33 \text{ lb}$$

c. Bulkheads (1/4 in. x 6 in.; total of 2)

$$w_3 = 10.2\ (1/2)\ (80/12)\ (2) = 68 \text{ lb}$$

d. Longitudinals (total of 8):

14 gage x 1 1/16 in.	= 50/16 (1.0625/12) (7.5)	= 2.08
1/8 in. x 1 1/8 in.	= 5.1 (1.125/12) (7.5)	= 3.18
	Total	= 5.26 lb each

$$w_4 = 5.26\ (8) = 42 \text{ lb}$$

e. Floor (total of 2):

14 gage x 6 in.	= 50/16 (1/2) (80/12)	= 10.4
1/8 in. x 1 1/8 in.	= 5.1 (1.125/12) (80/12)	= 2.9
	Total	= 13.3 lb each

$$w_5 = 13.3\ (2) = 27 \text{ lb}$$

f. Total weight of model:

$$w = \sum_{n=1}^{5} w_n = 435 \text{ lb}$$

5. Calculation of model mass m_s:

$$\text{Ave } m_s = \frac{435}{90(80)} \frac{1}{32.2(12)} = 1.57(10)^{-4} \text{ lb-sec}^2/\text{in.}^3$$

6. Calculation of impact pressures:

By Equation [6.2], the equation of motion can be written as

$$p(w,t) = m_s\ddot{w} + c_p\dot{w} + kw \qquad [6.13]$$

Since the structural damping for the welded structure is small, therefore

$$c_p \to 0$$

Thus

$$p(w,t) = m_s\ddot{w} + kw \qquad [6.14]$$

For plastic response, k = 0. Thus

$$p(w,t) = m_s\ddot{w} \qquad [6.15]$$

Since the model has elastoplastic response, Equations [6.14] and [6.15] may be combined to become

$$p(w,t) = m_s\ddot{w} + k\,[w]_{\substack{\text{corrected for} \\ \text{plastic flow}}} \qquad [6.16]$$

When Equation [6.16] is applied to the calculations for the model at a point of concern, Equation [6.3a] may be written as

$$(PE\text{-}3) = 1.57(10)^{-4} \frac{\Delta(VM\text{-}1)}{\Delta t} + 70\,[MD\text{-}6]_{\substack{\text{corrected for} \\ \text{plastic flow}}} \qquad [6.17]$$

Calculations are tabulated in Table 2, and the plot is shown in Figure 38. The comparisons between the calculated and the recorded values of the impact pressure time histories showed reasonably good agreement also.

TABLE 2

Calculations of Impact Pressure (PE-3)

t msec	Measured PE-3 psi	VM-1 fps	Measured MD-6 in.	Corrected MD-6 (Note 1) in.	Δ(VM-1) fps	$\frac{\Delta(VM-1)}{\Delta t}$ ft/sec^2	$m_p \frac{\Delta(VM-1)}{\Delta t}$ (Note 2) psi	k(MD-6) Corrected (Note 3) psi	Calculated PE-3 (Note 4) psi
0	0	0	0	0	0	0	0	0	0
2.5	1	0	0	0	0	0	0	0	0
5	5	1.2	0.05	0.05	+1.2	$5.76(10)^3$	0.9	3.5	4.4
7.5	20	5.1	0.20	0.22	+3.9	18.72	2.9	15.4	18.3
10	36	10.2	0.55	0.55	+5.2	25	3.9	38.5	42.4
12.5	40	14.0	1.05	0.67	+3.8	18.2	2.9	46.9	49.8
15	41	17.0 12.9	1.45	0.67	nil	---	---	46.9	46.9
17.5	43	7.2	1.57	0.67	-5.7	-27.4	-4.2	46.9	42.7
20	42	6.0	1.48	0.58	-1.0	- 4.8	-0.8	40.6	39.8
22.5	30	6.2	1.38	0.48	+0.2	+ 0.96	+0.2	33.6	33.8
25	19	5.7	1.25	0.35	-0.5	- 2.4	+0.4	24.5	24.9
27.5	10	7.4	1.12	0.22	+1.7	+ 8.2	+1.3	15.4	16.7
30	1	7.6	1.09	0.19	+0.2	+ 0.96	+0.2	13.3	13.5
32.5	-2	7.2	0.96	0.06	-0.4	- 1.92	-0.3	4.2	3.9

Notes: 1. Assume permanent set = 0.9 in. for correction of (MD-6) due to plastic flow.

2. $M_p = 1.57(10)^{-4}$ lb-sec^2/in.^{3}

3. k = 70 lb/in.^{3}

4. Calculated (PE-3) = $m_p \frac{\Delta(VM-1)}{\Delta t} + k\,(MD-6)_{corrected}$

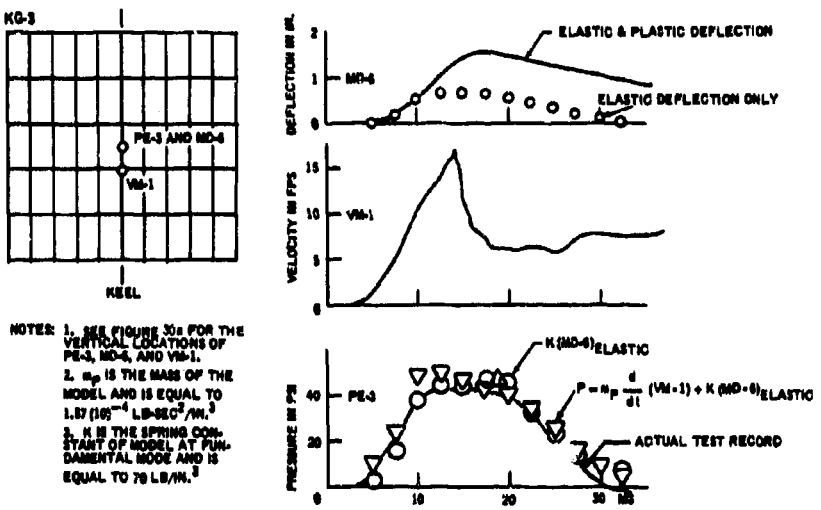

Figure 38 - Comparisons of Calculated and Recorded Values of Pressure Histories for 6-Foot Drop Test of Model KG-3

E. STRAIN RECORDS VERSUS DEFLECTION RECORDS

The structural behavior during and after the impact can be examined from the deflection time histories in Figure 32 and the strain time histories in Figure 33. The information provided by the deflection histories is not as detailed and direct as the strain histories. This is illustrated by comparing Figure 32 with Figure 33. The deflection histories, for instance MD-1 in Figure 32a, do not provide sufficient information to determine the stress of the plate or its supporting member at the point measured unless other information is available. Strain histories, such as those for ST-4 and ST-5 in Figure 33a, can answer immediately whether the strain of the plate or its supporting member in the direction measured has exceeded elastic limit with permanent set, is still within the elastic limit, or has created lock-in stresses.

The strain time histories measured at the plate panel provide and amplify the panel vibrations, for instance, the ST-4 strain histories shown in Figure 33a. Calculations on the vibratory frequencies indicate that this excited vibration is the fundamental mode of the plate panel. However, the panel vibrations were excited on 2-ft drops. On higher drops, these panel vibrations were not excited; see Figure 30. Panel vibrations are also shown in the deflection histories, but it is difficult to tell whether they are due to the higher modes of the grillage structure or to the fundamental mode of the plate panel.

Examination of the deflection and the strain histories gives sufficient evidence to conclude that essentially the excited vibrations are the fundamental mode of the whole grillage structure and that of the plate panel. The panel vibrations were not excited for drops higher than 2 ft.

F. ANGLE OF ATTACK

As indicated by the pressure histories in Figure 31, the impact surface of both models did not strike the water surface evenly for all the drops; this was especially obvious for the 2-ft drop height. The record of Model KG-3 (Figure 31a) showed that at the 2-ft drop height, the pressure measured by PE-20 rose first. The PE-10 pressure rose when the

positive pulse of the PE-20 pressure was almost over. The records of Model KG-4 (Figure 51d) showed that at the 2-ft drop height, the pressure measured by PE-2 rose first, followed in sequence by PE-3, PE-4, ..., and PE-13. The calculation of the time lag between the pressure rises at different locations showed that at the 2-ft drops, both models hit the water surface at an angle of attack of about 1 deg.

G. MAXIMUM IMPACT PRESSURE

The measured maximum impact pressures of all test data of models KG-3 and KG-4 are plotted in Figure 39 and compared with those obtained from the rigid flat-bottom model given in Section II and the elastic plate model given in Section V. Since the structural models were more rigid than the plate model, the pressures acting on the bottom plating of the structural models were comparatively closer to the rigid flat-bottom impact pressures than those of the plate model. However, because of the irregularity of the water surface (illustrated in Figure 28), the measured maximum impact pressures of the structural models are more scattered than those of the plate model.

H. UNDERWATER PRESSURE VERSUS BOTTOM IMPACT PRESSURE

Figure 40 indicates good agreement between the underwater pressure and nearby bottom impact pressure. Because the underwater pressures were measured some distance away from the impact surface, they were somewhat lower than those at the impact surface. Theoretical investigations on the underwater pressures are not within the scope of the present study.

I. QUASI-STATIC APPROXIMATION

The quasi-static approximation has been suggested by Heller and Jasper for the structural design of planing craft.[19] Therefore, it is worthwhile to investigate whether the drop test of the types of models used in the present study can be considered quasi-static in nature. To do this, it is first necessary to examine the applied pressure p_t. As discussed in Section IV-A, this p_t is the sum of p_r (the pressure generated by the impact of the rigid body on the water surface) and p_i

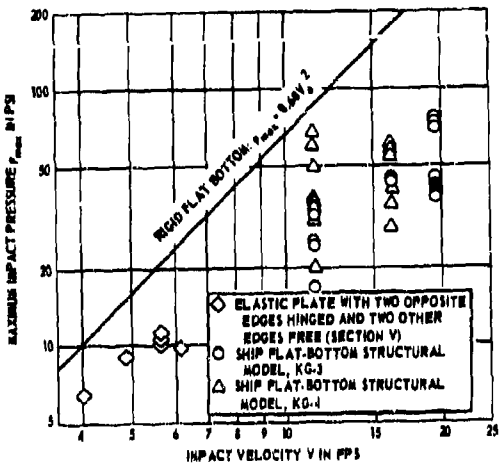

Figure 39 - Maximum Impact Pressures Obtained from Flat-Bottom Impact of Models KG-3 and KG-4

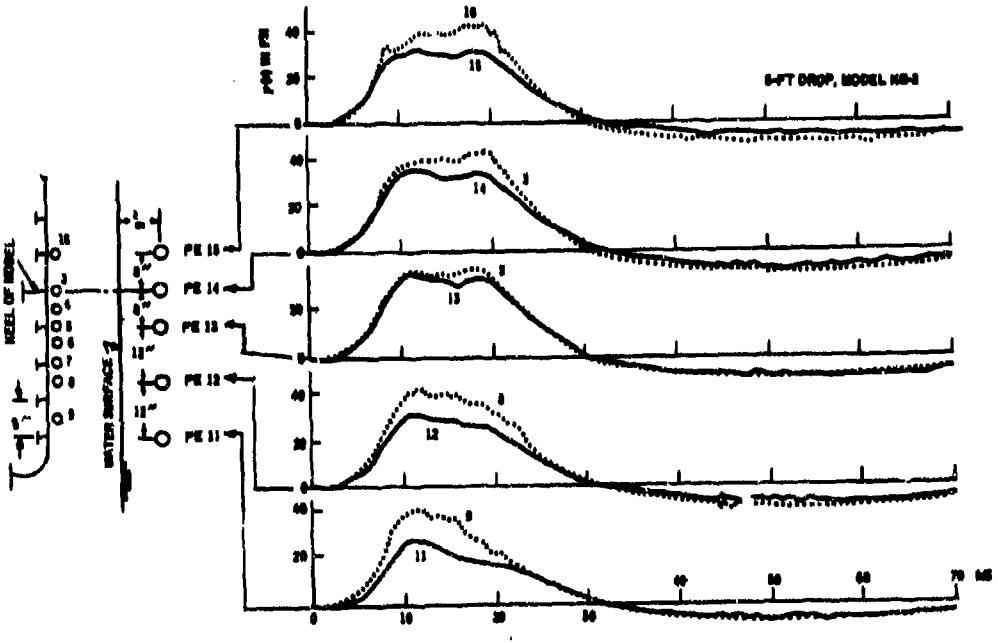

Figure 40 - Comparisons of Underwater Pressure with Nearby Bottom Impact Pressures

(the interacting pressure caused by the movement of the elastic body with respect to the fluid). Since the grillage models are quite rigid, p_r is about equal to p_t. As can be seen in Figure 38 and Table 2, the inertial term $m_s \frac{d}{dt}$ (VM-1) is insignificant when compared with the spring force k(MD-6). This shows that the problem is quasi-static in nature. In other words, the deflection of the structure is in direct proportion to the applied load as if applied statically. This relationship can also be determined by comparing the pressures with the strains given in Figure 41.

J. SHORT SUMMARY

On the basis of experimental work on the impact of ship structural models with flat bottom, it is concluded that:

1. The equation of motion expressed in Equation [4.3] of Section IV-A may represent the behavior of a grillage-type ship bottom subjected to bottom impact with water. This applies when the interaction between the ship bottom structure and fluid should be considered. However, if the grillage type of ship bottom is relatively rigid, it is reasonable to assume that the rigid-body impact loads can be applied quasi-statically to the impact area as the practical design loads for the ship bottom.

2. The underwater pressure produced by ship bottom impact diminishes with the distance away from the impact surface of the ship bottom.

VII. IMPACT OF SHIP BOTTOM WITH 10-DEGREE DEADRISE ANGLE

Since a portion of the test results of this series has been presented elsewhere,[24-26] it is intended to show here some of the test results which are used to verify findings given in the previous sections. In this section, models and tests are described, and the test results on maximum impact pressures are compared with the findings given in Section III for the wedge with 10-deg deadrise angle. In addition, the structural damage caused by repeated loading is explored, and the ineffectiveness of using backing material to reduce structural damage is explained by the dynamic interaction given in Section IV-A. A short summary is provided at the end of the section.

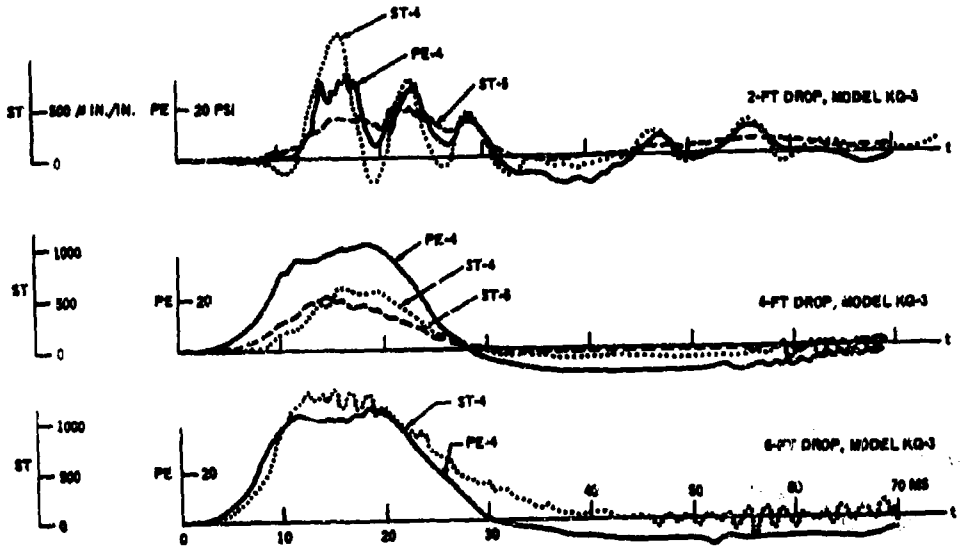

Figure 41 - Interaction between Bottom Pressure and Strain of Deformable Body

A. DESCRIPTION OF MODELS AND TESTS

The models were essentially similar to those of the ship flat bottom described in Section VI except that the present models had a V-shaped bottom with a 10-deg deadrise angle and a 2-in. flat bottom at the keel; see Figure 42. The total drop weight was also 8910 lb for each model, excluding the weight of backing material.

The test facility and test conditions described in Section VI and shown in Figure 28 were used. The tests and the instrumentation were identical to those used for the drop test of ship flat-bottom models. For quick references, the test schedule of this series of tests is given in Table 3. The table also gives the amount and kind of backing material used in the individual models. The backing materials used were water, oil, sand, ML-D2, and PVC-PVA. The ML-D2 is a polyamide-epoxy aluminum-oxide filled material that weighs 4.5 lb for each 12- x 12- x 1/2-in. section, and the PVC-PVA is a polyvinyl-chloride-polyvinylacetate material that weighs 5.1 lb for each 12- x 12- x 1/2-in. section. As stated previously, the drop height is defined as the vertical distance between the keel of the model and the water surface.

B. MAXIMUM IMPACT PRESSURE

The measured maximum impact pressures of eight models (see Table 3) are plotted in Figure 43. The drop heights ranged from 2 to 25 ft, with the free-fall impact velocity from 11.4 to 40.1 fps.

Since the models were relatively rigid, the measured values were close to the values calculated by Equation [3.8] (obtained experimentally from the rigid body impact test of the wedge with 10-deg deadrise angle) of Section III. For purposes of comparison, Equation [3.8] is also plotted in Figure 43. However, since large deformations of Models A-1 and KG-2 were caused by the 25-ft drops, the measured maximum pressures were well below the values given by Equation [3.8]. Because of the irregularity of the water surface, as illustrated in Figure 28, the measured maximum impact pressure was scattered.

The test results also indicate that the addition of backing material, which thus increases the total drop weight of the model, does

TABLE 3

The 10-Degree Ship Bottom Models and Test Conditions

Model No.	Backing Material		Shot No.	Drop Height ft	Remarks
	Port	Starboard			
A-1	None	None	5530	2	
			5531	4	
			5532	6	
			5533	8	
			5534	25	
B-4	None	None	5544	2	
			5545	4	
			5546	6	
			5549	12(A)	Repeated drops at same drop height of 12 ft
			5550	12(B)	
			5551	12(C)	
			5553	12(D)	
C-2	None	None	5766	8	
			5767	9(A)	
			5768	9(B)	
			5769	9(C)	
			5770	9(D)	
D-3	Water	Oil	5812	4(A)	77 percent = 689 lb
			5813	4(B)	89 percent = 787 lb
			5814	4(C)	100 percent = 885 lb
			5815	4(D)	67 percent = 591 lb
			5816	10(A)	
			5817	10(B)	77 percent
			5818	10(C)	(= 689 lb each side)
KG-1	None	None	5819	4	
			5820	10(1)	
			5821	10(2)	
			5822	10(3)	
			5945	10(4)	
			5946	10(5)	
			5947	10(6)	
			5948	10(7)	
			5949	10(8)	
			5950	10(9)	
			5951	10(10)	
			5952	10(11)	
			5953	10(12)	
			6033	10(13)	
			6034	10(14)	
			6035	10(15)	
			6036	10(16)	
			6037	10(17)	
			6038	10(18)	
			6039	10(19)	
			6040	10(20)	
			6041	10(21)	
			6042	10(22)	

Table 3 (Continued)

Model No.	Backing Material		Shot No.	Drop Height ft	Remarks
	Port	Starboard			
KG-2	Sand	ML-D2	5823	4	Weight of backing material = 689 lb each side
			5824	10(A)	
			5825	10(B)	
			5826	10(C)	
			5899	25	
MG-1	1/4 in. PVC-PVA	1 in. PVC-PVA	7076	3(A)	
			7077	3(B)	
			7078	10(1)	
			7079	10(2)	
			7080	10(3)	
			7081	10(4)	
			7082	10(5)	
			7083	10(6)	
			7086	10(7)	
			7088	10(8)	
			7089	10(9)	
			7090	10(10)	
MG-2	1/2 in. ML-D2	1/2 in. PVC-PVA	7051	3(A)	
			7052	3(B)	
			7053	10(1)	
			7054	10(2)	
			7055	10(3)	
			7056	10(4)	
			7057	10(5)	
			7058	10(6)	
			7059	10(7)	
			7060	10(8)	
			7061	10(9)	
			7062	10(10)	

Notes:

1. Tests were performed at the semiconfined bay area of the Norfolk Navy Shipyard, Portsmouth, Va.
2. Models are identical to have 10-deg deadrise angle except as noted in Remarks Column.
3. 1/2 in. ML-D2 is a polyamide-epoxy, aluminum-oxide filled material weighing 4.5 lb per 1/2-in. x 1-ft x 1-ft section.
4. PVC-PVA is a polyvinyl-chloride-polyvinylacetate material weighing 5.1 psf for 1/2-in. thickness.
5. Models D-3, KG-1, KG-2, MG-1, and MG-2 were separated longitudinally by installing a thin vertical plate from the top plate of the keel to the level of the tank top. The partition was made as light as possible so that the properties of the model would not be affected appreciably.

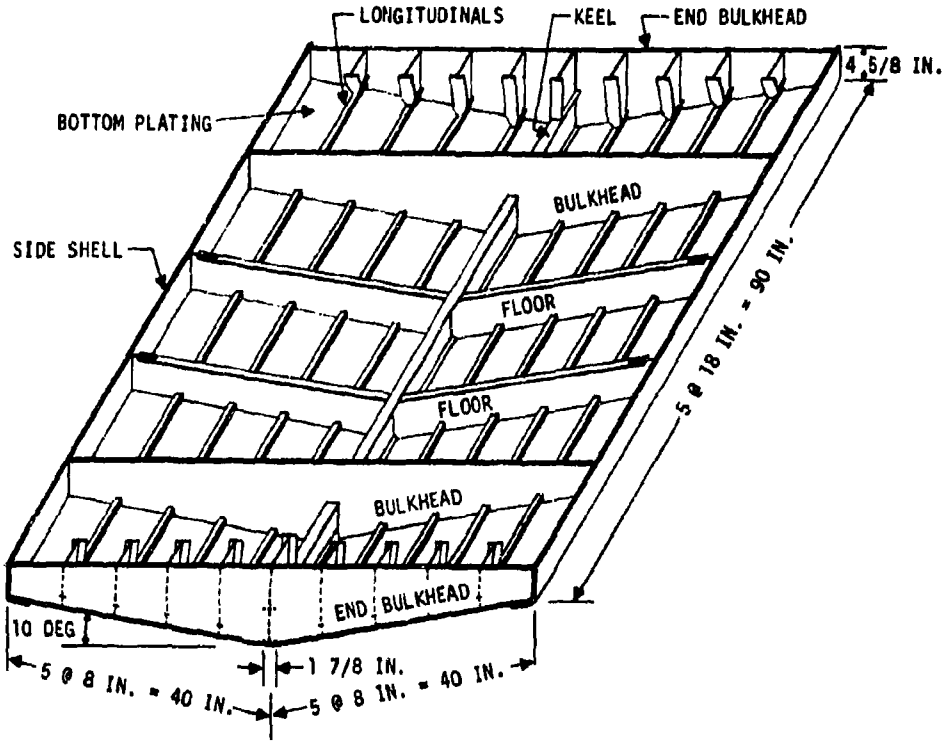

SCANTLINGS:

BOTTOM PLATING	-	1/8 IN. HTS PLATE
BULKHEAD	-	1/4 IN. M.S. PLATE
FLOOR	-	WEB: 14 GA HTS PLATE
		FLANGE: 1/8 IN. X 1 1/8 IN. HTS PLATE
LONGITUDINALS	-	WEB: 14 GA X 1 35/64 IN. HTS PLATE
		FLANGE: 12 GA X 1 1/64 IN. HTS PLATE
KEEL	-	1 7/8 IN. X 6 IN. X 4.4 LB I, M.S.
SIDE SHELL	-	3/8 IN. M.S. PLATE

Figure 42 - 1/4-Scale Structural Model with 10-Degree Deadrise Angle

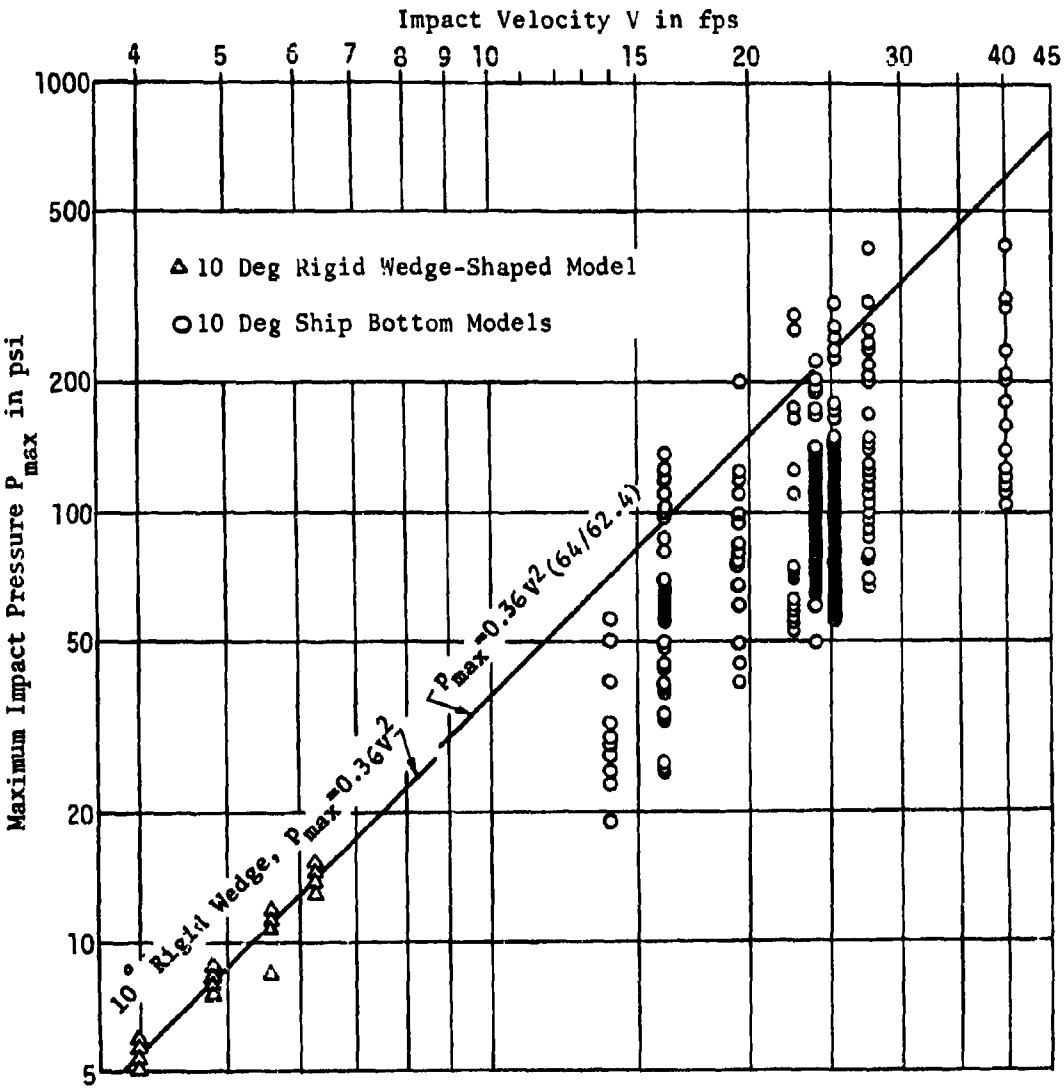

Figure 43 - Maximum Impact Pressure Obtained from Drop Tests of Eight Ship Bottom Models with 10-Degree Deadrise Angle

not affect the maximum impact pressure at all. This independence of total drop weight agrees with findings given in Section IV and in Reference 13.

Samples of records of this series of tests are illustrated in Figure 44.

C. EFFECT OF REPEATED LOADS ON STRUCTURAL DAMAGE

Repeated drops at the same drop height were performed for most of the models except Model A-1 (see Table 3). An analysis of the test results was performed for Model B-4, the first in this series to be subjected to repeated drops.* The findings from the test results of this model are in general agreement with those of the other models.

The offsets of Model B-4 were measured manually before and after each repeated drop. The permanent deformation of each of 50 panels could then be calculated. The mean values of net changes in permanent deformations at the center of each panel caused by 12-ft repeated drops are shown in Figure 45.

Permanent deformations were also recorded at several selected locations by means of deflection gages; see Figure 44. Results of the permanent deformations are shown in Figure 46. A comparison indicated that the manual measurements and measurements by deflection gages agreed very well.

From the observations of the test, it is concluded that the structural damage may occur on the plate panel and/or on the supporting members, such as keel, floors, longitudinals, etc. The following conclusions have been drawn regarding the structural damage caused by repeated drops at the same drop height:

1. The change of permanent deformation of panels was confined essentially to the first 12-ft drop and was gradually reduced after every repeated drop. This shows that there is considerable further strengthening due to membrane stretching (shape hardening). This membrane stretching would usually be present in ship grillages.

---

*Reported informally by S.L. Chuang in NSRDC Technical Note SML 760-70 (May 1964).

Figure 44 - Samples of Records (Test Results from Four 12-Foot Repeated Drops of Model B-4)

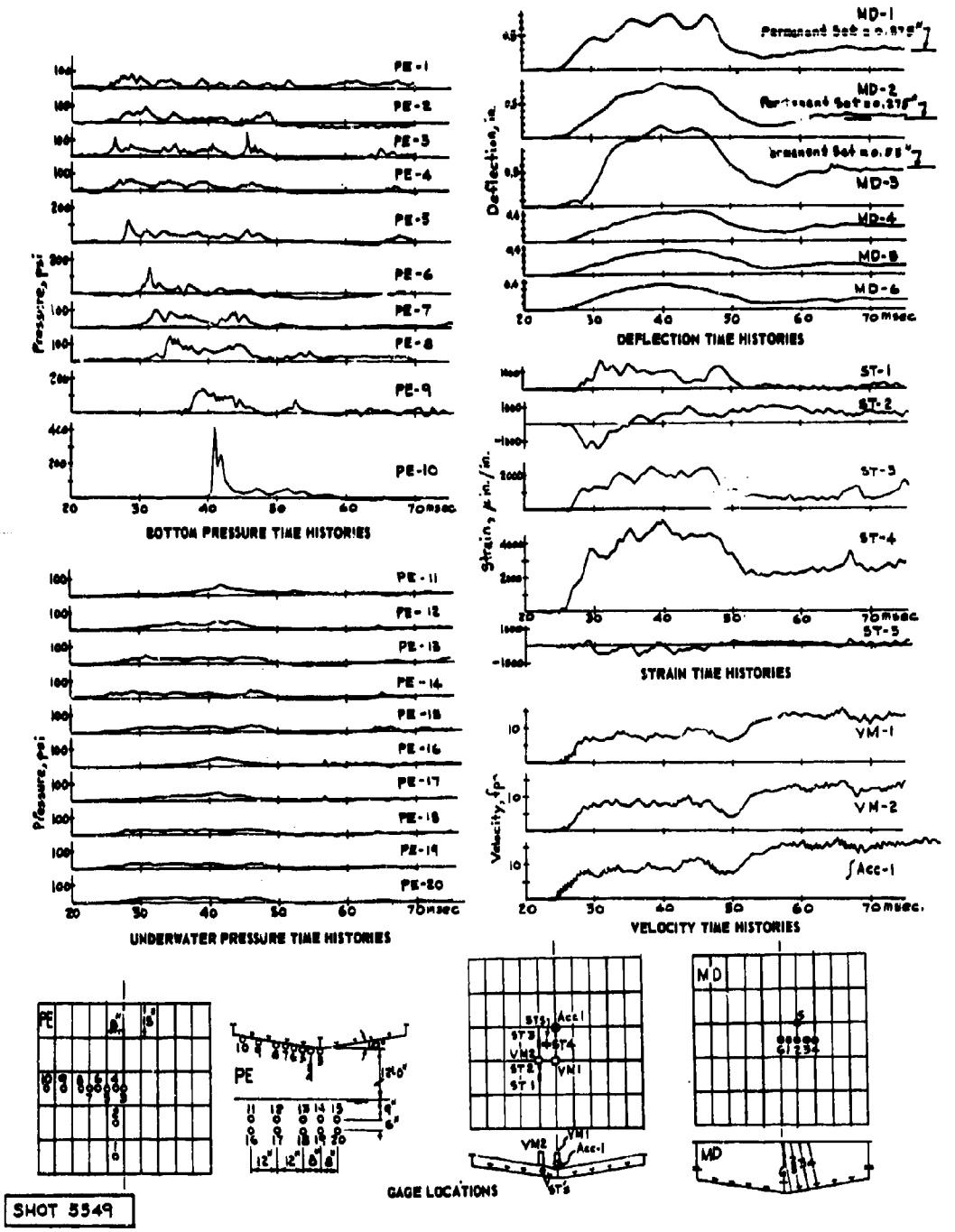

Figure 44a – Test Results for First 12-Foot Repeated Drop of Model B-4

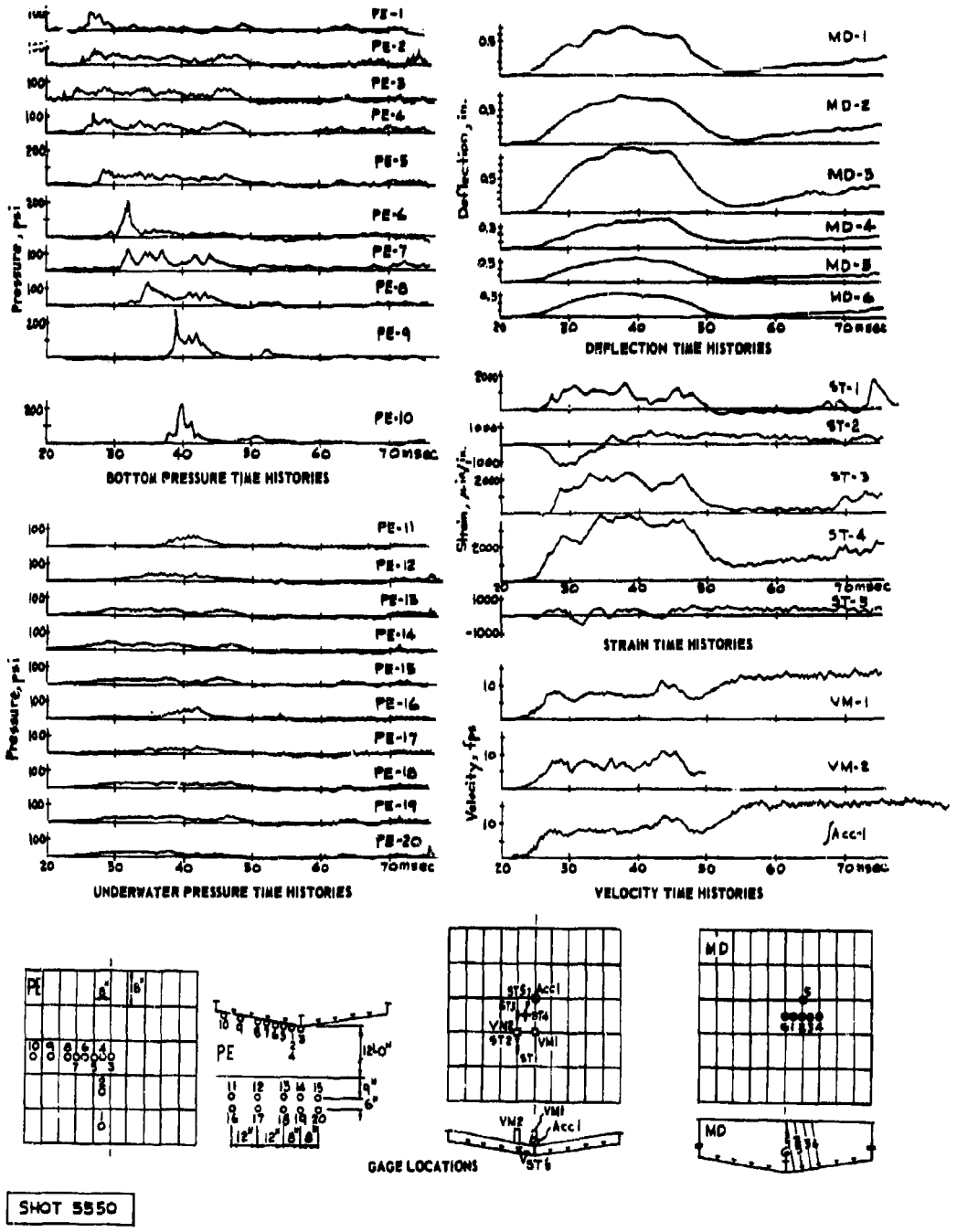

Figure 44b — Test Results for Second 12-Foot Repeated Drop of Model B-4

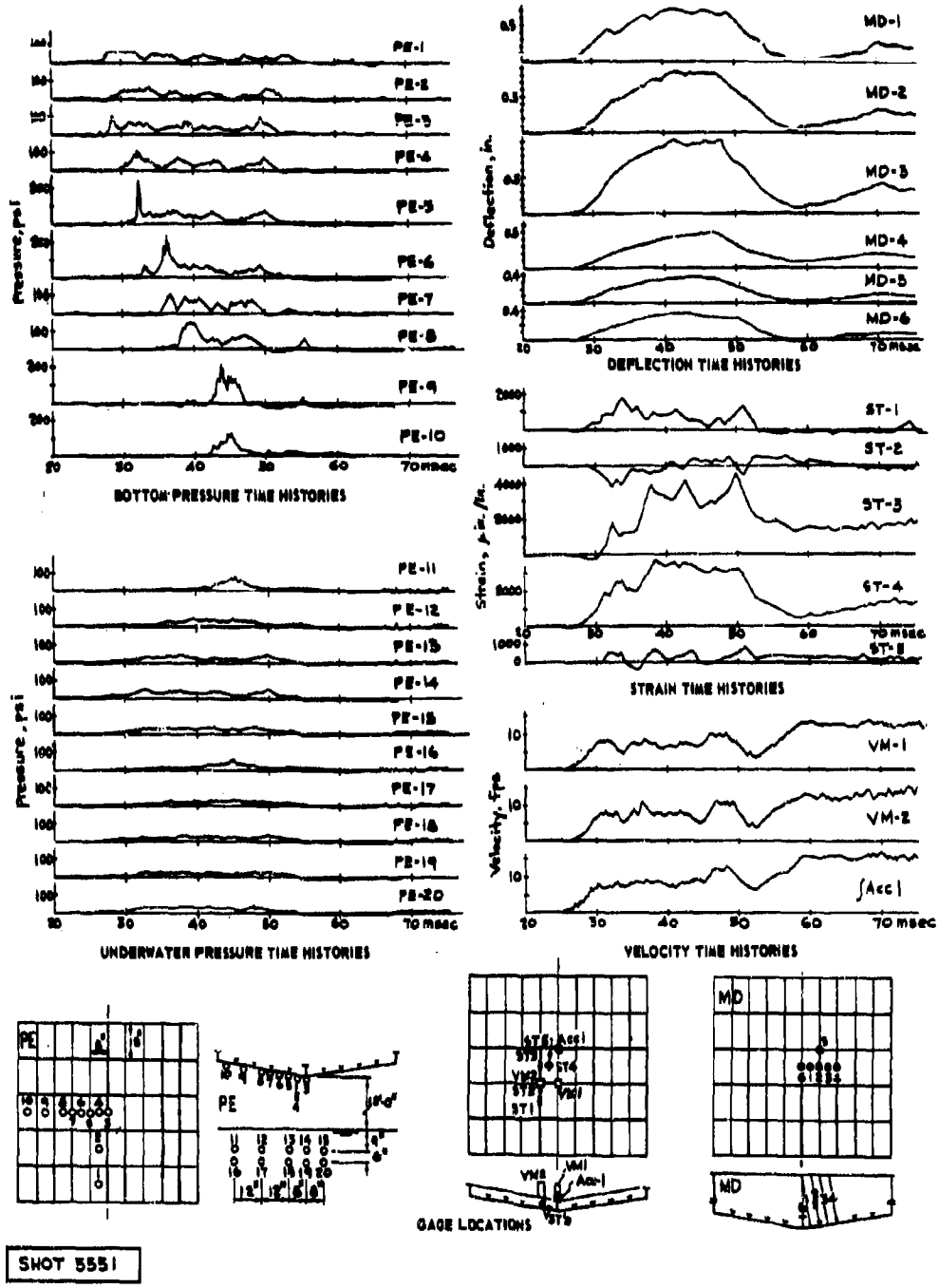

Figure 44c — Test Results for Third 12-Foot Repeated Drop of Model B-4

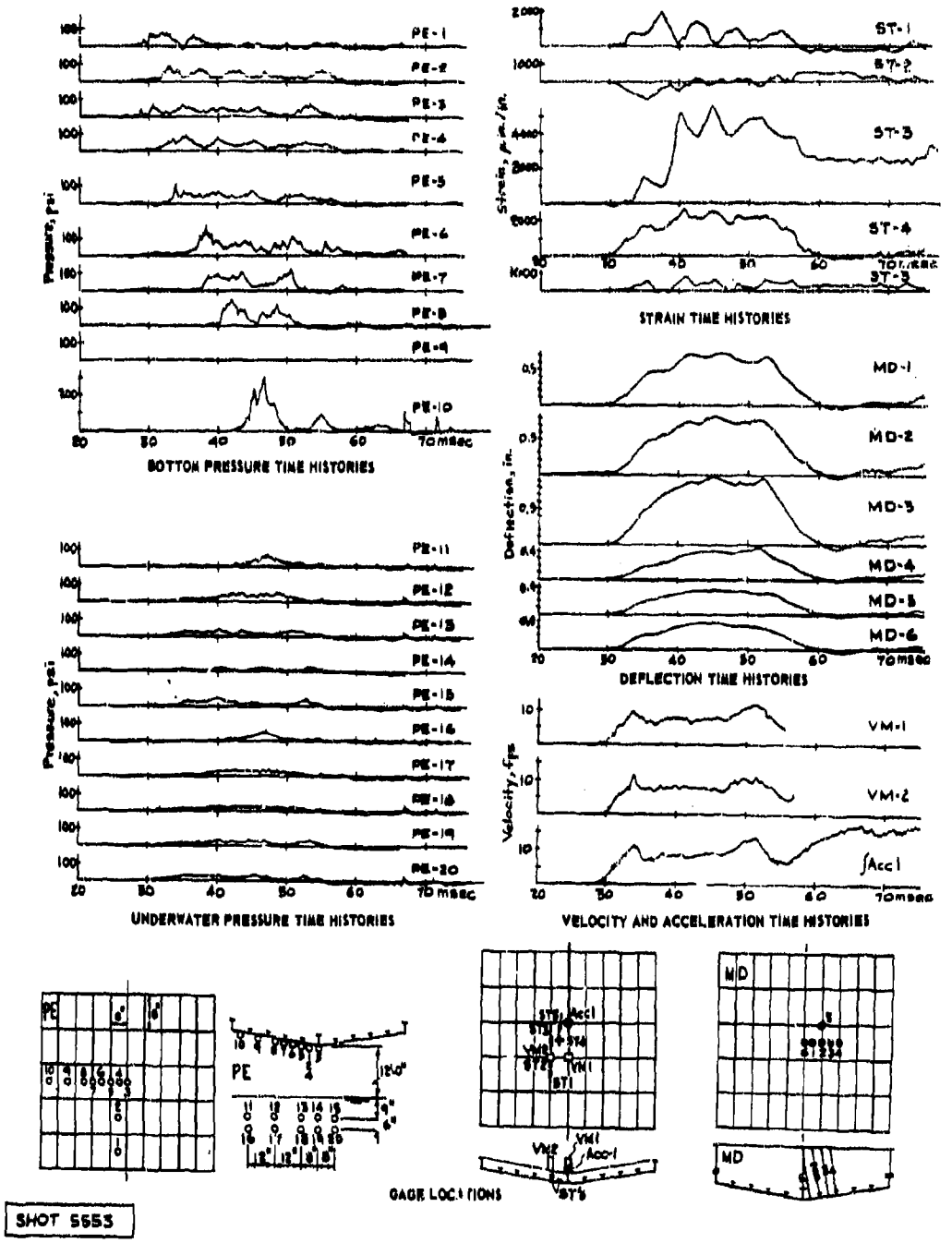

Figure 44d — Test Results for Fourth 12-Foot Repeated Drop of Model B-4

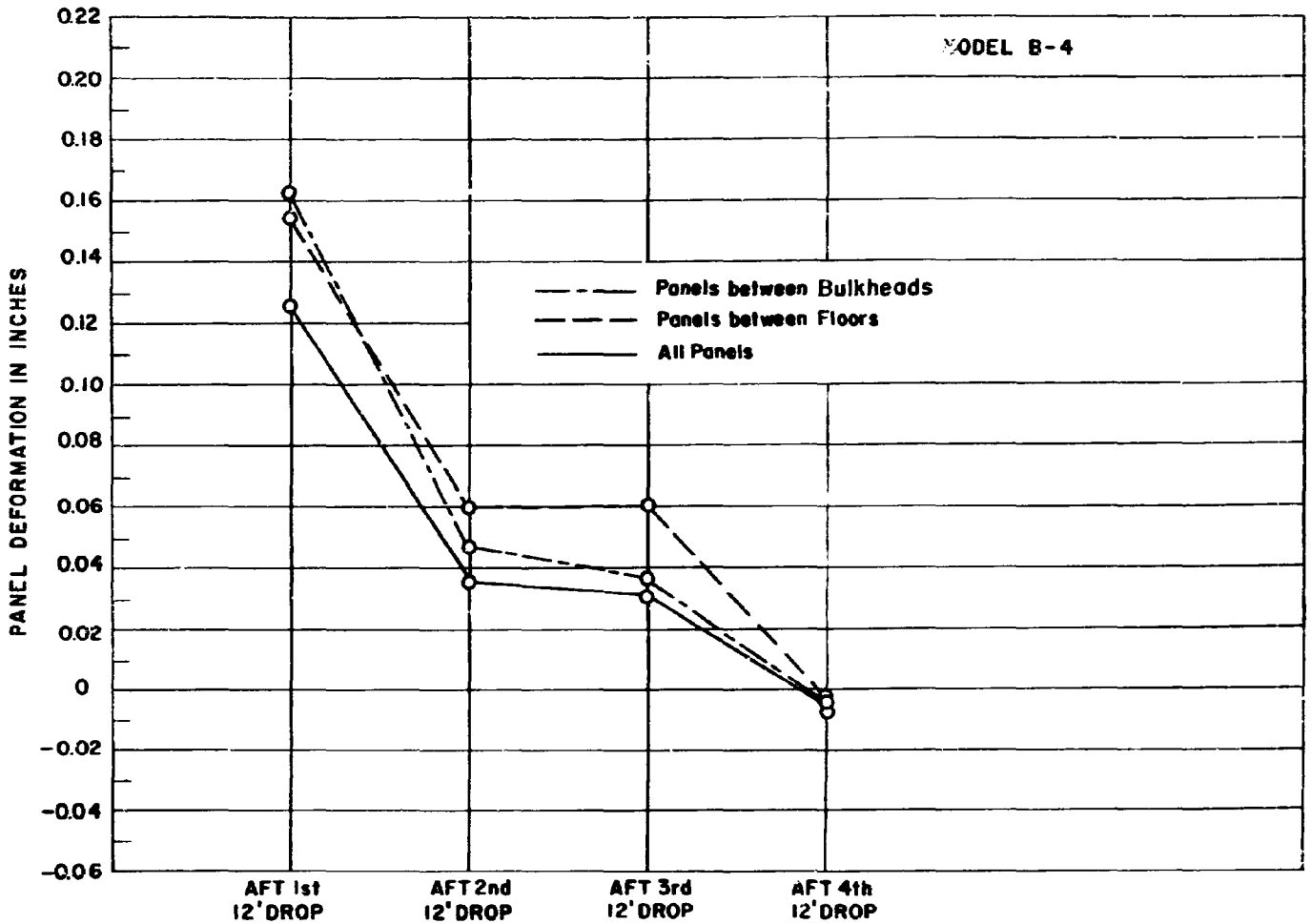

Figure 45 - Mean Value of Net Change of Permanent Deformation at Each Center of 50 Panels Caused by 12-Foot Repeated Drops

2. The change of permanent deformation of keel and bulkheads was gradually reduced after every repeated 12-ft drop. This shows that there is considerable further strengthening due to bending action. However, it is felt that the rate of change of permanent deformation of the keel will not be reduced since dishes at the center vertical keel started to form after the fourth 12-ft drop.

3. Floors showed considerable damage after the first 12-ft drop. Not only did dishes begin to form at webs, but flanges warped and webs also began to warp with visible buckled traces at the ends. Warping, buckling, and dishing formed rapidly after each repeated 12-ft drop.

4. Longitudinals showed permanent deformation after the first 12-ft drop. The net change of permanent deformation was gradually reduced thereafter.

Since this topic is beyond the scope of the present study, the theoretical investigation on repeated loads has been omitted.

D. EFFECTIVENESS OF BACKING MATERIAL IN REDUCING STRUCTURAL DAMAGE

It was concluded from this series of tests that structural damage cannot be substantially reduced by backing material up to 1.75 times the weight of the bottom plating.[26] This finding can be explained by the dynamic interaction theory given in Section IV-A.

As indicated in Section IV-A, the equation of motion of the grillage ship bottom subjected to bottom impact is given by Equations [4.3] and [4.5], i.e.,

$$(m_s + m_{zz})\ddot{w} + c_v\dot{w} + \left[D_x\frac{\partial^4}{\partial x_1^4} + 2H\frac{\partial^4}{\partial x_1^2\,\partial y_1^2} + D_y\frac{\partial^4}{\partial y_1^4}\right]w = p_r \quad [4.3]$$

for the ship bottom with no backing material and

$$(m_s+m_{zz}+m_b)\ddot{w} + (c_v+c_b)\dot{w} + \left[D_x\frac{\partial^4}{\partial x_1^4} + 2H\frac{\partial^4}{\partial x_1^2\,\partial y_1^2} + D_y\frac{\partial^4}{\partial y_1^4}\right]w = p_r \quad [4.5]$$

for the ship bottom with backing material.

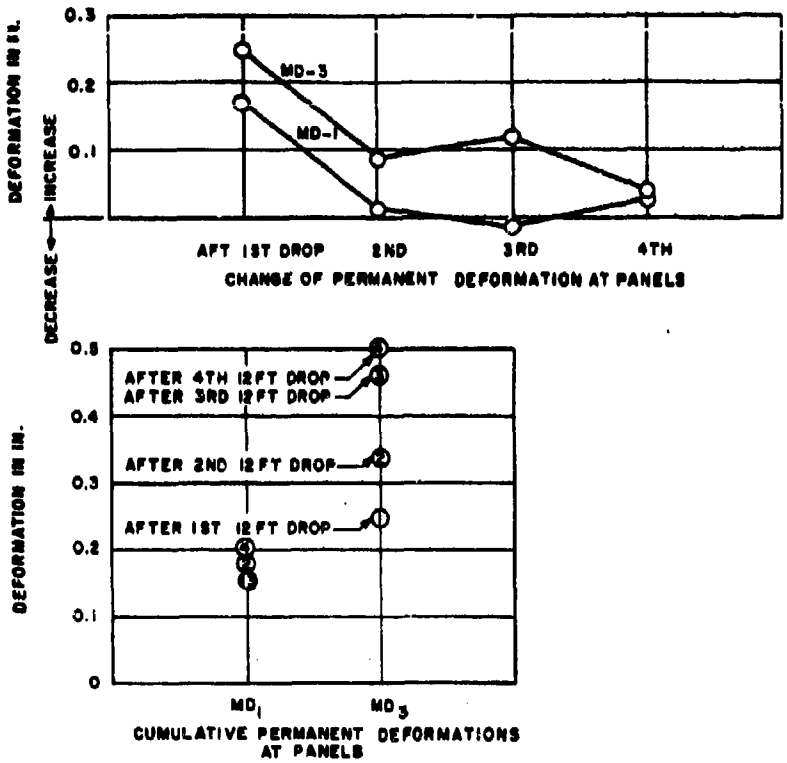

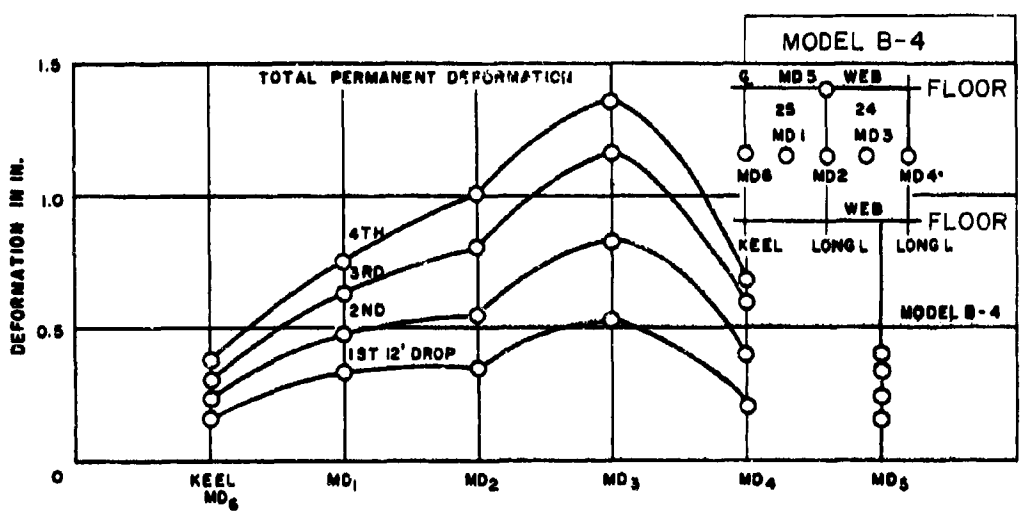

Figure 46 - Permanent Deflection Recorded by Deflection Gages

In the above two equations, the spring force and the rigid-body impact load remain the same, with or without the backing material. The inertial force and the damping force are affected by the addition of the backing material. Therefore, it is necessary to examine the first two terms in the equations and to determine how the backing material influences the dynamic response of the structure.

As given in the example in Section VI, the structural mass is found to be

$$m_s = 1.57(10)^{-4} \text{ lb-sec}^2/\text{in.}^3$$

with the weight of the plate 265 lb and the total weight of the model 435 lb. If a total of 435 lb of backing material is added to the model, then

$$m_s + m_b = 3.14(10)^{-4} \text{ lb-sec}^2/\text{in.}^3$$

But, calculated from

$$m_{zz} = \frac{\pi}{2} \rho L^2/2L$$

$$= 2.94(10)^{-3} \text{ lb-sec}^2/\text{in.}^3$$

the value of the added mass of fluid is almost 10 times larger than the value of $(m_s + m_b)$. This means that the addition of the backing material will not change the inertial force very much.

The effectiveness in damping can be detected by the change of excited frequency of the model caused by the addition of the backing material. Harmonic analysis of the test results of Models D-3, KG-1, KG-2, MG-1, and MG-2 indicated that changes in fundamental frequencies were insignificant (see Figure 47); all were around 50 Hz. (The harmonic analysis was performed by feeding the actual digitized test record into the computer.) Therefore, the addition of damping by the backing material will not change the damping force very much.

Calculation from Equation [6.17] for the ship flat-bottom model (shown in Table 2 and Figure 38) indicates clearly that the spring force is much larger than is the inertial force due to the mass of the structure.

Thus the omission of the inertial force due to the mass of the structure will not affect the maximum value of the structural response very much. Since the mass of the backing material is in the same order as that of the structure, it will not affect the structural response very much either. Therefore, this suggests that backing material is not very effective in reducing structural damage.

E. COMPARISON OF INTERACTION FREQUENCIES AMONG PRESSURE, DEFLECTION, ACCELERATION, AND STRAIN TIME HISTORIES

As indicated in Section IV-A, the total impact pressure p_t generated by the elastic body falling on the water surface can be separated into the rigid body impact pressure p_r and the interacting pressure p_i. This can be expressed by

$$p_t = p_r + p_i$$

$$= p_r - (m_{zz}\ddot{w} + c_{zz}\dot{w} + k_{zz}w) \qquad [4.1]$$

Since in Equation [4.1] the terms $(c_{zz}\dot{w})$ and $(k_{zz}w)$ are much smaller than the term $(m_{zz}\ddot{w})$, this equation can actually be represented by Equation [3.1] with proper correction for small deadrise angle of wedge (where $z = -\ddot{w}$). Therefore, p_t is predominated by the same frequency as for $\ddot{w}$, but it is an 180-deg out-phase of $\ddot{w}$, and hence p_t is an in-phase with w. This phenomenon has been illustrated in Figure 22 (Section V).

To prove this interaction phenomenon for the present series, a harmonic analysis by computer was performed for Models D-3, KG-1, KG-2, MG-1, and MG-2. A sample of the results is illustrated in Figure 47 which is traced from the actual charts plotted by the computer. The figure shows that for the 10-ft drop height, the pressure, the deflection, the acceleration, and the strain time histories all have the same frequency of about 50 Hz. This 50 Hz is the fundamental frequency for Model MG-2.

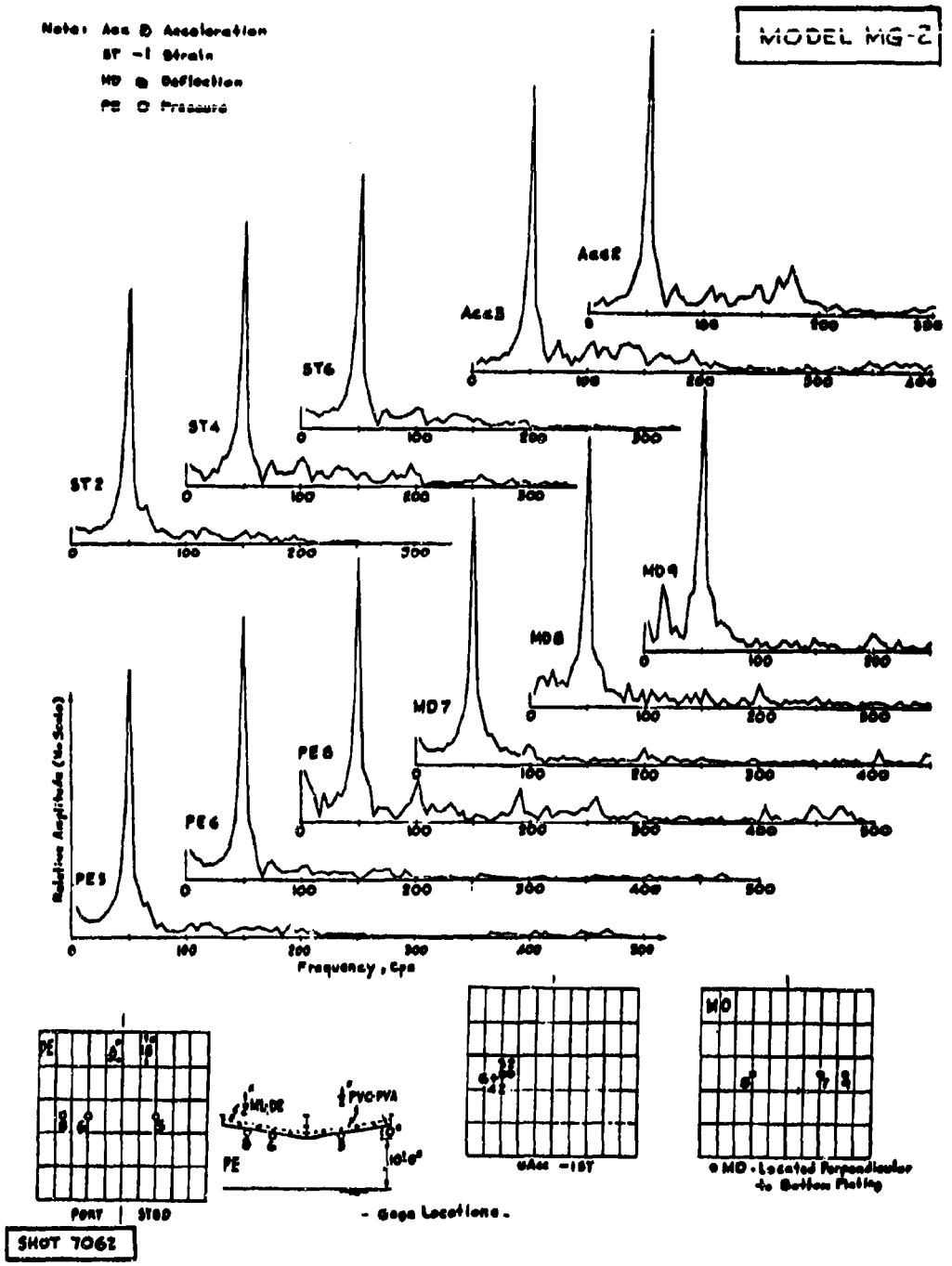

Figure 47 - Harmonic Analysis Obtained from Computer Results

F. SHORT SUMMARY

On the basis of experimental work on the impact of ship structural models with 10-deg deadrise angle, with and without backing material, it is concluded that:

1. The harmonic analysis indicates that the pressure, the deflection, the strain, and the acceleration time histories all had about the same frequencies as the predominant fundamental frequency of the structure. This was caused by the dynamic interaction between the vibration of the impact surface and the fluid.

2. The measured maximum pressures at the impact surface of the structural models were close to the values obtained from the impact test of the rigid wedge-shaped body with 10-deg deadrise angle.

3. The addition of as much as 10 percent of the original drop weight did not affect the maximum impact pressure at all.

4. For higher drops, both the plate panel and the supporting members will deform into the plastic region to cause permanent set. Repeated tests at the same drop height indicated that the rate of change of permanent set in plate panel caused by each drop is confined essentially to the first drop.

5. The use of backing material is not very effective in reducing structural damage because the added-on mass and the damping effect of the backing material do not contribute significantly.

VIII. SUMMARY

It has generally been believed that the impact of a ship bottom with a large deadrise angle, say 15 deg and larger, is an unsteady hydrodynamic phenomenon. If the ship has a flat bottom, the impact of such a surface has been considered a combined acoustic and unsteady hydrodynamic phenomenon. This assumption is made because the hydrodynamic theory would predict infinite impact pressure for the flat bottom. However, the situation has never been clearly defined for the impact of a ship bottom with small deadrise angles (say, below 15 and above 0 deg).

Theories for determining the structural response on the ship-bottom impact have been treated in two different ways: as impact on an incompressible fluid and as impact on a compressible fluid. But none of these theories has been rigorously verified by experiments.

The objectives of the present study were therefore:

1. To clarify whether the flat-bottom impact is an acoustic or a hydrodynamic phenomenon.

2. To determine the impact pressure for rigid wedge-shaped bodies at small deadrise angles.

3. To resolve the basic nature of the structural response resulting from ship-bottom impact.

Two series of test programs were conducted to accomplish the above objectives. The first series of tests investigated the impact of rigid bodies with water; one rigid flat-bottom model and five rigid wedge-shaped models with respective deadrise angles of 1-, 3-, 6-, 10-, and 15-deg were used for this investigation. The second series of tests investigated the impact of deformable and elastic bodies with water; two inflatable fabric ship sectional models, one elastic plate model, two ship flat-bottom models, and eight ship-bottom models with 10-deg deadrise angles were used for this investigation.

On the basis of the two series of experimental investigations, the following conclusions are drawn:

A. IMPACT OF RIGID BODIES WITH WATER

1. During rigid-body impact of the flat bottom, the first positive pulse of the impact pressure occurs at the instant when the air is trapped momentarily between the falling body and the fluid. Only the flat bottom and 1-deg wedge trap considerable amounts of air; wedges with deadrise angles of 3 deg or higher do not trap very much air.

2. The existence of trapped air acts as a cushioning medium during the flat-bottom impact and causes the impact pressure to rise and decay gradually. Thus the maximum impact pressure is much lower than the hydrodynamic infinite pressure or the acoustic ρcV_o pressure.

3. Since no acoustic $\rho c V_o$ pressure is detectable from the impacts of flat bottom and wedges with different deadrise angles, water may always be considered an incompressible fluid.

4. Because of the trapped air phenomenon, the Wagner hydrodynamic theory does not apply very well for wedges with small deadrise angle. Equation [3.8] and Figures 10 to 13 were prepared for the purpose of estimating the maximum impact pressure of a rigid wedge-shaped body with any deadrise angle.

B. IMPACT OF DEFORMABLE AND ELASTIC BODIES WITH WATER

1. Test results of this series revealed that the dynamic interaction caused by ship-bottom impact is closely related to the hydrodynamic phenomenon and that water may be considered incompressible. In other words, to include the interaction in the analysis is to include the hydrodynamic added mass of the fluid and the fluid damping in the equation of motion for the structural response.

2. The impact pressure for the inflatable fabric hull is considerably lower than that for the rigid-body hull. This is attributed to the fact that a deformable body affords relief from the impact load.

3. During the impact of the elastic plate model, the first positive pulse of the impact pressure occurs when the air is also trapped momentarily between the falling body and the water. However, when compared with the record from the rigid flat-bottom impact test, it is obvious that the plate stiffness and boundary conditions affect the time required for the trapped air to escape.

4. The maximum impact pressures were independent of drop weight for two inflatable models and eight 10-deg ship structural models.

5. From the practical point of view, the damping effect may be omitted without introducing noticeable error in the design of the ship bottom subjected to impact load.

6. Also from the point of view of practical design, because the grillage type of ship bottom is relatively rigid, it is reasonable to assume that the rigid-body impact loads are applied quasi-statically to the impact area of ship bottom.

7. The use of backing material (such as water, oil, sand, ML-D2, or PVC-PVA) is not very effective in reducing structural damage because the added-on mass and the damping effect of backing material do not contribute significantly.

8. If the plate panels and the structural members deform into the plastic region to cause permanent set as a result of repeated drops with an identical impact velocity, this permanent set is essentially confined to the first drop.

9. The underwater pressure produced by ship-bottom impact diminishes with the distance away from the impact area of the ship bottom.

ACKNOWLEDGMENTS

The author is indebted to Dr. M.C. Soteriades for his technical guidance during the course of this work. The course taken under Dr. Soteriades enabled the author to successfully analyze the test data on the structural response to impact loads.

Many thanks are extended to Dr. S.R. Heller, Jr. and to Dr. and Mrs. M.K. Ochi for their expert advice. Dr. Heller and Dr. Ochi read the manuscript in detail; their helpful assistance and valuable suggestions added to the clarity and interest of the work.

Acknowledgments will not be complete without extending thanks to Mrs. Nan L. Cook for her efforts in revising and editing the thesis to its present form.

This work was supported by the Naval Ship Research and Development Center. However, the opinions expressed are those of the author alone and should not be construed to reflect the official views of the Center, the Navy Department, or the naval service at large.

BLANK PAGE

APPENDIX

THEORETICAL INVESTIGATION OF FLAT-BOTTOM IMPACT

The theory under development assumes that a layer of air is trapped between the falling body and the fluid. Further, the theory is based on the fact that the energy stored in the falling body prior to the occurrence of impact is a function of position and impact velocity only, and is not dependent on the presence of air under the falling body. It is obvious from this that the impulse produced when the falling body strikes the fluid is the same whether air is present or not. However, even though the impulse is the same, the resulting pressure-time curves with and without air are very different.

Since the air is more compressible than the fluid, it functions as a cushioning layer to relieve the sharp rise of the impact pressure. This cushioning effect causes the impact pressure to rise more gradually from zero to its maximum and to be distributed evenly over the entire contact area. To reach this maximum pressure requires $2L/c_{air}$ units of time because the pressure waves travel in the air layer at the speed of sound in the air as well as in the fluid at the speed of sound in the fluid. For this same reason, the impact pressure takes $2L/c_{air}$ units of time to return to zero. This makes the duration of pulse T:

$$T = 4\ L/c_{air} \qquad [A.1]$$

providing that c_{air} is considered constant. The values of T obtained from Equation [A.1] check reasonably well with the experimental results, such as shown in Figures 3 and 5. However, if c_{air} varies within the duration of pulse T, Equation [A.1] has to be revised accordingly. This will be shown later. If the air is absent during the flat-bottom impact, the impact pressure rises almost immediately at the instant of impact and dies down at 2L/c units of time.[4]

From the foregoing discussion, the following hypotheses may be drawn:

1. During flat-bottom impact, the total impulse produced is the same whether the layer of air is or is not present between the impact body and the fluid, i.e.,

$$(I)_{\text{without air}} = (I)_{\text{with air}} \qquad [A.2]$$

2. The speed of sound in the trapped air c_{air} varies with the pressure in the confined space between the falling body and the fluid. Assuming the compression of air to be isentropic, then

$$\frac{p}{p_a} = \left(\frac{\rho_1}{\rho_a}\right)^{\gamma}$$

$$\frac{dp}{d\rho_1} = c_{air}^2$$

From these two equations,

$$\frac{p}{p_a} = \left(\frac{c_{air}}{c_a}\right)^{\frac{2\gamma}{\gamma-1}}$$

or

$$c_{air} = c_a\left(\frac{p}{p_a}\right)^{\frac{\gamma-1}{2\gamma}} \qquad [A.3]$$

where p_a is the atmospheric pressure, c_a is the speed of sound in the atmosphere at p_a, and γ is the ratio between the specific heat at constant pressure and that at constant volume. At the normal condition of atmosphere, $\gamma = 1.4$ may be used.

In Equation [A.3], p is referred to the absolute-zero pressure. If it is referred to the atmospheric pressure as zero, then Equation [A.3] becomes (with $\gamma = 1.4$)

$$c_{air} = c_a\left(\frac{p_a + p}{p_a}\right)^{\frac{1}{7}} \qquad [A.4]$$

3. In a time dt, the pressure wave travels a distance of (c_{air} dt) in the trapped air region. This distance is also equal to $d\ell$. This gives

$$d\ell = c_{air}\, dt \qquad [A.5]$$

During the flat-bottom impact, the time required within the duration of pulse is T; and during that duration, the pressure wave has traveled a distance of 4L. Therefore,

$$\int_0^{4L} d\ell = \int_0^T c_{air}\, dt \qquad [A.6]$$

The above equation shows that if c_{air} is considered as constant during the process of pulse, then $T = 4L/c_{air}$ which is Equation [A.1]. However, because c_{air} is a function of impact pressure (by Equation [A.4]), Equation [A.1] is therefore replaced by Equation [A.6] for the present investigation.

4. Since the pressure wave travels in the trapped air region at the speed of sound, the impact pressure distribution on the flat bottom would be similar to Figure 10 of Reference 4. This figure indicates that the impact pressure at the center of the flat bottom decays later than pressures at other locations in the flat bottom. This phenomenon is evident in Figure 5 which compares pressure histories at the center and the edge. However, the differences are small because the cushioning effect of the trapped air tends to distribute pressures more evenly. To avoid tedious mathematical operations, therefore, we assume that the impact pressure distributes evenly over the entire area of the flat bottom, even though physically the impact pressure has to be distributed unevenly for the pressure wave to travel. This gives

$$p \cong p(t) \qquad [A.7]$$

5. From the experimental results, the impact pressure time history curve may be approximated empirically in the form of

$$p(t) = 2\, p_{max}\, e^{-1.4\, t/T} \sin \pi \frac{t}{T} \qquad [A.8]$$

with $p(t) \geq -15$ psi.

Equation [A.8] is nothing but a sine wave with decreasing amplitude. Although better fitted equations may replace Equation [A.8], the final results of the maximum pressure will not deviate very much from those

determined by Equation [A.8]. The use of a triangle pulse for approximation would give much higher maximum pressures as they are compared with the experimental results.

The total impulse for idealized flat-bottom impact (no air layer) may be expressed as[12]

$$(I)_{\text{without air}} = \frac{m_{zz}\, V_o}{1 + \frac{m_{zz}}{M_o}} \qquad [A.9]$$

where m_{zz} is the added mass of the fluid and M_o is the total mass of the impact body. If $M_o >> m_{zz}$, which is generally true for the actual ship, then

$$(I)_{\text{without air}} = m_{zz}\, V_o \qquad [A.10]$$

Use $m_{zz} = \pi\, \rho L^2/2$, which is the conventionally used expression for added mass; then

$$(I)_{\text{without air}} = \frac{1}{2}\, \pi\, \rho L^2\, V_o \qquad [A.11]$$

Equation [A.11] is valid whether the flat-bottom impact is treated as a hydrodynamic phenomenon[12] or as an acoustic phenomenon.[4] (V_o is considered constant here.) Therefore, Equation [A.2] can be rewritten as

$$\frac{1}{2}\, \pi\, \rho L^2\, V_o = A \int_{t_o=o}^{t=T} p(t)\, dt \qquad [A.12]$$

where the right side of the equation is the total impulse for actual flat-bottom impact (with air layer). Substituting Equation [A.8] into Equation [A.12] yields

$$\frac{1}{2}\, \pi\, \rho L^2\, V_o = A \int_o^T 2\, p_{max} e^{-1.4\, \frac{t}{T}} \sin \pi\, \frac{t}{T}\, dt \qquad [A.13]$$

where A is the area of the flat bottom per unit length or

$$A = 2\, L \qquad [A.14]$$

Since T and p_{max} are two unknowns contained in Equation [A.13], one more equation is therefore needed. This can be obtained by combining Equations [A.4], [A.6], and [A.8]. This yields

$$4\,L = c_a \left(\frac{1}{p_a}\right)^{\frac{1}{7}} \int_0^T \left(p_a + 2\,p_{max} e^{-1.4\,\frac{t}{T}} \sin \pi \frac{t}{T}\right)^{\frac{1}{7}} dt \qquad [A.15]$$

which also contains T and p_{max}. From Equations [A.13] and [A.15],

$$p_{max} \cong 4.3\,V_o^{1.1} \qquad [A.16]$$

where p_{max} is in pounds per square inch and V_o is in feet per second.

REFERENCES

1. Lewis, E.V. and Gerard, G., "A Long-Range Research Program in Ship Structural Design," Ship Structure Committee Serial SSC-124 Final Report (Nov 1959).

2. Saunders, H.E., "Hydrodynamics in Ship Design, Vol. III," Society of Naval Architects and Marine Engineers (1965), Chapter 16, pp. 288-296.

3. Von Karman, Th., "The Impact on Seaplane Floats during Landing," National Advisory Committee for Aeronautics TN 321 (1929).

4. Ogilvie, T.F., "Compressibility Effects in Ship Slamming," Schiffstechnik Vol. 10, No. 53 (1963).

5. Sharov, Y.F., "Slamming Stresses in Ship Bottom Plates," Sudostroenie, Vol. 24, No. 4, pp. 5-9 (1958).

6. Meyerhoff, W.K., "Die Berechnung hydroelastiacher Stösze," Schiffstechnik Vol. 12, No. 60 and 61 (1965).

7. Fujita, Y., "On the Impulsive Pressure of a Circular Plate Falling upon a Water Surface," Journal of Zosen Kiokai, Vol. 94, pp. 105-110 (1954).

8. Tanaka, N., "On the Impact of a Body Falling upon the Water Surface," Journal of the Society of Naval Architects of West Japan, Vol. 72 (1952).

9. Wagner, V.H., "Über Stosz-und Gleitvorgänge an der Oberflache von Flüssigkeiten," Zeitschrift fur Angewandte Mathematik und Mechanik, Vol. 12, No. 4, pp. 193-215 (Aug 1932).

10. Bleich, H.H., "Dynamic Interaction between Structures and Fluid," Proceedings of the First Symposium on Naval Structural Mechanics, Pergamon Press (1960).

11. Egorov, I.T., "Impact on a Compressible Fluid," National Advisory Committee for Aeronautics TM 1413 (1956).

12. Ochi, K.M. and Bledsoe, M.D., "Hydrodynamic Impact with Application to Ship Slamming," 4th Symposium on Naval Hydrodynamics, Office of Naval Research (Aug 1962).

13. Ochi, M.D. and Schwartz, F.M., "Two-Dimensional Experiments on the Effect of Hull Form on Hydrodynamic Impact," David Taylor Model Basin Report 1994 (May 1966).

14. Verhagen, J.H.G., "The Impact of a Flat Plate on a Water Surface," Journal of Ship Research (Dec 1967).

15. Johnson, R.S., "The Effect of Air Compressibility in First Approximation to the Ship Slamming Problem," Journal of Ship Research (Mar 1968).

16. Lewison, G. and Maclean, W.M., "On the Cushioning of Water Impact by Entrapped Air," Journal of Ship Research (Jun 1968).

17. Ochi, M.K., "Ship Slamming - Hydrodynamic Impact between Waves and Ship Bottom Forward," Fluid-Solid Interaction Symposium, American Society of Mechanical Engineers (Nov 1967).

18. Chuang, S.L., "Theoretical Investigation of Dynamic Interaction between Ship Bottom and Fluid during Slamming," NSRDC Report 2403 (Dec 1967).

19. Heller, S.R., Jr. and Jasper, N.H., "On the Structural Design of Planing Craft," Quarterly Transactions of the Royal Institution of Naval Architects (Jul 1960).

20. Warburton, G.B., "The Vibration of Rectangular Plates," Proceedings of the Institution of Mechanical Engineers, Vol. 168, No. 1, pp. 371-384 (1954).

21. Hearmon, R.F.S., "The Frequency of Flexural Vibration of Rectangular Orthotropic Plates with Clamped or Supported Edges," Journal of Applied Mechanics, pp. 537-540 (Dec 1959).

22. Huffington, N.J., Jr. and Hoppmann, W.H., II, "On the Transverse Vibrations of Rectangular Orthotropic Plates," Journal of Applied Mechanics (Sep 1958).

23. Norris, C.H. et al., "Structural Design for Dynamic Loads," McGraw-Hill Book Company (1959).

24. Clevenger, R.L. and Melberg, L.C., "Slamming of a Ship Structural Model," M.S. Thesis, Massachusetts Institute of Technology (May 1963).

25. Goodwin, J.J. and Kime, J.W., "Slamming of a Ship Structural Model with Backing Material," M.S. Thesis, Massachusetts Institute of Technology (May 1964).

26. Gardner, J.T. and Morris, C.C., "Slamming of a Ship's Structural Model Backed with Damping Material," M.S. Thesis, Massachusetts Institute of Technology (May 1965).

UNCLASSIFIED
Security Classification

DOCUMENT CONTROL DATA - R & D

(Security classification of title, body of abstract and indexing annotation must be entered when the overall report is classified)

1. ORIGINATING ACTIVITY (Corporate author) Naval Ship Research and Development Center Washington, D.C. 20007	2a. REPORT SECURITY CLASSIFICATION Unclassified 2b. GROUP

3. REPORT TITLE
INVESTIGATION OF IMPACT OF RIGID AND ELASTIC BODIES WITH WATER

4. DESCRIPTIVE NOTES (Type of report and inclusive dates)
Final

5. AUTHOR(S) (First name, middle initial, last name)
Sheng-Lun Chuang

6. REPORT DATE February 1970	7a. TOTAL NO. OF PAGES 122	7b. NO. OF REFS 26
8a. CONTRACT OR GRANT NO. b. PROJECT NO. c. Subproject Z-R011 01 01 Task 0401 d.	9a. ORIGINATOR'S REPORT NUMBER(S) 3248 9b. OTHER REPORT NO(S) (Any other numbers that may be assigned this report)	

10. DISTRIBUTION STATEMENT
This document has been approved for public release and sale; its distribution is unlimited.

11. SUPPLEMENTARY NOTES Ph.D. thesis, Catholic University of America, June 1969	12. SPONSORING MILITARY ACTIVITY Naval Ship R&D Center Washington, D.C. 20007

13. ABSTRACT

Impact tests of rigid flat-bottom models indicated that the maximum impact pressure is nowhere near the theoretical infinitely large hydrodynamic pressure nor near the theoretical acoustic pressure. The cushioning effect of the compressible air trapped between the impact body and the water surface reduces the maximum impact pressure to about one-tenth of the acoustic pressure. However, the nature of the trapped air phenomenon is not very stable. Much more air was trapped for the impact of a flat bottom and a 1-deg wedge than for a wedge with deadrise angles of 3 deg or higher. Tests of elastic models verified the fact that the pressure generated by the impact is affected by the vibratory movement of the impact surface and that it can be separated into rigid body impact pressure and interacting pressure. This dynamic interaction is closely related to the hydrodynamic phenomenon rather than to the acoustic phenomenon. In summary, the present study demonstrates that for the impact of rigid and elastic bodies, (1) water can be treated as an incompressible fluid regardless of the size of the deadrise angle, (2) trapped air must be taken into consideration for small deadrise angles, and (3) the structural response to impact can be treated as the impact of a deformable body on an incompressible fluid, with or without trapped air.

14. KEY WORDS	LINK A		LINK B		LINK C	
	ROLE	WT	ROLE	WT	ROLE	WT
Dynamic interaction						
Elastic body impact						
Hydrodynamic impact						
Hydroelasticity						
Impact of flat bottom						
Impact of wedge-shaped body						
Rigid body impact						
Ship bottom slamming						
Slamming damage						
Structural dynamic response						